NASA CONTRACTOR REPORT

NASA CR-1134

C. 1

NASA CR-1340

CORRELATION OF FLUCTUATING FORCES WITH THE SOUND RADIATION FROM RIGID FLOW SPOILERS

by Hanno H. Heller, Sheila E. Widnall, and Colin G. Gordon

Prepared by
BOLT BERANEK AND NEWMAN INC.
Cambridge, Mass.
for Langley Research Center

NATIONAL AERONAUTICS AND SPACE ADMINISTRATION • WASHINGTON, D. C. • MAY 1969

NASA CR-1340

CORRELATION OF FLUCTUATING FORCES WITH THE SOUND RADIATION FROM RIGID FLOW SPOILERS

By Hanno H. Heller, Sheila E. Widnall,
and Colin G. Gordon

Issued by Originator as BBN Report No. 1734

Prepared under Contract No. NAS 1-7552 by
BOLT BERANEK AND NEWMAN INC.
Cambridge, Mass.

for Langley Research Center

NATIONAL AERONAUTICS AND SPACE ADMINISTRATION

For sale by the Clearinghouse for Federal Scientific and Technical Information
Springfield, Virginia 22151 – CFSTI price $3.00

TABLE OF CONTENTS

page

page

LIST OF ILLUSTRATIONS

page

page

page

ABSTRACT

This report presents the results of a theoretical and experimental study of the correlation of fluctuating forces on rigid flow spoilers with the resulting sound radiation. For this experiment, we developed a system of force transducers to measure simultaneously, yet independently, the drag and lift components of the fluctuating forces on flow spoilers within an experimental jet-pipe system.

This study is a continuation of an earlier study* which suggested that the noise from flow spoilers in a confined environment – such as a hard-walled pipe – is of quadrupole (rather than of dipole) nature, for which the sound sources would be located in the free shear layer past the flow spoiler. The present study aimed to solve this question by correlating the fluctuating lift and drag forces measured on flow spoilers, both under confined and freefield environmental conditions, with the sound transmitted from the experimental jet pipe system into the freefield.

The results of the study suggest strongly that spoiler-generated noise is of dipole character, since a direct correlation of fluctuating forces with the radiated sound was found.

For evaluation of the data, we developed a theory to predict the sound power radiated from pipe-immersed flow spoilers. This theory considered the effect of the enclosure upon the sources and the effect of pipe end reflection. Both monopole and dipole sources were treated. An increase of the dipole sound power output by a factor of 3 for frequencies below the pipe cut-off frequency was predicted and experimentally confirmed.

---

*NASA Contract No. NAS 1-4974: "Influence of Upstream Flow Discontinuities on the Acoustic Power Radiated by a Model Air Jet." NASA CR-679 (also BBN Report No. 1426, 1966).

I. INTRODUCTION AND SUMMARY

A. The Noise of Fan-Jet Engines

Use of high-bypass-ratio fan-jet engines for the new generation of large subsonic aircraft has led to concern about the noise generated by this type of engine. Figure I-1 shows a schematic sketch of the noise sources associated with a turbofan-jet engine. The two primary sources are the fan and the jet exhaust; noise from the fan is radiated through the intake and the fan discharge duct, and noise from the jet is radiated directly into the atmosphere. Jet exhaust noise, which predominates in fan-less jet engines, typically has a low-frequency, broad-band character, whereas the noise emitted from the fan discharge duct consists of higher-frequency broadband and superposed discrete frequency components. As evident from Fig. I-2, which shows a noise spectrum for a typical modern fan-jet engine, the noise radiated from the fan discharge may exceed the jet exhaust noise by 10 to 20 dB. The need to reduce the intense fan noise has led to the pursuit of a number of noise reduction programs. Two approaches are currently being studied [Ref. 1]: (1) treatment of the engine nacelle with acoustical lining, and (2) adjustment of engine parameters to minimize noise generation. Taking the latter, more ideal, approach, however, requires a thorough understanding of the basic mechanisms responsible for the generation of fan noise. The present study aims to contribute to the understanding of the noise-generating mechanisms in the fan sections of fan-jet engines.

B. Previous Study

Our study is a continuation of an earlier investigation [Ref. 2] of the effect of upstream flow discontinuities on the acoustic power radiated by an air jet. The rotor and stator blades of a fan in essence are "flow-spoilers" that disturb the flow in the annular duct in which they operate; the associated acoustic phenomena observed outside the discharge duct result from the interaction of these "flow-spoilers" with the oncoming flow, from acoustic transmission properties of the enclosure, and from the acoustic propagation characteristics in and out of the duct. The earlier study dealt with the noise generated by a flow-spoiler of arbitrary shape, in a hard-walled pipe as sketched in Fig. I-3. The empirical scheme that was developed permits the prediction of the overall noise from the experimental configuration from known steady-state aerodynamic parameters.

Because of unsteady forces (acting on the obstruction and thus on the fluid) that result from turbulence in the oncoming flow and from the shedding of vortices from the obstruction, the interaction of flow with rigid obstructions produces noise. Curle [Ref. 3] considered the sound radiation from these unsteady forces and showed that under certain conditions, applied forces on a fluid correspond to acoustic dipoles, with the sound power due to a fluctuating force varying as the square of the force amplitude and as the square of a characteristic frequency. It is important to note that it is the unsteady aerodynamic components that result in sound generation, and not the steady-state components. In the previous study, the magnitude of the fluctuating forces were assumed to be proportional to the steady-state forces. The validity of this assumption was substantiated by the good correlation that was obtained between acoustic and steady-state force parameters.

The steady drag force on the spoiler equals the static pressure drop Δp across the spoiler times the pipe area. The pressure drop across the spoiler was found to be the most important parameter in the previously developed equation for overall acoustic power Π_{OA} associated with the spoiler-generated noise:

$$\Pi_{OA} = k \cdot \Delta p^3 \cdot d^2/\rho_a^2 c_a^3 , \qquad (I-1)$$

where Π_{OA} is the sound power radiated from the pipe exit, **d** is the pipe diameter, and ρ_a and c_a the atmospheric density and the speed of sound, respectively. The geometry of the spoiler does not enter this equation, but is implicit in the pressure drop. This equation is based on a dipole model of spoiler noise; and the variation of overall spoiler noise with the sixth power of flow velocity predicted from this equation has been observed experimentally.

However, some data points for sound power in the higher frequency bands were found to fit an eighth-power dependence on velocity better than the above mentioned sixth-power law. As is well known, however, an eighth-power law holds for quadrupole sources. It was therefore suggested that spoiler-generated noise is of quadrupole nature, and assumes dipole characteristics below the pipe cut-off frequencies because of the solid pipe-walls. If this suggestion is true, then spoiler-generated noise within a confined space would be ascribable to the quadrupole sources present in the free shear-layer in the flow past the spoiler. Thus, the very fundamental question concerning the nature of the noise sources associated with flow past obstructions in confined environment remained to be resolved; it is at this point that the present study begins.

C. Present Investigation

To determine the validity of the "quadrupole-theory", we measured the fluctuating drag and lift forces on flow-spoilers and the associated radiated sounds under both simulated free-field and confined environment conditions. An important fraction of our total effort was devoted to development of a system of transducers capable of measuring simultaneously the fluctuating lift and the drag forces on a flow spoiler.

Our experimental results indicate that spoiler-generated noise is indeed related to the fluctuating forces, and that it results from dipole, rather than from quadrupole, sources. However, we have also shown theoretically that the confinement provided by the pipe wall enhances the sound power radiated by dipole sources, and we have observed this enhancement experimentally.

In developing the theoretical expressions, we have also looked into the changes that monopole radiation characteristics would suffer from an immersion into a confined environment. We have to this extent also performed a simple experiment whereby an acoustic monopole source was immersed into a hard-wall pipe without flow to investigate its radiation characteristics. In addition, we studied the effect of reflection at the pipe end on the power radiated to the freefield from both the monopole and dipole sources. Further, we have investigated how the degree of turbulence in the flow, impinging on the spoiler, affects the fluctuating forces and the associated sound. We substantiated some results of the earlier study by checking the relationship between the fluctuating forces and the steady-state forces experienced by one particular spoiler.

Because we obtained good correlation between fluctuating forces and sound radiation and because our experimental results

agree with theoretical predictions, we felt that the originally planned additional studies of rotating-jet/slot configurations would not add to our present understanding of flow-spoiler noise, and therefore we did not undertake them.

The following sections of this report summarize the four phases of our effort:

(1) Development of a system for measuring fluctuating drag and lift forces on flow spoilers.

(2) Development of theory for (a) sound radiation from aerodynamic dipole sources in a hard-walled enclosure, and (b) sound propagation within and out of a hard-walled pipe.

(3) Studies of the relation between forces and sound, for a variety of flow spoilers under both freefield and confined conditions.

(4) Comparison of theoretical prediction of Phase 2 with experimental findings of Phase 3.

II. FORCE MEASURING SYSTEM

A. Fluctuating-Force Transducer

The force transducer (Fig. II-1) that was developed for our program consists of a pair of barium titanate elements, polarized in the thickness direction, assembled with the faces of like polarity adjacent to each other and joined to a common platinum foil electrode. The barium titanate elements are held between stainless steel plates; the lower plate has a threaded-stud for fastening the transducer to a supporting structure. A thin cover plate, cemented to the top of the transducer, provides a smooth surface for the spoiler assembly to contact. The function of the layer of rubber and of the additional metal cover shown in the figure are explained in Sec. C, below.

B. Calibration

The frequency response of the force transducers was found to be completely flat from 20 Hz to beyond 20 kHz. The transducers, therefore, were calibrated at only one frequency, 100 Hz. Each transducer was mounted on a vibration exciter (Fig. II-2) and was subjected to an acceleration of 1 g at 100 Hz. An added 10-gram mass was fastened atop the cover-plates (whose total mass is 0.65 gram). The combined masses of the cover-plates and the additional weight thus experienced a sinusoidal acceleration of 1 g amplitude, so that the transducer experienced a fluctuating force of 10,500 dynes. Our force measuring system used a total of four force transducers. The peak-to-peak output voltages of each transducer responding to the aforementioned force were found to range from 116 to 134 mV; their sensitivities were

found to range from 3.9×10^{-3} to 4.5×10^{-3} RMS millivolt output per dyne.

C. Force Measuring Apparatus

A schematic of the force measurement set-up appears in Fig. II-3. Since we were interested in both the lift and drag forces, we mounted two transducers on each supporting strut, with their sensitive axes at right angles. Disks rigidly attached to the ends of the flow spoiler serve to transfer the force on the spoiler to the transducers. Set screws with rubber tips were used to hold the disks against the transducer faces.

Figure II-4 is a photograph of the force measuring apparatus for one particular test configuration in which the spoiler is located at the pipe exit. Figure II-5 shows one of the two struts, removed from the jet-pipe. Figure II-6 is a close-up view of the cavity in which the force transducers are mounted.

To be able to measure the two fluctuating-force components independently, one must keep the interaction between the lift-force transducer and the drag-force transducer to a minimum. We checked the "cross-talk" of each transducer pair by magnetically exciting a spoiler in only the lift or the drag direction and recording the signals of both transducers over the frequency range of interest. Our original force measuring system showed very poor cross-talk characteristics. We overcame this difficulty by adding the previously mentioned rubber layer and an additional cover plate onto the transducer, as shown in Fig. II-1, to provide a connection that is stiff in the axial direction and flexible in the lateral direction. The cross-talk characteristics for this improved version of the transducers were very satisfactory, as illustrated by Fig. II-7.

It was also essential to structurally isolate the cover plates of each transducer from the pipe system, so that the transducer would respond only to the forces on the spoiler and not to the pipe systems' vibration. Therefore, we used flexible wire connections for the center conductor and for the ground conductor (from the cover plate to the plug) of each transducer.

III. EXPERIMENTAL FACILITIES AND TECHNIQUES

A. Air Flow Facility and Measurement Chamber

In the present study we used essentially the same airflow system as in our previous work described in detail in Ref. 2. A diagrammatic sketch of the air-flow system and the measurement chamber appears in Fig. III-1. The flow produced by an aircraft engine supercharger is fed through a noise muffler via a flexible hose into the experimental jet system. Controlling the speed of the driving engine and bleeding air from the system upstream of the pipe leading to the jet exhaust keeps the rate of airflow constant.

The jet pipe exhausts into an acoustically-treated chamber that is essentially anechoic for frequencies above 250 Hz. The chamber measures approximately 12 ft by 12 ft by 7 ft. Figure III-2 is a photograph of the chamber with the experimental jet-pipe system.

B. Flow Spoilers

1. Spoiler types

We performed experiments with spoilers of three different cross-sectional shapes as shown in Fig. III-3:

(1) A spoiler of rectangular cross-section (1.27 × 0.63 cm), subsequently called the "strip-spoiler",

(2) A spoiler with a cross-section of 0.3 cm × 2.3 cm with a rounded leading edge and a sharp trailing edge, subsequently called the "airfoil",

(3) A spoiler of circular cross-section (1.6 cm in diameter), subsequently called the "cylindrical-spoiler".

Our reasons for choosing these spoiler configurations are given below.

Spoiler No. 1, the strip-spoiler, was chosen to study noise phenomena dominated by fluctuating drag forces. Flow over this spoiler separates at the sharp-edged corners, leading to high fluctuating forces, particularly drag, and to high associated noise radiation in the drag direction.

Spoiler No. 2, the airfoil (an "aerodynamically well-shaped body"), was chosen to study noise phenomena controlled by fluctuating lift forces. Since, flow separation for small angles of attack occurs only close to the trailing edge, the unsteady lift forces are an order of magnitude larger than the unsteady drag forces. In addition, fluctuating forces on airfoils are important noise sources in rotating machinery.

The aerodynamic and acoustic phenomena due to flow interaction with the airfoil were tested under freefield conditions. It was not possible to observe sound that might have been generated by the airfoil within the pipe, since the rather weak drag components of the fluctuating force on the airfoil, at zero or small angle of attack, did not generate enough noise above the background noise of emanating pipe flow. Noise generation by the airfoil due to fluctuating lift forces under freefield conditions, however, exceeded the jet noise — allowing the correlation of noise and fluctuating force data.

The airfoil was mounted onto the side disks so that its quarter chord line corresponded to the center line between the disks. Since aerodynamic forces on an airfoil act at about the quarter chord distance from the leading edge, this placement minimized undesirable moments.

Spoiler No. 3, the cylindrical spoiler, was chosen to check the results obtained from Spoiler No. 1 with a spoiler of a

different shape. One might expect discrete frequency phenomena in certain Reynolds number ranges due to periodic vortex shedding and could then study associated sound and force phenomena.

2. Influence of the first bending mode frequency

In measuring fluctuating forces on a bar-like spoiler, the presence of modes influences the response at frequencies at and above its first bending mode frequency and thus distorts experimental results. One should then expect useful data from the experiments only at frequencies well below the fundamental resonance. Extending of the useful frequency range requires a spoiler with the highest possible fundamental resonance. We increased the first bending mode frequency of the strip-spoiler and the airfoil by decreasing the mass per unit length (through the use of Balsawood) and by increasing the rigidity of the spoilers (by inserting a reinforcing rib into those two spoilers).

The first bending mode frequency of the strip-spoiler was 4500 Hz, of the airfoil 1500 Hz, and of the cylindrical spoiler 4500 Hz.

Although these still relatively low resonance frequencies seemed to restrict our experiments, by normalizing the force data with respect to a dimensionless frequency, we determined the shape of the force spectrum over a wide frequency range, in spite of the measurement restrictions imposed by the spoiler resonance.

3. Spoiler arrangements

Since our experiment aimed to study the fluid-dynamic and acoustic phenomena for spoilers both under freefield conditions and under constrained-environmental conditions, we used two different arrangements (Figs. III-4 through 6). Figure III-4 shows

the spoiler-transducer assembly employing the airfoil externally of the jet pipe in the "freefield". In this arrangement, we inserted a 1-inch-diameter converging nozzle into the exit plane of the jet pipe. We thus avoided impingement of the high speed air flow on the two struts and consequently eliminated an additional noise source not related to the forces measured by the transducers. Figure III-5 shows a photographic view of the arrangements with one strut removed for clarity.

The velocity profile and the turbulence characteristics of a jet emanating from a converging nozzle (which acted upon the airfoil) differ grossly from that of fully developed turbulent pipe flow (which acted upon the spoilers). However, the characteristics of the impinging flow do not influence the relationship between fluctuating forces and radiated sound.

The spoiler-transducer assembly to study flow spoilers under the "constrained environment" within the hard-walled pipe is shown in Fig. III-6. Here the spoiler pierces the pipe through wall cut-outs shaped to provide minimum clearance to the spoiler. Adding various lengths of pipe downstream of the spoiler allowed the spoiler to be located in the pipe at varying desired distances from the exit plane of the jet-pipe.

For the in-pipe studies, the spoiler was exposed to fully developed turbulent pipe flow. In one test, we changed the degree of in-pipe turbulence by inserting a fine mesh wire screen upstream of the spoiler. We will describe the arrangements in Chap. V.

C. Data Acquisition Systems

1. Flow properties

The stagnation and static pressures upstream of the flow spoiler for in-pipe locations were measured using a Pitot-static tube. This determined the mean flow velocity inside the jet-pipe, as well as in the core of the jet emanating from the converging nozzle. Using DISA hot wire anemometer equipment, the overall turbulence levels and the turbulence levels in frequency-bands were measured in the pipe for conditions of fully developed pipe flow and for conditions of changed flow turbulence downstream of the fine mesh wire screen inserts. Similar measurements were performed in the jet.

2. Fluctuating-force data

To measure the fluctuating forces in frequency bands, the signal of each force transducer was fed into a 1/3-octave band analyzer (B+K type 2111) via an impedance match and a preamplifier. The RMS output voltage in 1/3-octave bands was plotted versus frequency on a graphic level recorder (B+K type 2305) and the output voltage was subsequently converted into force in dynes using the earlier determined sensitivity of each transducer. We simultaneously observed the signal on an oscilloscope. Figure III-7 presents a block diagram of the force measuring system.

3. Sound data

The sound radiated from the experimental jet system was measured with a 1/2-inch-diameter condenser microphone (B+K type 4133) and the acoustic signal was fed through a high pass filter (with a cut-off frequency of 250 Hz to avoid the frequency range for which the measurement chamber was not essentially anechoic)

into an analyzing system consisting of a 1/3-octave-band analyzer (B+K type 2111), a graphic level recorder (B+K type 2305), and a tape recorder (Kudelski type NAGRA III-5). Figure III-8 shows a block diagram of the acoustic data acquisition system. An oscilloscope was used to check that the signal was free from distortions.

The microphone in the anechoic chamber was suspended from a boom so that it could traverse a circular arc with a 3-ft radius around the jet exit in a horizontal plane between 10° and 150° from the downstream axis of the jet. Sound pressure level spectra could also be measured at various fixed angles from the jet axis. The overall signal output of the microphone sweeping on its traverse around the sound source (either the exit plane of the jet-pipe, or the externally located spoiler) could be recorded and stored for later processing.

D. Data Reduction Techniques

1. Fluctuating force data

Figure III-9 shows typical recordings of force signals obtained from the two transducers responding to the fluctuating drag force component. All force signals were recorded and analyzed in 1/3-octave bands in a frequency range from 20 Hz up to 40,000 Hz. The signals in the frequency range at and above the first bending mode of the particular spoiler, however, were not used for further analysis, since the spoiler at and above this frequency could no longer be considered "rigid" and the signals from two corresponding transducers (either the two "drag-transducers" or the two "lift-transducers") could not therefore be construed to represent the total force on the spoiler. Since the

validity of the sound pressure data measured in the free field outside the pipe held only for frequencies above 250 Hz, the frequency range within which sound and force data could be compared is, in fact, restricted to the range bordered at the low end by the "cut-off frequency" of the anechoic chamber and by the first bending mode frequency of the spoiler at the high end. The range of comparison can, however, be "extended" by using force data obtained at lower flow speed and by assuming a universal normalized Strouhal frequency spectrum shape. Fluctuating forces scale with the dynamic pressure $1/2\ \rho U^2$, and hence one expects the force levels $20\ \log F/F_0$ to scale with the fourth power of a typical velocity. During the whole program we have normalized all force data by plotting $20\ \log\ (F/F_0) - 40\ \log\ (U/U_0)$ versus a normalized frequency $S = (f \cdot D/U)$. Here F is the fluctuating force in dynes, F_0 a reference force equal to 1 dyne, U is either the jet exhaust velocity or the in-pipe flow velocity in cm/sec and U_0 is a reference velocity equal to 1 cm/sec, f is the center frequency in Hz of a third-octave band and D is a length dimension in cm related to a typical dimension of the spoiler. Normalized plots of force spectra are presented in Chap. V.

2. Sound data

Sound pressure data were always recorded at a fixed distance of 3 ft (radius of the microphone traverse), usually at 90° and 45° from the downstream axis of the jet, to obtain directivity information.

Sound data were also normalized versus the same nondimensional frequency $S = f \cdot D/U$ to allow direct comparison with normalized force data. Sound pressure levels were normalized with the sixth-power of a typical velocity, since dipole radiation is characterized by a sixth power of velocity dependence.

Sound data were, therefore, plotted in terms of $20 \log p/p_0 - 60 \log U/U_0$ versus the Strouhal frequency $S = f \cdot D/U$.

Here p is the sound pressure in dynes/cm^2 and p_0 is the reference sound pressure of 2×10^{-4} dynes/cm^2. Typical normalized plots of sound spectra will appear in Chap. V.

IV. THEORETICAL CONSIDERATIONS OF THE AERODYNAMIC NOISE RADIATED BY FLOW SPOILERS IMMERSED IN A PIPE.

A. Introduction

The classic work in the theory of aerodynamic noise radiated by flow separation from a spoiler is that of Curle [Ref. 3]. He demonstrated that for a small flow spoiler in free space the radiated sound was dipole in character and was proportional to the time rate of change of the unsteady forces acting upon the object. Small, in this context, means small in comparison to the wavelength of sound at the frequency in question – insuring that the flow field in the neighborhood of the spoiler may be treated as incompressible. The coupling between an incompressible inner region and resulting acoustic radiation to an outer region is one of the key ideas in this discussion. This separation gives great insight into the mechanism of sound radiated by flow spoilers immersed in a pipe.

The theoretical expression for sound radiated by a fluctuating force on a stationary object in free space is

$$\Pi(\omega) = \frac{\omega^2 F^2}{12\pi\rho c^3} \qquad \text{(IV-1)}$$

For sea level standard conditions this is:

$$\Pi(f) = f^2F^2 \times 2.2 \cdot 10^{-11} \qquad \text{(IV-2)}$$

where F is the force in dynes, f is the frequency in Hz, and Π is the power in dyne-cm/sec.

If we wish to consider sound radiated by this same flow spoiler immersed in a pipe, we must investigate how the duct

walls affect the sound power. In this case, the flow spoiler is still small compared to a wavelength, but, at low frequencies, the pipe diameter is also small, compared to a wavelength. Thus, the incompressible inner region of the flow is modified and the resulting acoustic radiation changed.

If the flow spoiler is not too large, the fluctuating forces on it due to flow separation will be unaffected by the presence of the duct. In any case, the fluctuating forces on the flow spoilers can be measured and we are therefore in a direct position to assess the effect of the duct upon the sound power radiation by a known fluctuating force.

In a recent paper, Davies and Ffowcs Williams [Ref. 4] noted that, when a sound source is confined in an infinitely long duct of diameter small in comparison to a wavelength, the character of the problem changes from a three-dimensional to a one-dimensional situation. The acoustic impedance of the surroundings changes and thus the amount of sound power radiated by the source changes. More important from an aerodynamic noise viewpoint, the dependence of the power upon the frequency of the source changes by a factor f^2.

In aerodynamic noise theory, the characteristic frequency of an aerodynamic source is assumed to increase in proportion to flow velocity. Therefore, at low frequencies, the familiar monopole, dipole, and quadrupole sources, when confined in a small diameter duct, would have sound power outputs increasing as U^2, U^4 and U^6, rather than the familiar U^4, U^6, and U^8 characteristics of these sources in an infinite fluid. As the frequency of the sound source increases, the sound power radiated by the source in the duct approaches the freefield case – as would be expected. We must now inquire whether the enhanced efficiency and increased sound power at low frequency will be measured in the free space beyond the end of the pipe.

Our earlier experiments on sound radiated into free space at the end of a pipe by fluctuating forces on flow spoilers [Ref. 2] indicated that the acoustical radiation was as if these sources were in an infinite fluid. Three remarks on these experiments are in order:

(1) While we did not measure the fluctuating forces on the flow spoilers, we did assume that they were proportional to the steady state drag. The overall power from a wide variety of flow spoilers was found to be proportional to the cube of the static pressure drop across the spoiler $(\Delta p_0)^3$ and to the sixth power of the flow velocity. Thus, a dipole noise source is indicated.

(2) When the normalized spectrum shapes for a given flow spoiler are collapsed using the Strouhal frequency, $S=f\ D/U$, there is good agreement at low frequencies, but some scatter at high frequencies.

(3) The effect of source confinement on the velocity dependence of the power radiated by a source at low frequencies was not found.

Obviously, a more complete examination is indicated. Since, in the present experiments, we have measured the spectrum of the fluctuating lift and drag forces on the flow spoilers under all test conditions for which free field sound measurements are available, we have the detailed information necessary to consider the problem directly. In the analysis following, we shall see the following results:

(1) For a monopole source confined in a narrow duct, the sound generated inside the duct is greater and differs by a factor f^2 from the sound generated by this same source in free space.

(2) When end reflections at the open end of the pipe are considered, an f^2 factor is introduced in the numerator that returns the dependence on frequency to the freefield case. The sound radiated into the free space is a small part of the total sound generated inside the duct.

(3) The monopole source radiates into the free space surrounding the end of the pipe, the same amount of power that it would generate in free space. At low frequencies, the directivity pattern from the end of the pipe is spherical.

(4) For a dipole source, effects similar to those in (1) and (2), are noted. There is an increase in efficiency with a factor f^2 due to the confinement of the dipole source. End reflections remove the dependence on f^2, restoring the U^6 behavior of the aerodynamic dipole.

(5) At low frequencies, there is a net increase in sound power radiated into the freefield by a factor of 3 above the power radiated by the dipole in free space. In addition, at low frequencies the radiation from the end of the pipe is, of course, spherical. At low frequencies, only the fluctuating drag forces contribute to the sound; at high frequencies, confinement in the duct does not affect the power radiated by the source.

The increase by a factor of 3 in sound power radiated into free space by a confined aerodynamic dipole source was an unexpected result. The agreement with the low frequency data from the experiment, however, is quite good. We can also detect in the experimental results the crossover from low to high frequency behavior, although the high frequency limit was not reached in the experiment since the pipe diameter was only 2 inches.

It would be inconsistent to consider the effect of source enclosure upon the sound power without considering end reflections. Both of these effects occur when the diameter of the pipe is small compared to a wavelength. In this case, both near the source, and at the end of the pipe, the incompressible part of the flow field dominates. Geometrical modification of the incompressible field affects the resulting sound radiation.

The problem of the effect of the pipe upon the sound power radiated into free space beyond the end of the pipe will be considered in the following steps, both for the monopole and dipole sources: First, we will consider the effect of enclosure in an infinite pipe. This will establish the simple model we will use for these sources. Second, we will consider the sound radiated to the freefield by a source enclosed in a semi-infinite pipe. We will also discuss, at the end of this Section, the qualitative behavior as the source location moves down the pipe into the freefield.

Our analysis will ignore the effect of mean flow upon the sound power generated and upon the mechanics of end reflections at the free end of the pipe. This question will be treated in the future.

In the experiments, flow velocities up to M=0.4 were achieved. The data show agreement with the theory and indicate no systematic trend with flow velocity.

B. The Effect of Enclosure Upon the Sources

The velocity potential at a point on the x-axis due to the monopole configuration shown in Fig. IV-1a is given by

$$\phi(x,R,t) = - \frac{\tilde{S}}{4\pi r} \cdot e^{i(\omega t - kr)} \quad , \qquad \text{(IV-3)}$$

where $r=\sqrt{R^2+x^2}$, and $\tilde{S}$ is the source strength. The power radiated into free space by this source is

$$\Pi = \frac{\rho\omega^2\tilde{S}^2}{4\pi c} \quad . \qquad \text{(IV-4)}$$

To account for enclosure in an infinite duct, one could place an infinite number of sources at suitable image points in the y,z plane as in Fig. IV-1b. For the case where the size of the duct is large in comparison to a wavelength, we are justified in placing a uniform density of sources of strength S' per unit area as in Fig. IV-1c and integrating over the y,z plane. This allows a clearer demonstration of the transition from three dimensions to one. The velocity potential for the configuration sketched in c is, then,

$$\phi(x,t) = - \frac{S'}{2} \int_0^\infty \frac{e^{i(\omega t - k\sqrt{x^2+R^2})}}{\sqrt{x^2+R^2}} \cdot RdR \quad . \qquad \text{(IV-5)}$$

Correct interpretation of this weakly convergent integral gives:

$$\phi(x,t) = i \frac{S'}{2k} e^{i(\omega t - Rx)} \quad . \qquad \text{(IV-6)}$$

This is, of course, the potential for a one-dimensional acoustic traveling wave from a piston oscillating with velocity $(S'/2)e^{i\omega t}$. The remaining half of the volume flow creates a one-dimensional acoustic wave traveling out along the negative x-axis.

For a source of strength $\tilde{S}$ enclosed in a duct of area A, $S'=(\tilde{S}/A)$. The power output from this source is then

$$\Pi_{duct} = \frac{\rho c \tilde{S}^2}{2A} . \qquad \text{(IV-7)}$$

We can obtain this same conclusion by considering the model sketched in Fig. IV-1d. Treating the flow in a small region about the source bounded by two imaginary surfaces upon which u is constant as incompressible, we see that the particle velocity upon these surfaces is $u=(\tilde{S}/2A)$. The sound power radiated into the duct by these pistons is

$$\Pi = 2\rho c \left(\frac{\tilde{S}}{2A}\right)^2 A \qquad \text{(IV-8)}$$

which is the same as Eq. (IV-7). Comparing Eqs. (IV-4) and (IV-8) shows the effect of the confinement upon the power. The power radiated into the duct depends upon the size of the duct. The latter formula is an approximation valid for low frequencies such that $\lambda >> \sqrt{A}$.

Similar conclusions can be drawn for the higher order acoustic sources. The vertical dipole, or fluctuating lift force, to this order would not radiate at all while the axial dipole or fluctuating drag force becomes, under confinement, a one-dimensional piston with a pressure of

$$p = \frac{F}{2A} \cdot \qquad \text{(IV-9)}$$

acting upon each face as sketched in Fig. IV-1e.

The power radiated by a dipole in free space is

$$\Pi_{free} = \frac{\omega^2 F^2}{12\pi\rho c^3} , \qquad \text{(IV-10)}$$

where F is the magnitude of the fluctuating force.

The power radiated into an infinite duct by this fluctuating force is

$$\Pi_{duct} = \frac{2}{\rho c} \left(\frac{F}{2A}\right)^2 A \cdot \qquad \text{(IV-11)}$$

The dependence of sound power upon frequency changes by a factor ω^2 for an "axial" dipole immersed in a pipe. In addition, the power depends not only upon the force, but upon the cross-sectional area of the duct.

Following the same argument, lateral quadrupole sources would be expected to radiate no sound while the longitudinal quadrupoles would display a change in the dependence of their power upon frequency. (This may prove useful in separating these two types of quadrupoles in jet noise experiments.)

These arguments pertain to the power delivered to the duct by these acoustic sources. The power which passes across the exit plane of the duct into the free environment in which we make our measurements will be further influenced by the impedance mismatch presented by the duct exit transition. This is called the end reflection effect.

C. End Reflections

Physically, reflection of sound back into a pipe of small diameter occurs because the free space surrounding the end cannot accept the large pressures associated with the one-dimensional acoustic waves in the duct. The boundary condition at a free end is approximately that of zero pressure. In this case, the sound would be completely reflected back into the pipe. In reality, however, the fluid at the end of the pipe can accept a small unsteady pressure proportional to the inertia or apparent mass of the fluid surrounding the end of the pipe. If there is no mean flow, we can idealize this end by considering a small piston oscillating with twice the particle velocity in the incident acoustic wave, the factor two coming from the almost perfect reflection at the pipe end. This is sketched in Fig. IV-2a.

The power radiated into free space by a piston, of area A and velocity 2u, enclosed in a baffle, is

$$\Pi_t = \frac{\rho c k^2 A^2}{2\pi} (2u)^2 \ . \qquad \text{(IV-12)}$$

However, our pipe end radiates into a solid angle of 4π rather than 2π. As is shown in [Ref. 5], this reduces by a factor of 2 the amount of power which the free space will accept. The power radiated at the pipe end is then

$$\Pi_t = \frac{\rho c k^2 A^2}{4\pi} (2u)^2 \ . \qquad \text{(IV-13)}$$

The transmission coefficient for the unbaffled end of a pipe at low frequencies is then

$$T = \frac{\Pi_t}{\Pi_i} = \frac{k^2 A}{\pi} \quad . \tag{IV-14}$$

Applying this result to the power generated in an infinite duct for a dipole and monopole source gives the expressions for the energy radiated to free space by these sources

$$\Pi_{monopole} = \left(\frac{\Pi_{monopole\ duct}}{2} \right) T = \frac{\rho \omega^2 \tilde{S}'^2}{4\pi c} \tag{IV-15}$$

and

$$\Pi_{dipole} = \left(\frac{\Pi_{dipole\ duct}}{2} \right) T = \frac{F^2 \omega^2}{\rho c^3 4\pi} \quad . \tag{IV-16}$$

For the monopole, the power radiated is the same; for the dipole, it is greater by a factor of three than the same source in free space. The directivity of the radiation of sound from the end of the pipe is spherical for both sources.

The simple considerations given above, although physically appealing, are not strictly valid, since disturbances do not die out with distance in one-dimensional acoustic waves. Therefore, the pipe end will affect the impedance seen by the source and thus give the amount of power generated by the source. It will turn out, after analysis of this problem, that Eqs. (IV-15) and (IV-16) are still valid and, although the source output is affected, that the sound is radiated upstream to infinity in the pipe.

D. Analysis of a Monopole and Dipole Near the End of a Duct.

The configuration of the monopole and dipole sources in the duct are sketched in Fig. IV-2b and c. The diameter is small in comparison with a wavelength, while the length ℓ is at least of the order of a wavelength. This latter restriction allows us to consider separately the region around the source and the free end coupled by a region that can only propagate plane acoustic waves.

Referring to the sketch in Fig. IV-2b for the monopole source, we make the following considerations:

The region surrounding the source may be treated as incompressible; the effect of the source is equivalent to two imaginary pistons of specified velocity essentially located at x=0. A massless piston of area A radiating into the free space may replace the free end of the pipe. The pressure is continuous across x=0, the source region. For $\ell>x>0$, we have both an upstream and downstream traveling wave; for $x<0$, we have only an upstream wave. These considerations are expressed below in the expressions and boundary conditions for the velocity potential.

$$0<x<\ell, \phi^+(x,t) = \phi_1 e^{i(kx-\omega t)} + \phi_2 e^{-i(kx+\omega t)}$$

$$-\infty<x<0, \phi^-(x,t) = \phi_3 e^{-i(kx+\omega t)} \qquad \text{(IV-17)}$$

$$P(\ell) = -\rho \frac{\partial \phi^+}{\partial t}(\ell) = 0$$

$$\frac{\partial \phi^+}{\partial x} - \frac{\partial \phi^-}{\partial x} = \frac{\tilde{S}}{A} \text{ at } x = 0$$

$$P^+(0) = P^-(0)$$

the solution to these equations is

$$\phi^{+}(x,t) = \frac{\tilde{S}}{2ikA} e^{-i\omega t}\left[e^{ikx} - e^{ik(2\ell-x)}\right], \qquad \text{(IV-18)}$$

$$\phi^{-}(x,t) = \frac{\tilde{S}}{2ikA} e^{-i\omega t}\left[1-e^{ik2\ell}\right] e^{-ikx} \ . \qquad \text{(IV-19)}$$

The solution is affected by ℓ, the distance of the source from the free end. However, the power measured in free space depends only on the particle velocity at the free end, $u(\ell)$. This is

$$u(\ell,t) = \frac{\tilde{S}}{A} e^{ik\ell} \ . \qquad \text{(IV-20)}$$

The effect of ℓ is to contribute only a phase shift.

From Eq. (IV-13), the power radiated into free space will be

$$\Pi_t = \frac{\rho\omega^2}{4\pi c} \cdot \tilde{S}^2 \ . \qquad \text{(IV-21)}$$

This is the same as the expression for the power radiated by this source in free space. The remaining power travels upstream to infinity in the model. For the case of a monopole in a finite duct, resonances are possible and the power is a very sensitive function of the frequency and the length ℓ. The experimental situation appears to be more closely approximated by the semi-infinite pipe, since there is a large upstream muffler in the duct.

A similar analysis for the dipole will now be done. The set of equations for the dipole source are similar to those of (IV-17), the differences being that we now require conservation of mass across the dipole, and now allow the pressure to be discontinuous by -F/A as sketched in Fig. IV-2c, where F is the

fluctuating force applied to the fluid by the flow spoiler.

$$\frac{\partial \phi^+}{\partial x}(0) - \frac{\partial \phi^-}{\partial x}(0) = 0 \ ,$$

$$P^+(0) - P^-(0) = \left[-\rho \frac{\partial \phi^+}{\partial t}(0)\right] - \left[-\rho \frac{\partial \phi^-}{\partial t}(0)\right] = \frac{F}{A} \ . \qquad \text{(IV-22)}$$

The solution to the set in (IV-17) with the appropriate conditions for a dipole is

$$\phi^+(x,t) = -\frac{iF}{2A\rho\omega}\left[e^{ikx} - e^{(2\ell - x)}\right] e^{-i\omega t} \ ,$$

$$\phi^-(x,t) = \frac{iF}{2A\rho\omega}\left[1 + e^{ik2\ell}\right] e^{-i(kx+\omega t)} \ . \qquad \text{(IV-23)}$$

The particle velocity at the end of the pipe is

$$u(\ell,t) = \frac{\partial \phi^+}{\partial x}(\ell,t) = \frac{F}{\rho c S} e^{ik\ell} e^{-i\omega t} \ . \qquad \text{(IV-24)}$$

The power radiated to free space by the hypothetical piston in the free end is

$$\Pi_t = \frac{\omega^2 F^2}{4\pi\rho c^3} \ . \qquad \text{(IV-25)}$$

This is considered the most important result in the analysis. It indicates that a confined aerodynamic dipole will radiate sound proportional to U^6 at both low and high frequencies but will have an increased power output by a factor of 3 at low frequencies. The details of the crossover to the high frequency case would require a complicated mathematical solution and would not give much additional information about the effect.

In the experimental situation, we can expect the constant of proportionality between Π and F^2f^2 to shift to the freefield value as the directivity changes from spherical to the more complex pattern, characteristic of the high frequency situation.

The preceding discussion is valid for sources located in the pipe a distance on the order of a wavelength. As this source is moved out into the freefield, a transition to the freefield case would occur (Fig. IV-3). We indicate a transition region near the end of the pipe where the constant of proportionality changes from its value in the pipe to that in freefield. Note the different behavior of the constant for lift as compared with that for drag. In the pipe, the lift forces do not radiate. In some of our experiments, the flow spoilers were located near the end of the pipe. Agreement with the expected trend was found.

V. EXPERIMENTAL RESULTS AND DISCUSSION

A. Introduction

The experiments on the sound radiated by flow spoilers were basically of two types:

(1) The confined environment experiments for the strip spoiler or cylindrical spoiler within the pipe, where sound radiation is due to fluctuating drag forces.

(2) The freefield experiments for the airfoil in a free jet at zero angle of attack, where sound radiation is due to fluctuating lift forces that exceed the fluctuating drag forces.

For the flow spoilers confined within the pipe, the simple considerations of Chap. IV apply for frequencies below the cutoff frequency of the 2"-diameter pipe (about 3800 Hz). In the experimental situation, this crossover to a more complex behavior might be seen as the directivity changes from spherical at low frequencies to a more directive pattern at high frequencies. Figure V-1, which shows sound data for a strip spoiler located 6" upstream of the end of the pipe, is typical in this regard. Up to about 3000 Hz, most of the sound data is within 2 dB of spherical. However, the fluctuating force data for this flow spoiler is also limited to the region well below 4500 Hz, which is the frequency of the fundamental bending mode. This effect can be seen, for example, in Fig. V-3, where fluctuating drag force data is presented: The resonance of the spoiler-transducer system shows up clearly. Similar effects for all the flow spoilers restrict our attention to the frequency range for which the theoretical consideration of Chap. IV apply for the confined flow spoilers.

We will discuss the experimental results of the confined experiments in Sec. B; the freefield experiment will be discussed in Sec. C.

B. Experimental Results for Flow Spoilers in a Confined Environment

1. Data presentation

We performed a series of experiments to determine the correlation between sound radiation and fluctuating forces for a flow spoiler within a pipe. The position of the flow spoiler was varied from zero to 9 pipe diameters upstream of the pipe exit plane and a cylindrical as well as a strip spoiler was used. Test results are summarized below:

Test 205* - Strip spoiler at pipe exit plane — Fig. V-9 to Fig. V-13.

Test 207 - Strip spoiler 3 pipe diameters upstream of the exit plane — Fig. V-1 to Fig. V-8.

Test 209 - Strip spoiler 9 pipe diameters upstream of the pipe exit plane — Fig. V-13 to Fig. V-15.

Test 210 - Cylindrical spoiler 9 pipe diameters upstream of pipe exit plane — Fig. V-16 to Fig. V-18.

The sound data for these experiments appear in Figs. V-9 (Test 205), V-1 (Test 207), V-13 (Test 209) and V-16 (Test 210). For most of the tests, the data below 3000 Hz show only slight directivity effects except where the jet noise dominates. We

*Test numbers mentioned in the report serve to identify particular tests.

can thus use the assumption of spherical directivity to calculate sound power. For greater accuracy, the actual directivity could be considered.

If we consider the exit plane of the jet-pipe exist to be the location of a spherically radiating sound source, then we can determine the sound power Π_1 from that source by

$$\Pi_1 = 4\pi r^2 \frac{p^2}{\rho c} , \qquad (V-1)$$

where p is the sound pressure at a distance r from the source. The sound power, radiated from the pipe exit, of course, was generated at the spoiler within the pipe as a result of the fluctuating forces acting on the spoiler.

Knowing the fluctuating forces that act on a spoiler, we can determine from Eq. (IV-1) the sound power Π_2 that it would radiate under freefield environmental conditions:

$$\Pi_2(\omega) = \frac{\omega^2 F^2}{12\pi\rho c^3} = \frac{\pi f^2 F^2}{3\rho c^3} = 2.2 \times 10^{-11} f^2 F^2 [\text{ergs/sec}] . \qquad (V-2)$$

For

$\rho = 1.21 \cdot 10^{-3}$ dyn sec^2/cm^4,

$c = 3.4 \cdot 10^4$ cm/sec,

F in dynes, and

f in Hz.

The analysis presented in Chap. IV suggested an effective increase in the sound power radiation of an aerodynamic dipole source in a confined environment: the power output was predicted to increase by a factor of 3 at low frequencies.

The change in radiated sound power is exhibited by the power ratio $R \equiv \Pi_1/\Pi_2$.

$$R \equiv \frac{\Pi_1}{\Pi_2} = \frac{4\pi r^2 p^2/\rho c}{\pi f^2 F^2/3\rho c^3}$$

$$= 12\, r^2 c^2 \left[\frac{p(f,r)}{F(f)\cdot f}\right]^2 . \qquad \text{(V-3)}$$

This power ratio can thus be determined experimentally by independently measuring (a) the sound pressure p at a distance r from the pipe exit in frequency bands and (b) the fluctuating force F (lift or drag component, as the case may be) in frequency bands.

We will now describe a typical test procedure using data from one particular test (Test 207). The strip spoiler was located 6 in. upstream of the jet-pipe exit plane, facing the oncoming pipe flow with its broad side (1.27 cm). The test set-up corresponds to that shown in Fig. III-6.

In this test we took data for the following pipe flow velocities: 12.5, 21, 46 and 74 m/sec. Figure V-1 shows 1/3-octave band sound pressure level spectra measured at α=45° and α=90° for various flow velocities. Background noise levels in the chamber for the aircraft supercharger running at full speed, but with no air flow in the jet-pipe system, are also plotted in this figure.

For each flow velocity, the spectral levels are within 3 dB up to about 3000 Hz for the two measurement positions, indicating essentially spherical directivity up to this frequency. If we normalize the spectra using only data up to this frequency, we

arrive at Fig. V-2. Normalized sound pressure levels are plotted versus Strouhal frequencies, S=fD/U, with the spoiler width of 1.27 cm as pertinent length dimension D. U, of course, is the pipe flow velocity and f the center frequency of the relevant 1/3-octave band.

We have thus obtained a normalized sound pressure level spectrum utilizing only "spherical-radiation pressure data" over a wide non-dimensional frequency range from S=0.03 to about 5.

Figure V-3 shows the *drag* force 1/3-octave spectra. In this figure we have already summed the output of the two drag-force transducers to obtain the total drag force. The first bending mode frequency of the spoiler, f_{crit}=4500 Hz, appears clearly in each spectrum. Higher modes give the spectra an irregular shape above f_{crit}. If we normalize the spectra with the pipe-flow velocity and plot them again versus Strouhal frequencies (Fig. V-4), we note that the first bending mode frequency appears at a different Strouhal frequency, of course; however, it is now very easy to infer the true spectral shape by omitting the f_{crit}-bumps and by following a tangent curve that touches all spectra "from below". This procedure allows us to determine the shape of the normalized drag force spectrum in a Strouhal frequency range from 0.003 to above 1.

Figure V-5 presents the fluctuating *lift* force spectra for various flow velocities. Their shape differs grossly from that of the drag-force spectra in that they have a very pronounced peak whose frequency increases with increasing flow speed. This peak is probably a result of an aerodynamic process, such as a periodic vortex-shedding from the spoiler, which reveals itself in strong lift-force fluctuations at a particular (i.e., the vortex shedding) frequency. The spoiler's first bending mode

frequency at f=4500 Hz, also appears in each spectrum. If we normalize the lift-force spectra with the pipe-flow velocity, and plot the data against Strouhal frequencies, (Fig. V-6), then the strong peaks collapse at one dimensionless frequency, S=0.2 to 0.3. This, incidentally, is close to the typical dimensionless frequency, which describes the vortex-shedding from rigid objects, such as cylinders of diameter D.

It is interesting to note that the strong peaks in the lift-force spectra do not show up in the sound spectra. As discussed in Chap. IV, we realize that the lift-fluctuations (which are, of course, oriented at right angles to the pipe-axis within the confined environment of the pipe) do not radiate at frequencies below the cutoff frequency of the pipe. Clearly, for this situation, there is no point in trying to correlate fluctuating lift-force data from internally-located spoilers with sound data observed in the freefield outside the pipe. This is, however, not necessarily so for externally located spoilers.

In all experiments, where the spoiler was located in the pipe, we therefore correlated the sound data measured outside the pipe with the fluctuating-*drag* force data measured on the spoiler.

Figure V-7 shows the ranges of both the normalized lift-force and drag-force spectra on one plot to emphasize their different shapes. This ability to measure such grossly different spectra at the drag and at the lift transducers indicates how well the drag and the lift transducers were decoupled, as discussed in Chap. II.

Figure V-8 presents 3 normalized spectra. The top spectrum (A) shows the normalized acoustic data in individual curves, as presented in Fig. V-2; the ordinate of this spectrum is labeled

20 log p/p_0-60 log U/U_0. The middle spectrum (B) shows the normalized total drag force spectrum, again in individual curves, equal to the presentation in Fig. V-4; here the ordinate is labeled 20 log F_{Drag}/F_0 - 40 log U/U_0. The lowest spectrum (C) is the difference between the top and the middle spectra and gives the normalized "difference-spectrum" in terms of

$$20 \log p/p_0 - 20 \log F_{Drag}/F_0 - 20 \log U/U_0 \ ,$$

where

$$p_0 = 0.0002 \text{ dyne/cm}^2 \ , \quad F_0 = 1 \text{ dyne} \ , \quad U_0 = 1 \text{ cm/sec} \ ,$$

plotted against the nondimensional Strouhal frequency, fD/U, where D=1.27 cm=spoiler width. We have "subtracted" the corresponding individual curves of the "force-level spectrum" from the "sound-pressure-level spectrum." By this procedure, we decrease the data scatter that would be inherent if we subtracted the spectral *ranges*, rather than individual curves. We have drawn a straight, best-fit line through the data points presented in spectrum C. This line of slope 2 corresponds to a constant power ratio R. For our test set-up, the distance r from the microphone to the pipe exit was 91.5 cm. From Eq. V-3 we thus find a power ratio

$$R = 2.95.$$

This ratio is about a factor of 3 higher than Curle's freefield value, as predicted in the previous chapter.

Having outlined the procedure to determine the discussed power ratio, we will now present the experimental results for the various spoiler types and locations.

1.1 Strip-spoiler at pipe exit plane (Test 205)

Sound pressure level spectra for the strip spoiler located at the pipe-exit plane are presented in Fig. V-9 for various flow velocities from 12.5 to 95 m/sec. The directivity pattern is essentially spherical in the frequency range below approximately 5000 Hz.

Fluctuating drag force data are shown in Fig. V-10. The first bending mode resonance of the spoiler shows up clearly in all spectra. The lift force spectra (which we do not present) were typically 10 dB below the drag force spectra. However, in the lift force spectrum at a Strouhal frequency of about 0.3, there is a peak which reaches the drag force levels at this frequency. We associate this peak with some periodic vortex shedding from the spoiler. We mentioned this phenomenon already in Sec. 1 of this chapter for the strip spoiler immersed 6 in. back in the pipe, where the lift force spectra showed a similar peak at about the same Strouhal frequency. Again, this "lift-force peak" did not appear in the sound spectra, although the strip-spoiler is now located at the exit plane of the pipe. This could be due to the fact that lift and drag forces are equal at this Strouhal frequency; any discrete frequency phenomena would be buried in the dominating drag-force related noise.

When the drag force data is normalized, then the spectrum for U=70 m/sec is lower than the other data, which collapse quite satisfactorily. However, the corresponding spectrum is also low in the normalized sound pressure data, presented in the summary of the test results in Fig. V-12. Subtracting the corresponding individual curves in the normalized sound and drag data keeps the scatter reasonably small. A straight line of slope 2 through the data points shown in Fig. V-12c corresponds

to a power ratio of

$$R = 2.6 \ ,$$

which is slightly lower than the value of R, predicted for a deep immersion of the spoiler into the pipe.

1.2 Strip-spoiler 3 pipe diameters upstream of pipe exit plane (Test 207)

In Sec. 1 of this chapter, we used this test to illustrate a typical data processing procedure. (Figure V-8 shows the summary of the data for Test 207.) The data suggested a power ratio

$$R = 2.95$$

for the strip-spoiler 3 pipe diameters upstream of the pipe exit plane.

1.3 Strip-spoiler 9 pipe diameters upstream of pipe exit plane (Test 209)

Figure V-13 displays the sound pressure spectra for the strip spoiler 18 in. upstream of the pipe exit plane. It appears that, for the higher flow velocities, jet noise determines the directivity pattern, since the directivity peak moves towards smaller angles α. We did not use the high velocity data for further analysis. In Fig. V-14 we present fluctuating drag force spectra for two flow velocities.

The normalized summary representation in Fig. V-15 exhibits some scatter both for the normalized sound pressure spectrum (A) and for the normalized drag force spectrum (B). In the Strouhal range where sound and force data can be compared, however, the scatter of the data points presented in spectrum (C) is relatively small.

A best fit straight line through the data points suggests a power ratio

$$R = 2.5 \ .$$

1.4 Cylindrical-spoiler 9 pipe diameters upstream of pipe exit plane (Test 210)

The sound pressure level spectra for the cylindrical-spoiler, located 18 in. upstream of the pipe exit plane, are shown in Fig. V-16. Again we observe a relatively pronounced directivity of the radiation pattern for high flow velocities.

The fluctuating drag force spectra are shown in Fig. V-27. The cylinders first bending mode frequency (f_{crit}=4500 Hz) appears very pronounced in these spectra.

The lift forces experienced by the cylindrical spoiler were slightly higher than the drag forces, typically by 6 to 12 dB in the frequency range below the bending mode frequency. However, we again correlated the drag forces with the sound data. The usual summary representation of the test data is given in Fig. V-18. The data suggest a power ratio

$$R = 2.35 \ .$$

2. Discussion of results

The results of our experiments, on the correlation between fluctuating drag forces acting upon a flow spoiler confined in a small diameter pipe and the resulting acoustic radiation to the freefield surrounding the end of the pipe, agree with the theory discussed in Chap. IV. The effect of source location upon the power radiated by the spoiler was expected to follow the sketch in Fig. IV-3. The actual experimental points are indicated in

this sketch. We found qualitative agreement, although the power ratio does not asymptote to 3 for increasing immersion of the sound into the pipe. This may be due to scatter in the data since only 2 dB will give a 60% increase in power. Also the upstream acoustics of the pipe, which changes in area by a factor of 3, (Fig. III-3), could have some influence on the power radiated by the source to the freefield.

C. Experimental Results for a Flow Spoiler in Freefield Environment.

In order to check the "freefield prediction" of the fluctuating-force/sound relationship, we exposed the airfoil to a free-jet flow emerging from a 1 in. diameter converging nozzle.

In experiments where the directivity pattern showed dipole characteristics, we measured the sound pressure $\hat{p}$ at the directivity peak and calculated the sound power Π_1^* from

$$\Pi_1^* = \frac{4\pi r^2 \hat{p}^2(f,r)}{3\rho c} \quad . \tag{V-4}$$

Equation (V-4) gives the sound power radiated from an acoustic dipole source as a function of the sound pressure at the peak of the figure-eight directivity pattern.

In this case the power ratio becomes

$$R \equiv \frac{\Pi_1^*}{\Pi_2} = 3r^2c^2\left[\frac{\hat{p}(f,r)}{F(f)f}\right]^2 \quad . \tag{V-5}$$

The airfoil was oriented at zero-angle of incidence with respect to the jet-axis. The airfoil's leading edge was located

2.3 cm (almost one nozzle diameter) downstream of the nozzle exit plane (Fig. III-5). The airfoil stretches across the potential core and the annular shear layer surrounding the jet.

1. Flow properties of the free jet

The velocity profile, the turbulence profile, and the turbulence spectra at various radial distances from the jet-axis were measured one nozzle diameter (equal to 1 in.) downstream of the nozzle exit plane.

Figure V-19 shows both the non-dimensional mean flow velocity and the turbulence intensities in percent of the mean flow velocity, plotted versus the radial distance from the jet axis. The overall turbulence intensities at the location of maximum shear reach almost 9% of the mean flow velocity in the core. In Fig. V-20 we have plotted turbulence intensities in 1/3-octave bands for some radial measurement locations. From these data we can determine the non-dimensional frequency, S=fD/U, at which maximum turbulence levels in the shear layer occur. If we take D equal to the nozzle exit diameter, then S_{max}=0.35 to 0.7. At this frequency we should expect maximum turbulence levels of about 2% in the peak 1/3-octave band.

2. Airfoil in "freefield environment" (Test 202)

The fluctuating lift force spectra, measured on the airfoil at zero-angle of flow attack, are presented in Fig. V-21. We do not present the drag force spectra; they had a similar shape, but were typically 10 dB below the lift force data. The similarity in spectral shape for the lift and the drag force data is not surprising, since the turbulence at the jet edge is responsible for both the unsteady lift and the drag forces; hence the equal

spectral shape. For an airfoil in a gust, however, the unsteady lift is larger than the unsteady drag. Due to the low bending frequency of the airfoil of about 1500 Hz, the fluctuating force data is valid only in the low frequency range.

Directivity studies of the sound radiated from the airfoil indicated that an energy maximum occurred at an angle of about 90° to the jet axis – the direction of the fluctuating lift. The fluctuating lift force data were used for correlation with the sound pressure levels measured at the 90°-point on our microphone trace.

Figure V-22 shows the sound pressure level spectra measured at α=90°; but in this figure we have also incorporated the undisturbed free-jet data to indicate where airfoil-generated noise dominates the spectrum. As one expects, the jet-noise increases more rapidly (i.e., typically with the eighth-power of velocity) than the airfoil-generated noise (which increases with a sixth-power of velocity dependence). At the high jet exit-velocities, which are close to sonic, most of the spectrum is due to the pure jet noise. At the frequency where the two spectra differ by 3 dB, we lowered the upper spectrum to let it intersect with the lower spectrum to infer the true spectral shape of the airfoil-generated noise. Due to the background noise of the free jet alone, good acoustic data for the sound radiated by the fluctuating lift was obtained only for high frequencies.

In Fig. V-23 we present the summary representation, i.e., the normalized sound pressure level spectrum (A), the normalized lift force spectrum (B), and the difference spectrum (C). Due to the very low bending mode frequency of the airfoil, the range of overlap of normalized sound and lift force data is extremely narrow. Only in the Strouhal frequency range of 0.2 to 0.3 is direct comparison possible. We have drawn a straight line of slope 2 through

the data points to infer the power ratio for this test. In determining R, we have used Eq. (V-4) to calculate the sound power radiated from the airfoil under its freefield conditions. The data points, presented in Fig. V-23, suggest a power ratio of only

$$R = 0.138 \ .$$

This data point is also shown in the sketch presented in Fig. IV-3. The power ratio seems to be rather low — although one certainly should expect a decrease when the ratio is compared to the freefield value for the spoiler location in the transition region. We presently have no explanation for such a drastic decrease in the power ratio.

D. Experiments of Supplementary Nature

1. Influence of upstream turbulence

Fully developed pipe flow is known to have typical overall turbulence intensities of 4 to 6% of the mean flow. To study the influence that turbulence in the oncoming flow (which impinges on the flow spoiler) has on the fluctuating forces and on the resulting noise generation, we attempted to change the pipe flow turbulence.

We tried insertion of (a) coarse grids, consisting of two crisscross layers of 1/8-in. or 1/4-in. tubing, and (b) very fine silk screens, supported by a mesh wire screen. The insertion of the coarse grids increased the turbulence levels only very slightly above the levels of fully developed pipe flow. And, in addition, the grids themselves act as flow spoilers that efficiently generated sound. Insertion of the actual flow spoilers (e.g., the strip-spoiler) at some small downstream distance from the grids did not increase the noise levels observed outside the

tube, so it was impossible to obtain useful data. Insertion of the fine silk screens however, reduced the turbulence levels quite markedly without generating additional noise in the frequency range of interest. The insertion of the strip-spoiler substantially increased the noise radiation from the system, thus allowing correlation of the spoiler-generated noise with fluctuating forces.

In Fig. V-24 we present the overall turbulence profiles, measured (a) 6 in. upstream of the pipe exit for fully developed pipe turbulence and (b) at the same location, but with the silk screen 2 in. upstream. The turbulence intensities in the center region of the pipe are approximately 5% for fully-developed pipe flow and approximately 1/2% with the silk screen insert. Turbulence spectra also measured were of broad band character.

In Fig. V-25 we show the summary representation of the test data for the strip spoiler located 2 in. downstream of the silk screen inserts and 9 in. upstream of the pipe exit plane (Test 188). Normalized sound pressure data can only be presented in a small Strouhal frequency range, since directivity effects did not allow the determination of the true shape of the spectrum above a Strouhal frequency of 0.5. Therefore we could evaluate the power ratio only for a rather limited frequency range. R was found to be 2.9.

Data from Test 188 can be compared with those test data for which the strip spoiler was located slightly further (6 in.) downstream, but exposed to fully turbulent pipe flow. (Test 207) Data are shown in Fig. V-8.

A comparison of the two tests indicates that the reduction in turbulence level in the oncoming flow lowers the drag forces that a flow spoiler experiences for a given flow speed. This

decrease in drag force is accompanied by a decrease in sound generation. This double reduction finally leads to the same power ratio as was observed for the strip spoiler in fully developed turbulent pipe flow.

2. Relationship of steady-state drag force and overall fluctuating drag force

One of the key assumptions of the earlier study [Ref. 2] had been the direct proportionality of the overall fluctuating forces and the steady-state drag force experienced by a flow spoiler in a pipe. Since we were able to measure fluctuating forces on each flow spoiler directly, we checked the relationship between steady-state and fluctuating forces.

Using the data from Test 207, where the strip-spoiler was immersed into the pipe 6 in. upstream from the pipe exit, we calculated the steady-state drag force $\overline{F}_{Drag}$ for a number of static pressure drops across the spoiler and compared it with the overall fluctuating drag force $\tilde{F}_{Drag}$ at the same static pressure drop. The ratio of the fluctuating overall and the steady-state drag force $(\tilde{F}/\overline{F})_{Drag}$ is plotted versus the static pressure drop in Fig. V-26. The ratio was indeed found to be constant and approximately equal to 2.3×10^{-3}.

VI. SUMMARY AND CONCLUSIONS

Within the present study, we examined the relationship of the fluctuating forces on rigid flow spoilers of various cross-sectional areas within an acoustically hard-walled pipe to the sound transmitted out of the pipe into the freefield. The result of the study is that pipe-immersed flow spoilers radiate sound due to the drag component of the fluctuating forces acting on the spoiler. Due to a cancellation effect from the nearby pipe walls, fluctuating lift forces do not contribute to the sound radiation from pipe-immersed spoilers.

It was shown on a theoretical basis that the efficiency of the sound power radiation from dipole-sources within a hard-walled pipe ("confined environment") increases by a frequency-squared-term which changes the sound-power/flow-velocity dependence to that of a quadrupole dependence, i.e., to an eighth-power law dependence. However, the effect of end reflection introduces an inverse-frequency squared term that restores the original sixth-power of velocity dependence of the dipole source power radiation.

In addition – and this is perhaps the most important result of the study – a net increase of the radiated sound power from dipole sources within a confined environment by a factor of 3 was predicted and was observed in the experiments.

In developing the theory for dipole sources in a confined environment, we extended Curle's well-known freefield expressions to take account of the effect (a) of the confinement, represented by the hard-walled pipe, and (b) of pipe end reflection.

For the experiment we developed a system of force transducers that allowed independent measurement of the drag and lift component of the fluctuating forces on the flow spoilers. The experimental

restrictions, imposed by the first bending mode frequency of the flow spoilers, were overcome by normalizing both the force and the sound data with a typical flow velocity. Thus, the possible range of correlation of force and sound data could effectively be extended.

In one experiment we studied a flow spoiler under simulated freefield conditions to check Curle's freefield expressions and found that the observed sound power radiation from fluctuating lift forces on this spoiler was lower than predicted by Curle. This decrease in sound power was ascribed to the influence of the nearby pipe exit, since the spoiler was, in fact, located in a transition region between the confined environment of the pipe and the true freefield. The result thus agreed qualitatively with the predictions developed in the present study.

Supplementary experiments served to round off our understanding of the phenomena associated with pipe-immersed flow spoilers. We found that changes in the degree of impinging flow turbulence directly changed the experienced fluctuating forces. However, changes in the degree of turbulence of the oncoming flow did not affect the force/sound relationship.

We also substantiated the direct proportionality of the overall fluctuating drag force and the steady-state drag force. This proportionality was a key assumption in the earlier study described in Ref. 2.

APPENDIX A: THE INFLUENCE OF PIPE ENCLOSURE — AN EXPERIMENT

In earlier sections of this report we discussed the influence of enclosing aerodynamic sources within the confines of the jet pipe. Two influences were identified: the influence of the hard wall environment on the intensity and frequency dependence of the source; and the frequency dependent transmissibility of the exist plane that limits the extent of noise radiation from the interior pipe environment to the exterior environment. We postulated that, as far as the frequency dependent influences are concerned, the effects of enclosure and end reflection are very nearly self-canceling.

Here, we present and discuss the results of an experiment in which, on a simple acoustic basis, we tried to obtain some verification of our theoretical findings. The experiment consisted of the following steps:

a. We carefully measured the power radiation from a high impedance acoustic monopole, having a characteristic diameter of about 1/4" and located in a freefield environment, as a function of frequency.

b. We then located this source in an (effectively) infinitely long pipe, having an internal diameter of 4", and measured the total power delivered to the pipe.

c. The pipe was truncated and the power transmitted through the exit plane of the pipe into a freefield environment was determined.

In the latter part of the experiment, two different locations of the source relative to the exit plane were used. In one case,

the source was deeply immersed in the pipe; in the other case, it was only shallowly immersed.

A. The Source

Since it was desirable that the acoustic source be physically small, the experimentation was limited to the simple monopole source.

The source was constructed by driving the air column in a 1/4"-diameter hollow pipe with a horn driving unit. So that variations of the external acoustic load would not influence the volume velocity at the exit of the source tube, the source had to have a relatively high internal impedance.

With this in mind, we selected two source design configurations (Fig. A-1). Both sources were driven with a JBL-375 horn speaker.

In the first configuration (Source #1), to control standing waves in the 48" tube and also to provide sufficiently high source impedance, strands of yarn were inserted into the exit plane of the tube as shown.

In the second configuration (Source #2), the length of tube was only 12". Tube termination in this case consisted simply of a 1/16"-thick plug of porous metal.

The freefield output of these sources for identical electrical inputs of third-octave bands of noise is illustrated in Fig. A-2. The high wall viscous losses of Source #1 have a very significant influence on the high frequency performance of this source.

B. Measurement System

Figure A-3 shows a schematic of the measurement system. To provide a good signal-to-noise ratio in these measurements, the source driver was supplied with third octave bands of noise. Third octave band filtering was also used in the acoustic measurement system. The input current to the driver was kept constant for each third octave band, for each source configuration, and for each experimental set-up.

The frequency range of measurement was 200 to 8000 Hz.

C. Freefield Environment

The freefield source data of Fig. A-2 were obtained with the source located in an anechoic chamber. For both source configurations, over the entire measurement frequency range, the directivity was closely spherical. Thus, the computation of source power involved two or three measurement locations and a simple area correction factor.

D. Enclosure in Infinite Pipe

For this experiment, the 1/4" diameter source penetrated the wall of a thick walled, 4" diameter steel pipe. The pipe was 16' long and the source was located midway between the ends. Both ends of the pipe were terminated with fiberglass "wedges" so that, as viewed by the source, the enclosing pipe seemed infinitely long. The effectiveness of the end treatments was checked by microphone probe and found to be satisfactory over the entire measurement frequency range.

The acoustic power delivered to the pipe was measured by sampling the sound pressure field in the pipe some 3 ft from the source for a number of different radial positions of the source and microphone. Power was calculated using the average measured sound pressure level at each third octave band setting and assuming plane wave propagation at all frequencies. We further assumed equal division of power between the two propagation paths available to the source. The result of this calculation is denoted the power delivered to the pipe (PWL_p).

In Fig. A-4 we present the difference between the power delivered to the infinite pipe (PWL_p) and the freefield power (PWL_f) as given in Fig. A-2. Data are presented for each of the source configurations.

E. Effect of Pipe Truncation

In the final experiment, we removed the acoustic termination at one end of the 4" diameter pipe and inserted this end into the anechoic chamber. The radiation field from the untreated end of the pipe was then scanned and estimates made of the sound power radiated through it. For the primary experiment, the distance between the source and the end plane was 8 ft (about 25 pipe diameters). To check the possible influence of shallow source immersion within the pipe, the source was later moved to a position 12 in. from the untreated end (corresponding to immersion of only 3 pipe diameters).

In scanning the acoustic radiation from the untreated pipe end, we found that even at high frequencies the directivity function was fairly smooth. Sound pressure levels were generally measured at four or five different angles and appropriate

areas taken into account in calculating the total radiated power.

Data relating to this experiment are given in Fig. A-5, showing the difference between the power radiated from the truncated pipe (PWL_t) and the power for the freefield source (PWL_f). Data are shown for both source configurations deeply immersed in the pipe and for the short tube configuration (Source #2) shallowly immersed.

F. Discussion of Results

Those data points shown circled in Fig. A-4 are believed to be the result of the influence of strong cross-modes upon the volume velocity of the long tube monopole source (#1 in Fig. A-1). If these points are neglected, the influence of source enclosure can be summarized by the dotted line given in Fig. A-4. This corresponds to an inverse frequency-squared dependence below about 1600 Hz asymptoting to a frequency independent difference of about 6 dB at higher frequencies. The latter effect perhaps derives from the fact that we have assumed plane wave propagation in calculating the pipe-transmitted source power. At frequencies above the cross-mode onset frequency (about 1600 Hz for the 4 in. diameter pipe), the sound field will, in fact, tend to be diffuse and thus cause the influence of enclosure to be overestimated by some 3 to 6 dB.

The data shown in Fig. A-4 are in general agreement with theoretical predictions: that the immersion of a monopole acoustic source in an infinitely long pipe modifies the freefield power of the source by an inverse frequency-squared term for frequencies below the cross-mode onset frequency and that the

source reverts to its freefield behavior for frequencies above this frequency.

The high frequency data scatter in Fig. A-5 can also be accounted for in terms of cross-mode interaction with the volume velocity of the acoustic source. If we neglect these points, we conclude that end reflection losses very nearly cancel the frequency dependent changes introduced by enclosure of the source within the pipe. It does not, furthermore, seem to matter whether the source is immersed three diameters or twenty-five diameters from the exit plane.

The influence of the truncated pipe upon the freefield source is not entirely frequency independent, however. The data show what might be construed as an inverse linear dependence upon frequency over the mid-frequency range encompassing the onset frequency for cross-modes. Presumably, the pipe enclosure effect is not exactly matched by the exit plane transmissibility.

REFERENCES

1. "Progress of NASA Research Relating to Noise Alleviation of Large Subsonic Jet Aircraft," NASA SP-189, 1968.

2. C.G. Gordon and G. Maidanik, "Influence of Upstream Flow Discontinuities on the Acoustic Power Radiated by a Model Air Jet," NASA CR-679, 1967.

3. N. Curle, "The Influence of Solid Boundaries Upon Aerodynamic Sound." *Proc. Roy. Soc.* 231A, pp. 505–514 (1955).

4. H.G. Davies and J.E. Ffowcs Williams, "Aerodynamics of Sound Generation in a Pipe." *J. Fluid Mech.* 32, Pt. 4, pp. 765–778 (1968).

5. P. Morse and U. Ingard, *Theoretical Acoustics*. New York: McGraw-Hill Book Co., Inc., 1968.

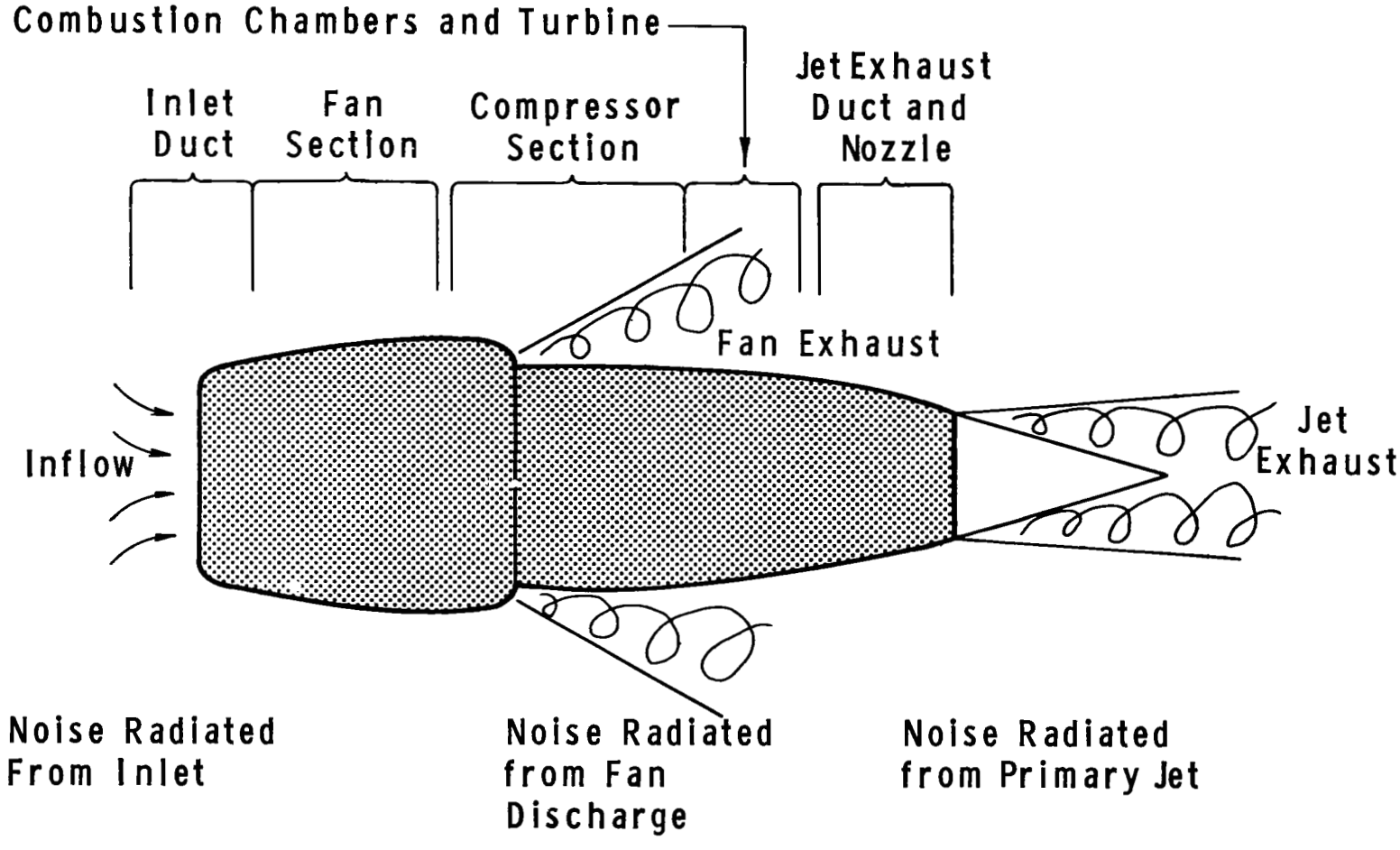

FIG. I-1 NOISE EMISSION OF A TURBO FAN-JET ENGINE

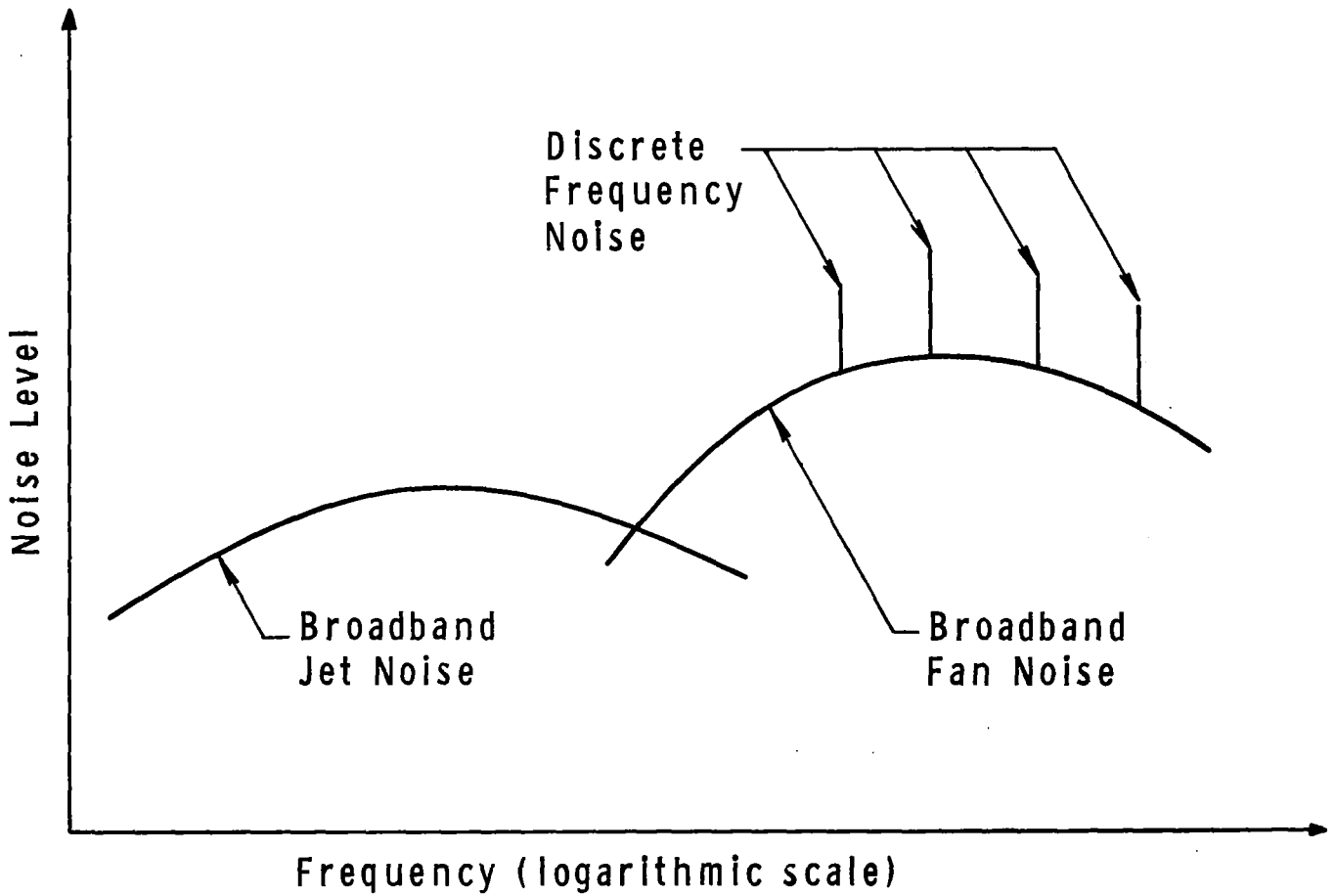

FIG. 1-2 TYPICAL NOISE SPECTRUM OF HIGH BYPASS-RATIO FAN-JET ENGINE

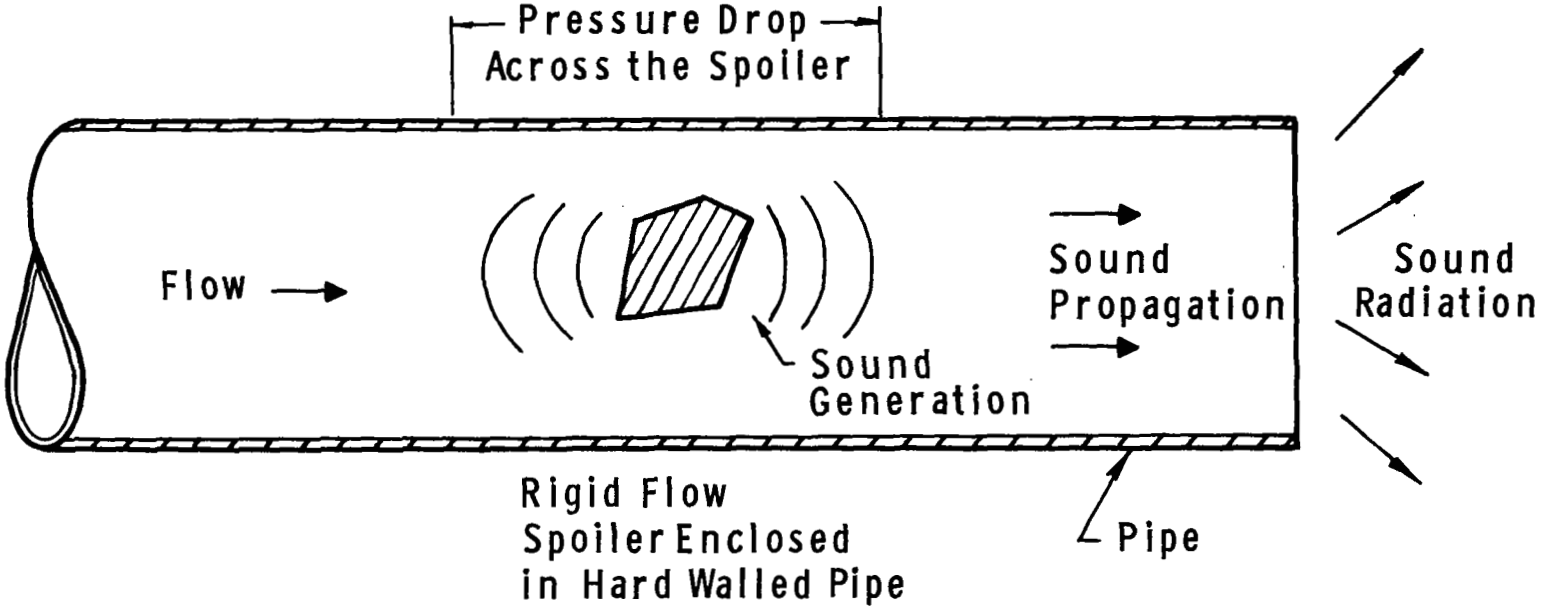

FIG. I-3 BASIC EXPERIMENTAL CONFIGURATION

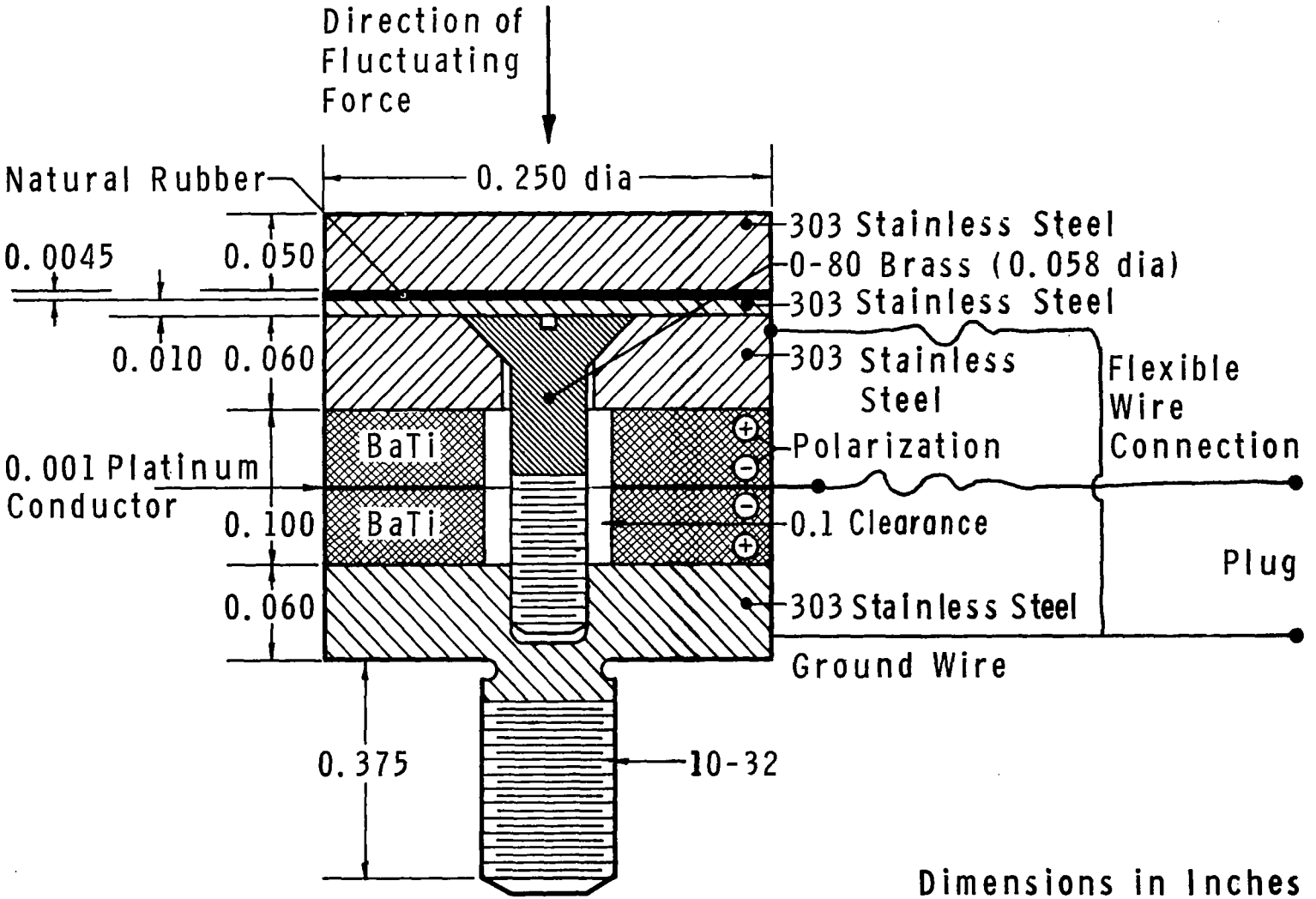

FIG. II-1 FLUCTUATING-FORCE TRANSDUCER

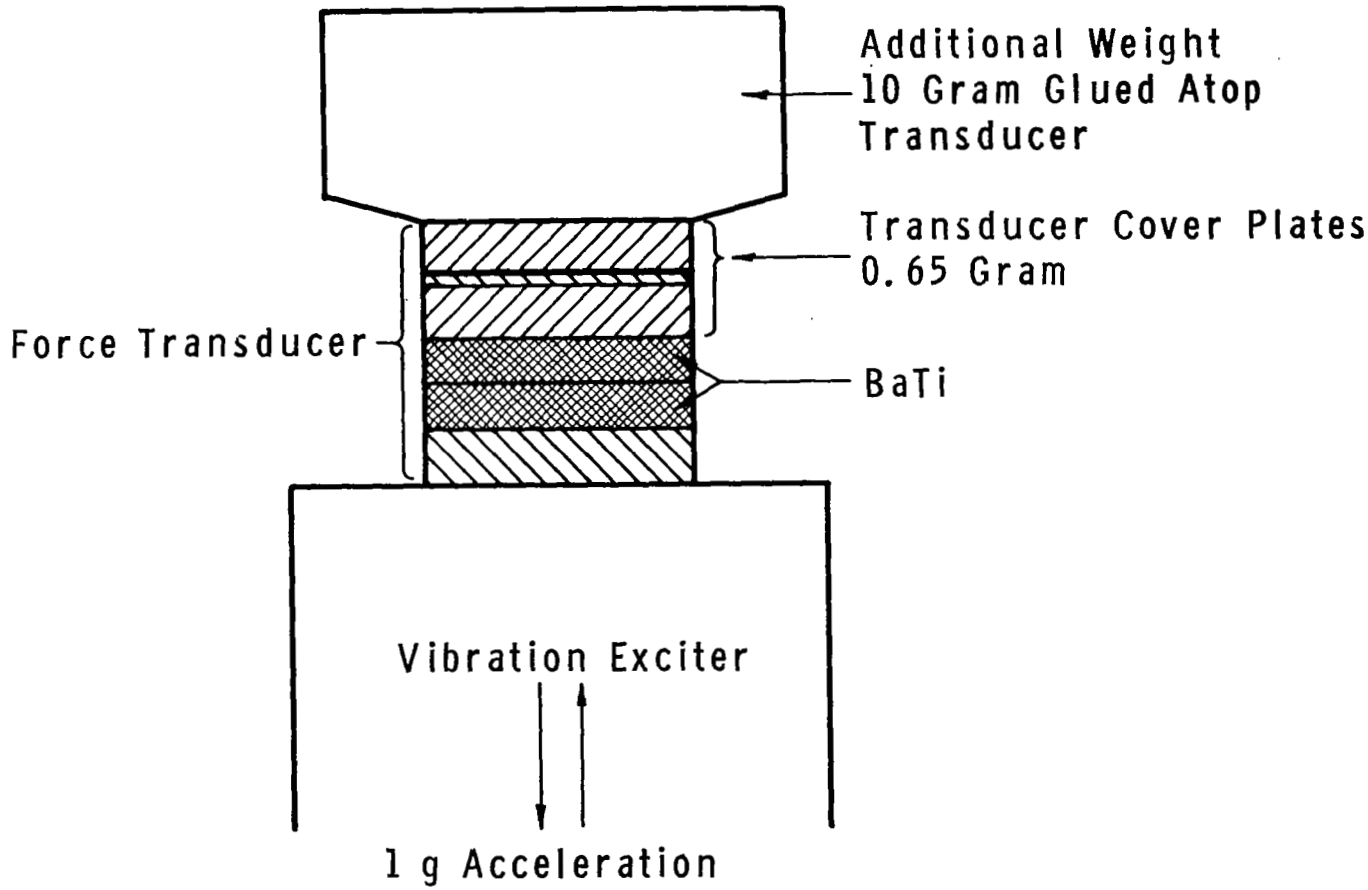

FIG. II-2 CALIBRATION OF FORCE TRANSDUCER

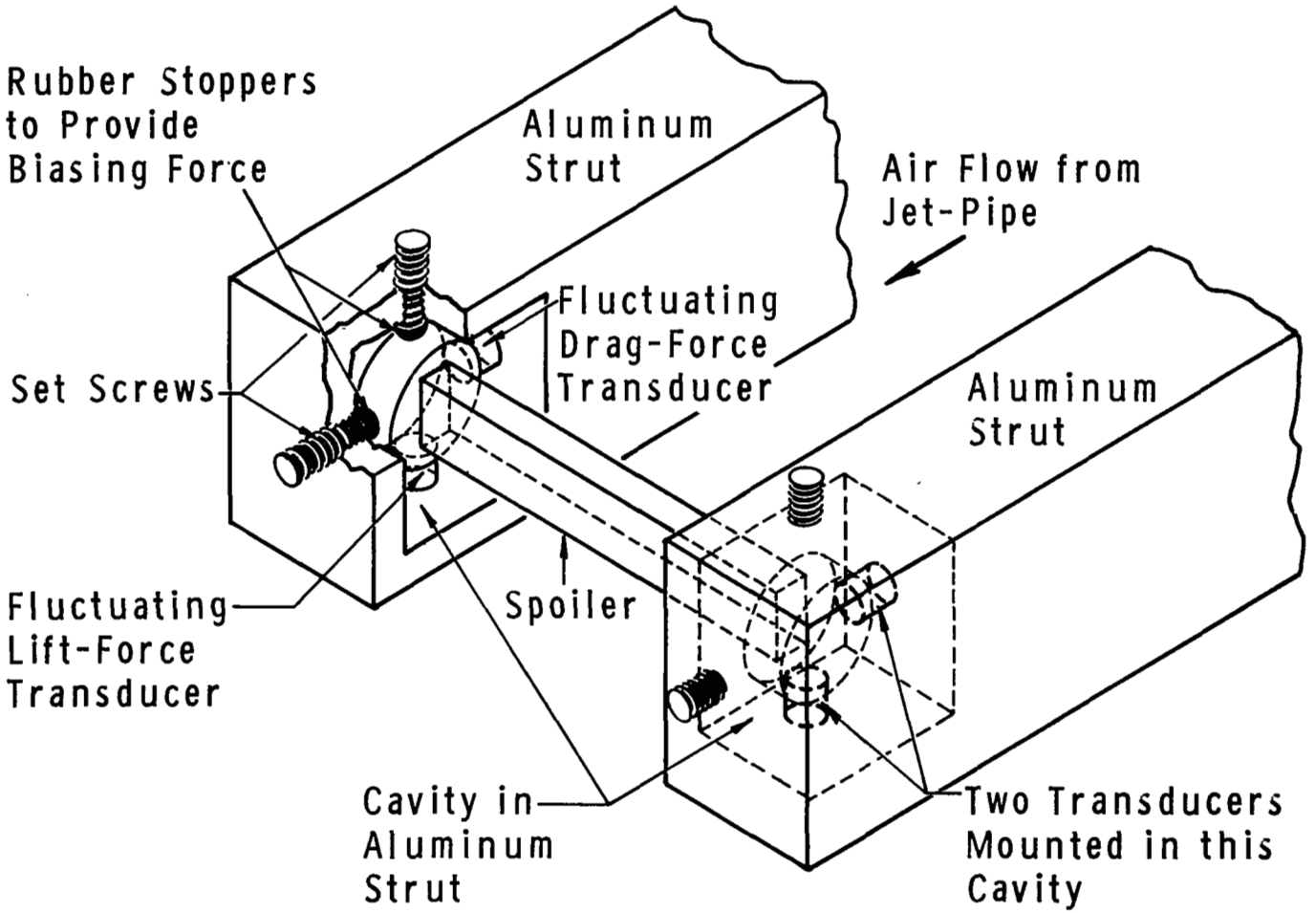

FIG. II-3 SCHEMATIC OF FLUCTUATING-FORCE MEASURING APPARATUS

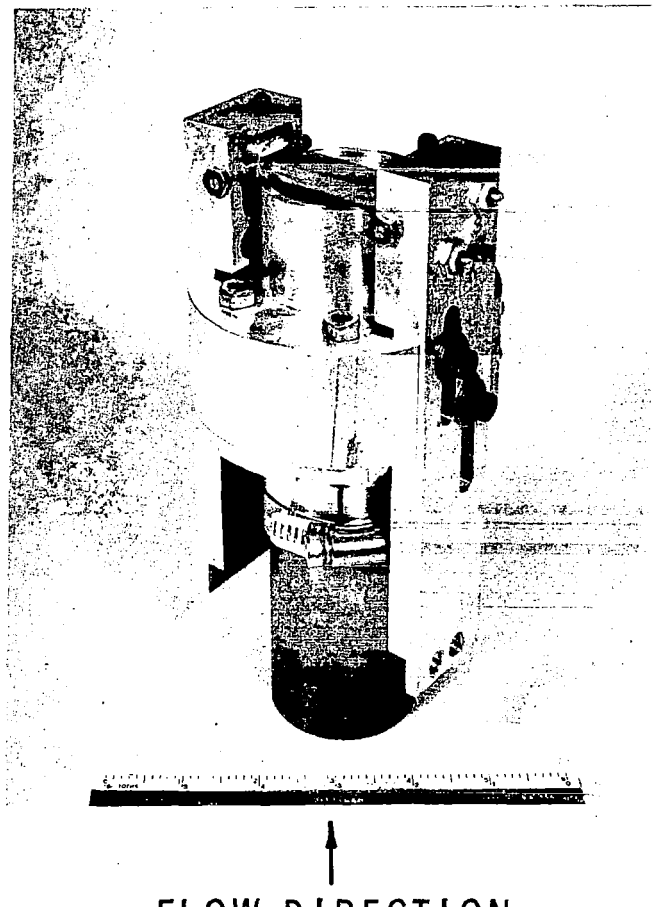

FIG. II-4 APPARATUS FOR MEASURING FLUCTUATING FORCES

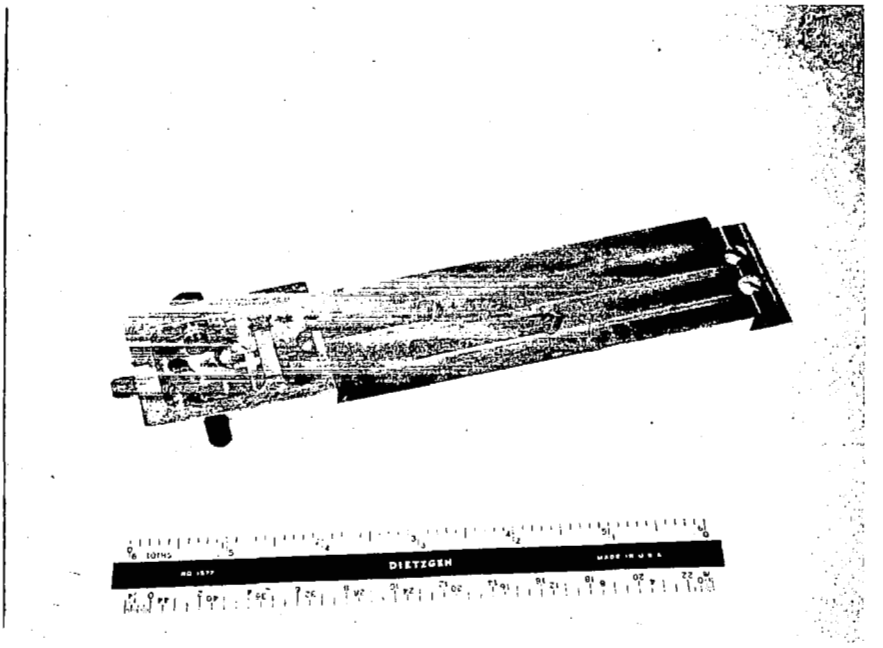

FIG. II-5 ALUMINUM STRUT INCORPORATING LIFT-FORCE TRANSDUCER AND DRAG-FORCE TRANSDUCER

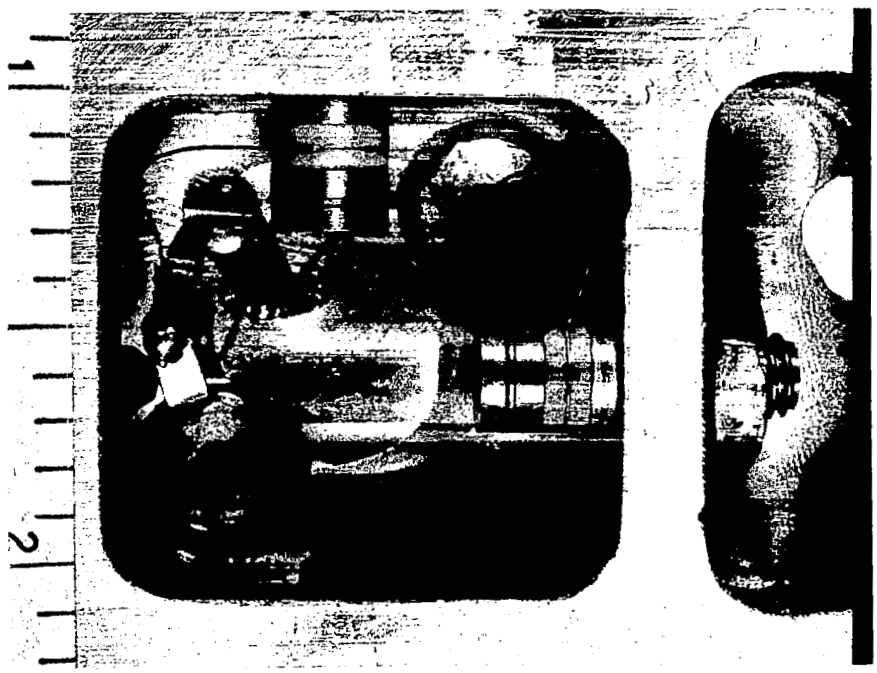

FIG. II-6 CAVITY WITH FORCE TRANSDUCER

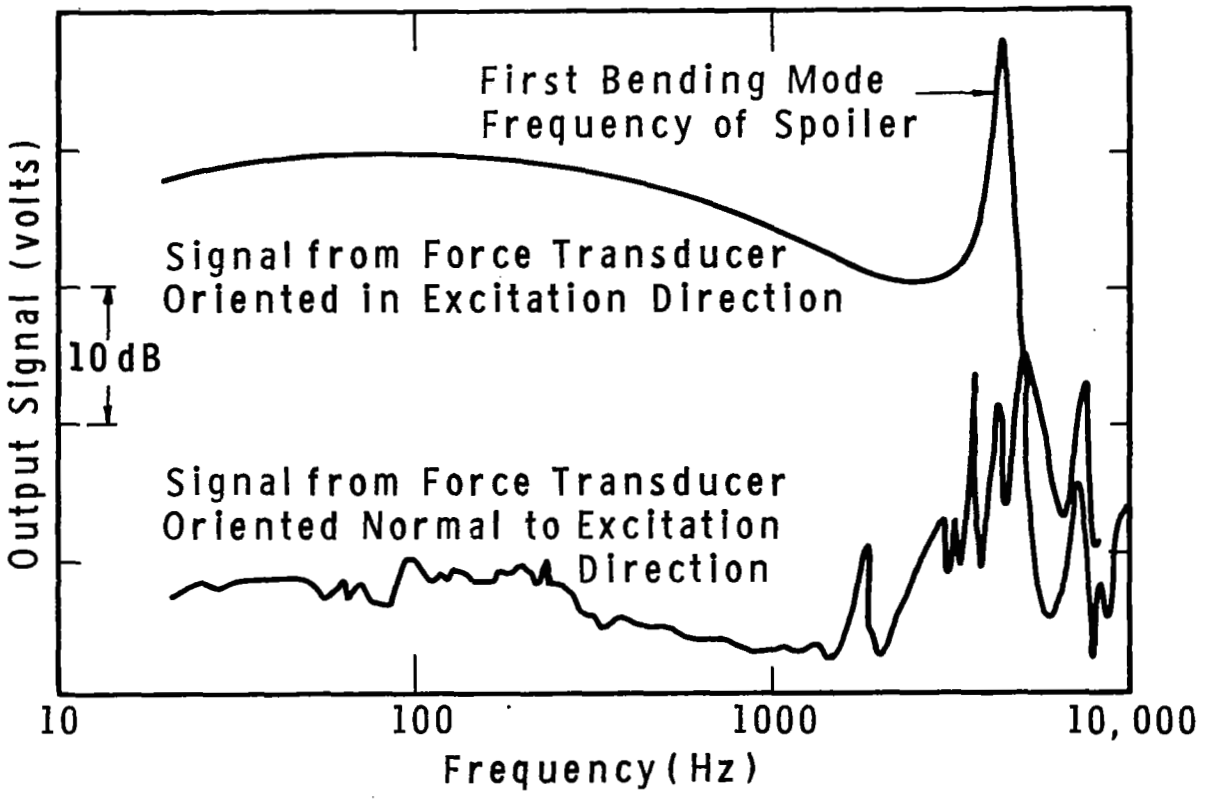

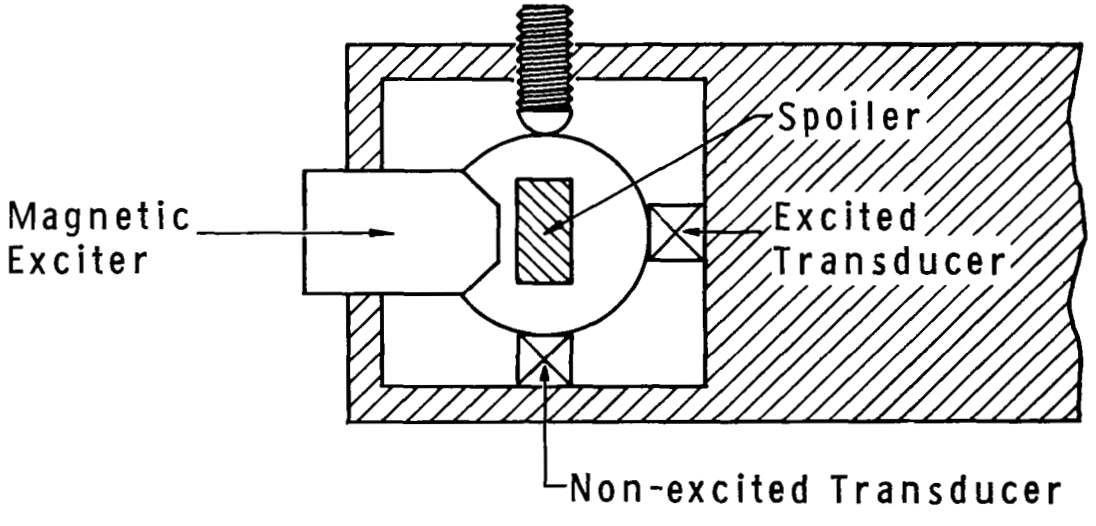

FIG.II-7 TYPICAL CROSSTALK CHARACTERISTIC OF TRANSDUCER PAIR

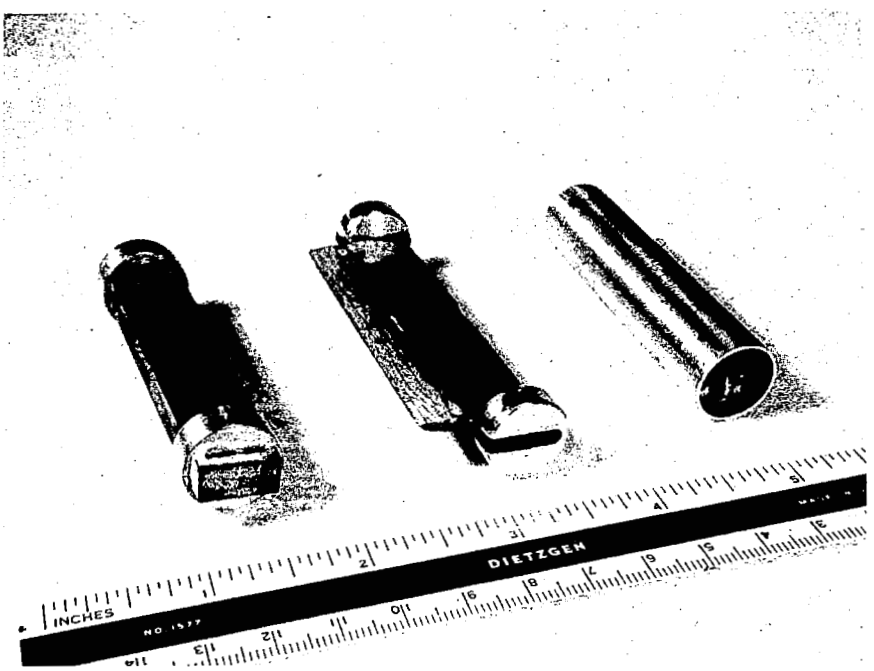

FIG. III-3 FLOW SPOILERS

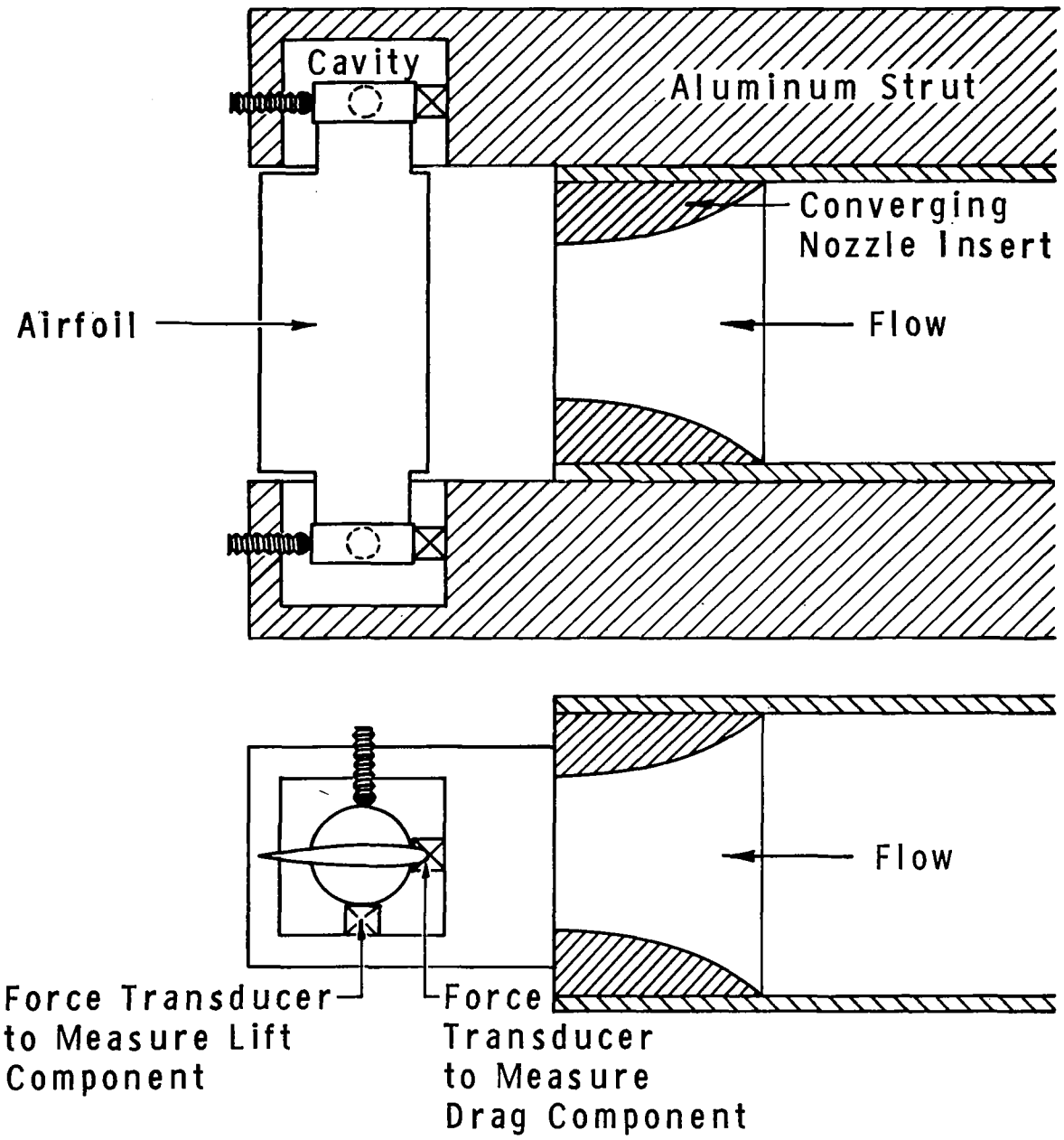

FIG. III-4 SCHEMATIC OF SPOILER/TRANSDUCER ASSEMBLY FOR FORCE MEASUREMENTS WITH THE SPOILER DOWNSTREAM OF THE JET-EXIT PLANE (FREE FIELD ENVIRONMENT)

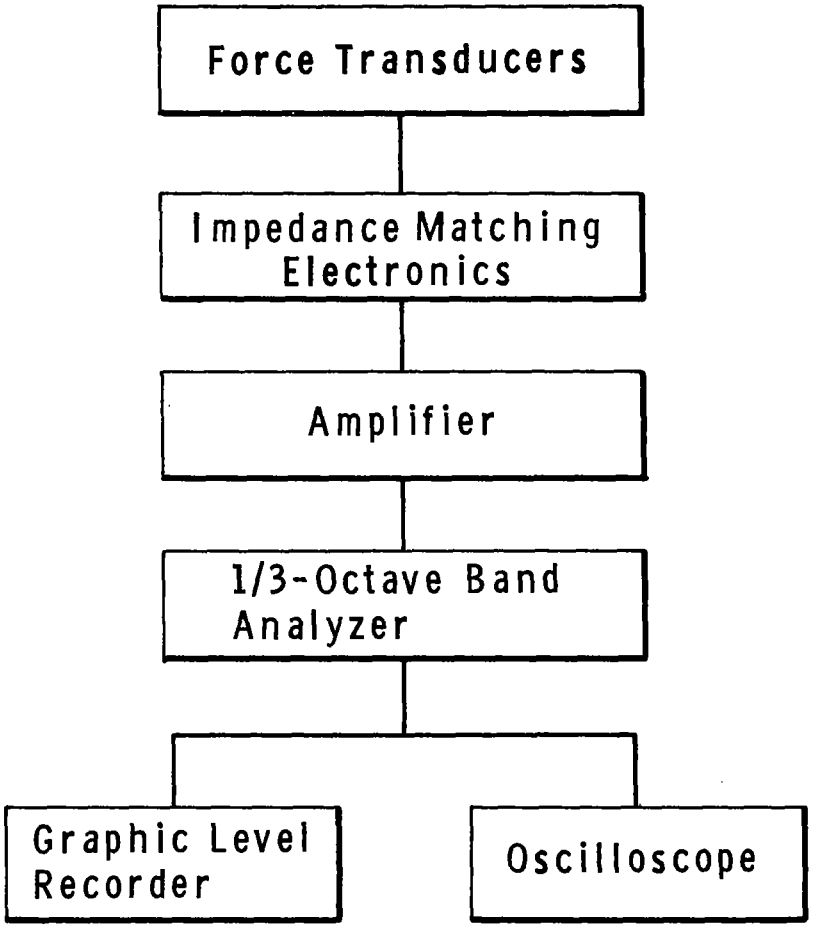

FIG. III-7 BLOCK DIAGRAM OF FORCE MEASURING SYSTEM

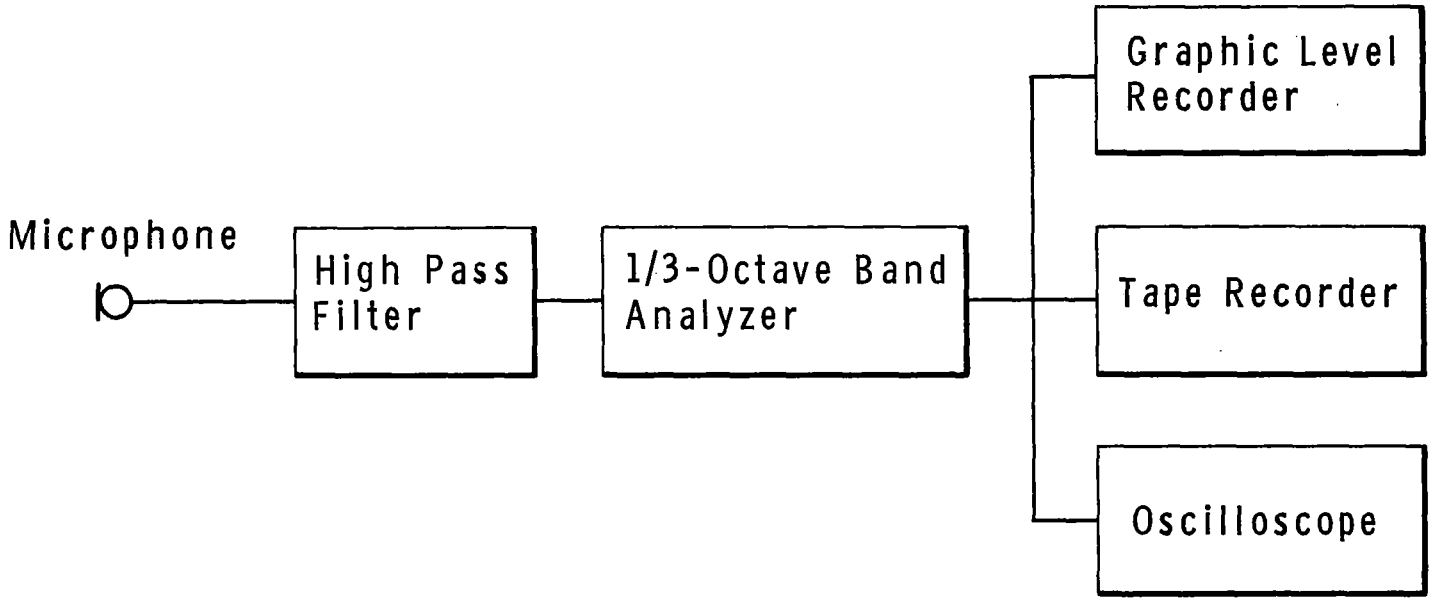

FIG. III-8 BLOCK DIAGRAM OF ACOUSTIC DATA ACQUISITION SYSTEM

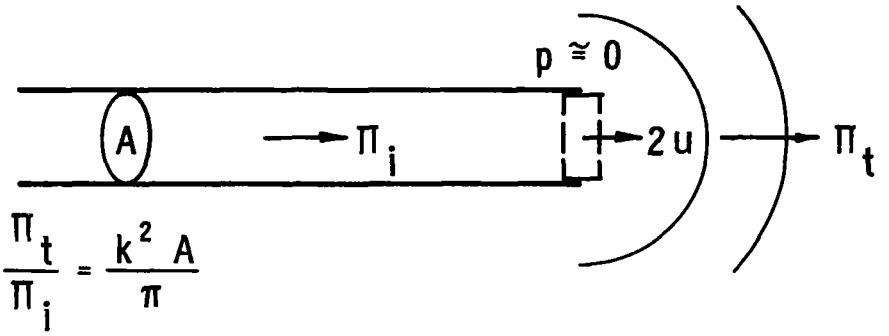

(a) Simple End Reflections

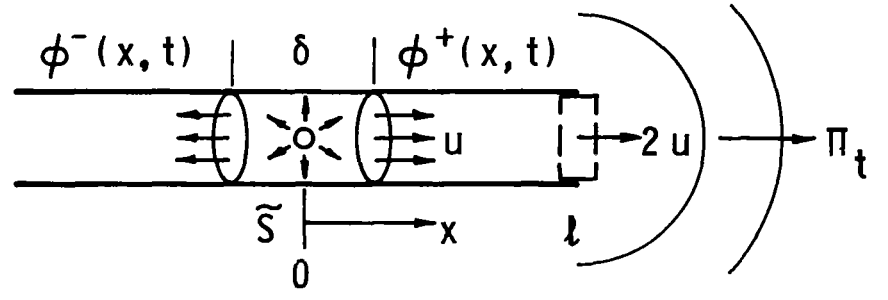

(b) Model for Monopole Near the End of a Duct

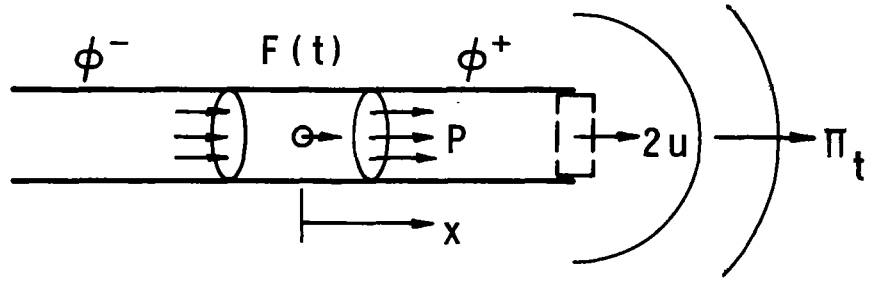

(c) Model for Dipole Near the End of a Duct

FIG. IV-2 ACOUSTIC MODELS FOR THE EFFECT OF THE PIPE END UPON THE POWER RADIATED TO FREE SPACE

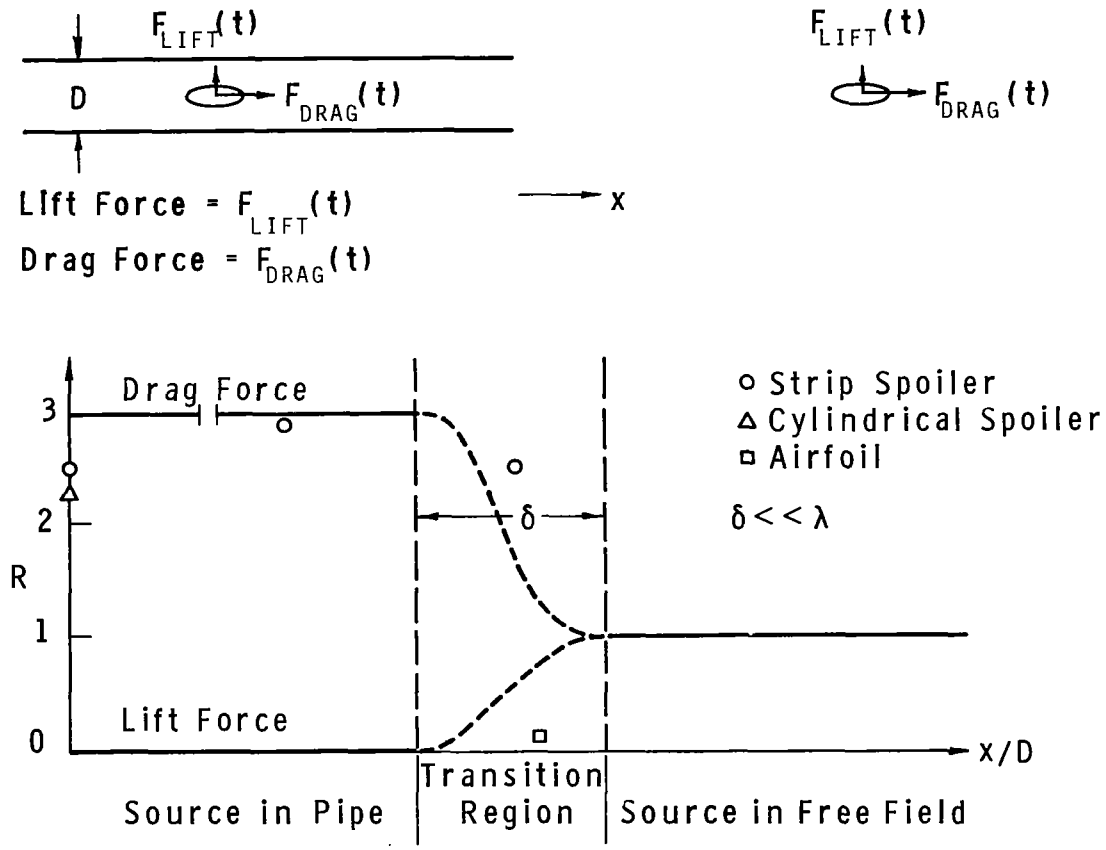

FIG. IV-3 PROPORTIONALITY BETWEEN ACOUSTIC POWER AND FLUCTUATING LIFT AND DRAG FORCES AS A FUNCTION OF FLOW SPOILER LOCATION AT LOW FREQUENCIES

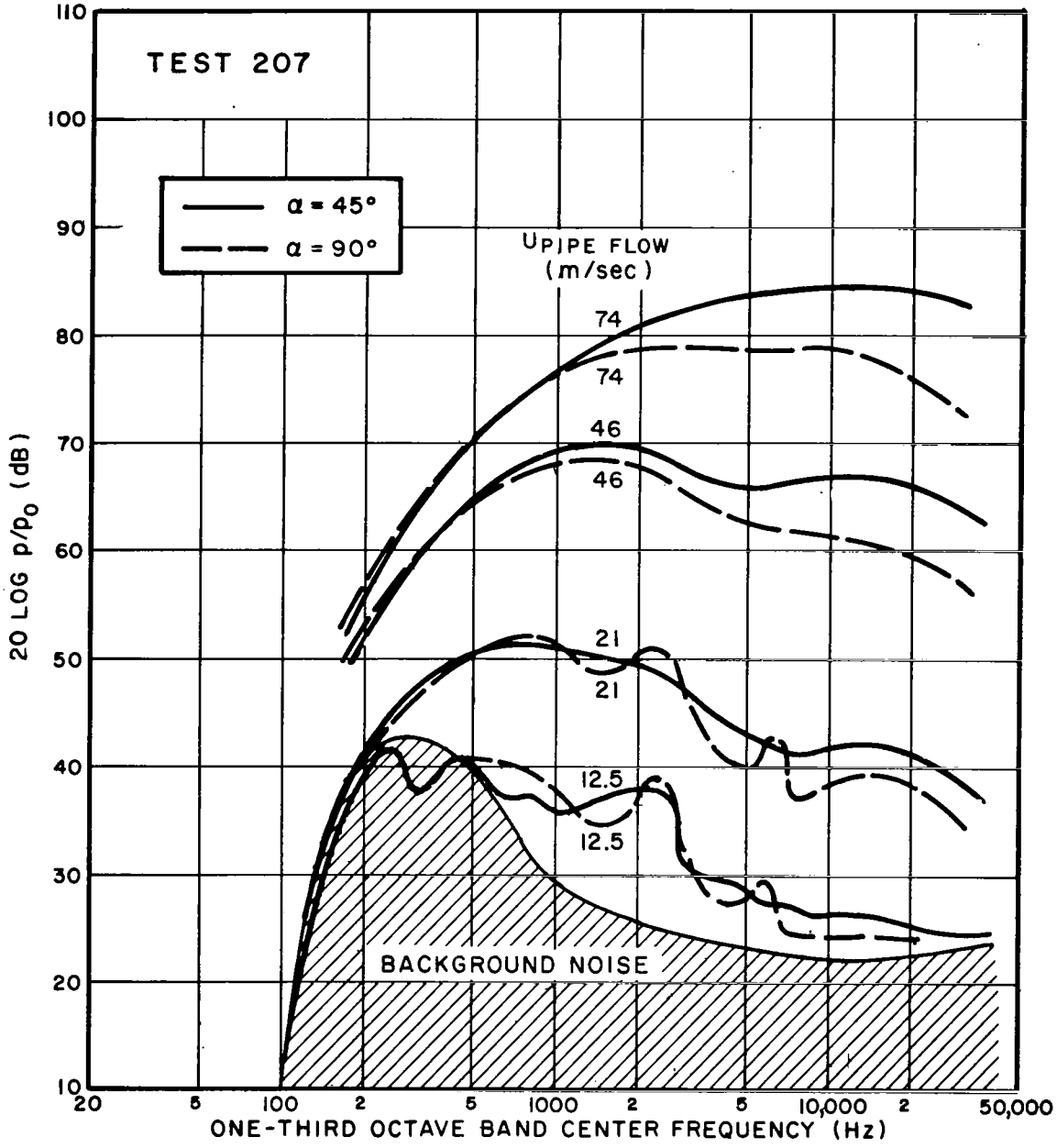

FIG. V-1 SOUND PRESSURE LEVEL SPECTRA (TEST 207: STRIP SPOILER 6 in UPSTREAM OF PIPE EXIT)

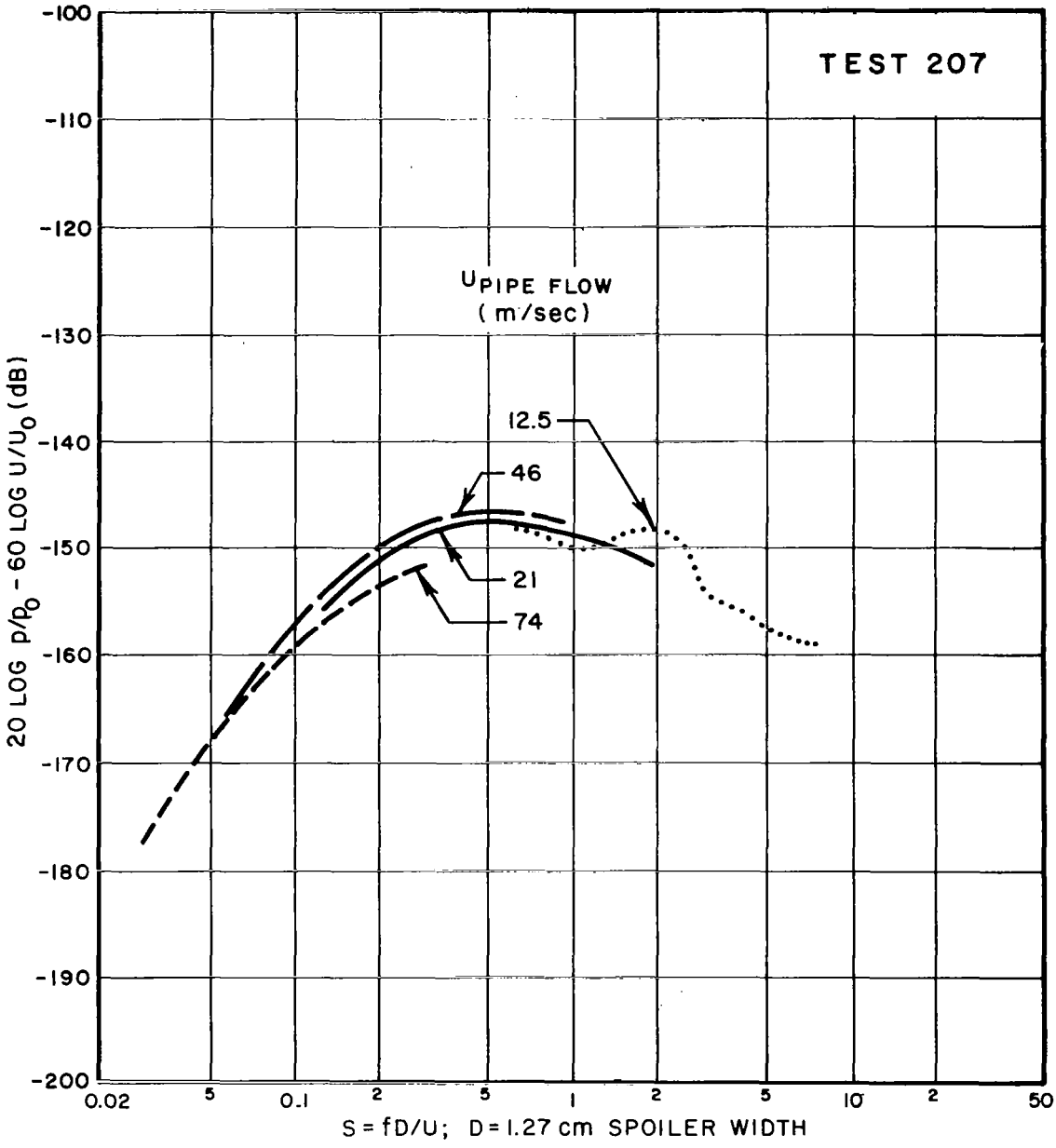

FIG. V-2 NORMALIZED SOUND PRESSURE LEVEL SPECTRUM (TEST 207: STRIP SPOILER 6 in UPSTREAM OF PIPE EXIT)

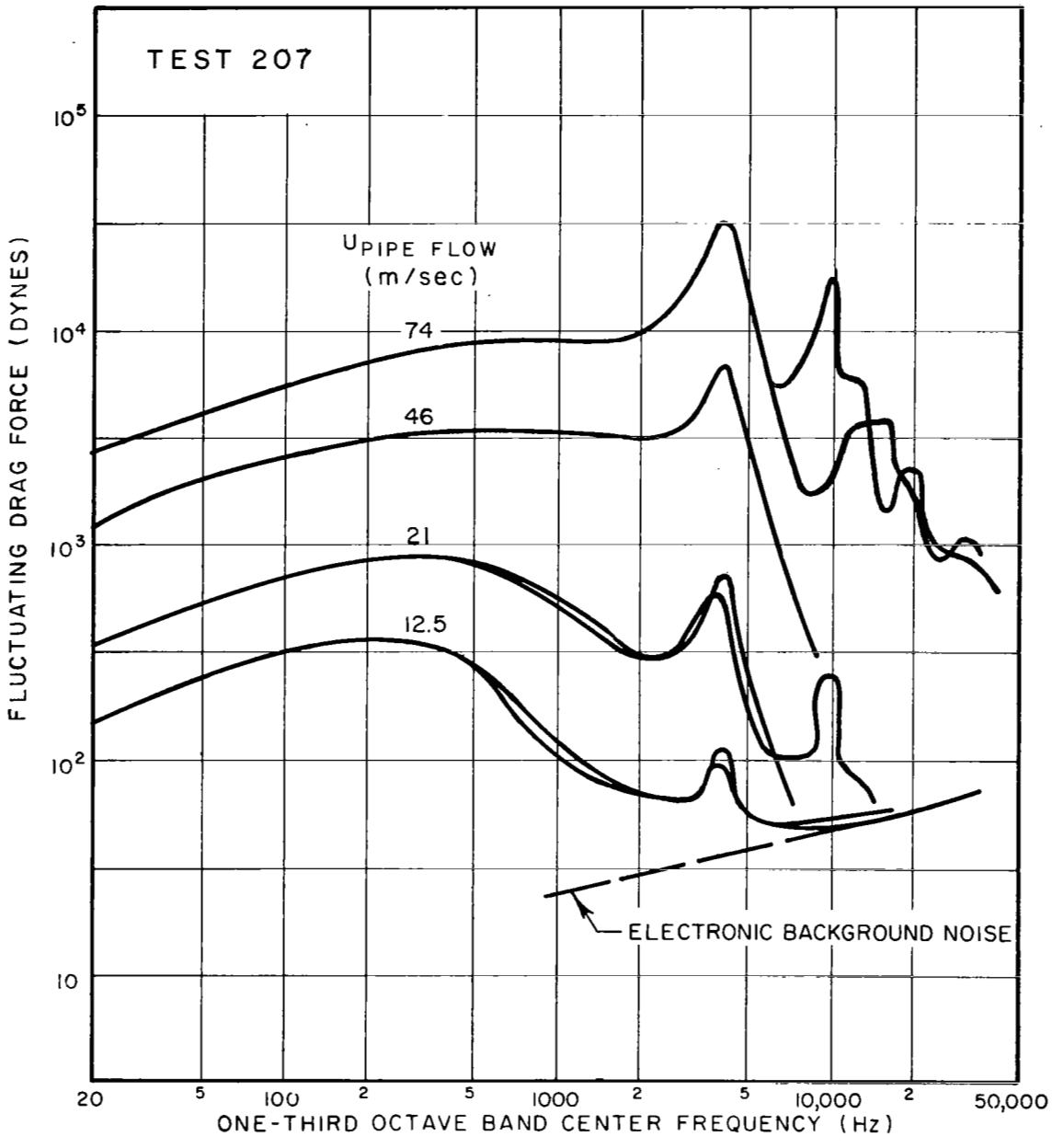

FIG. V-3 FLUCTUATING DRAG FORCE SPECTRA (TEST 207: STRIP SPOILER 6 in UPSTREAM OF PIPE EXIT)

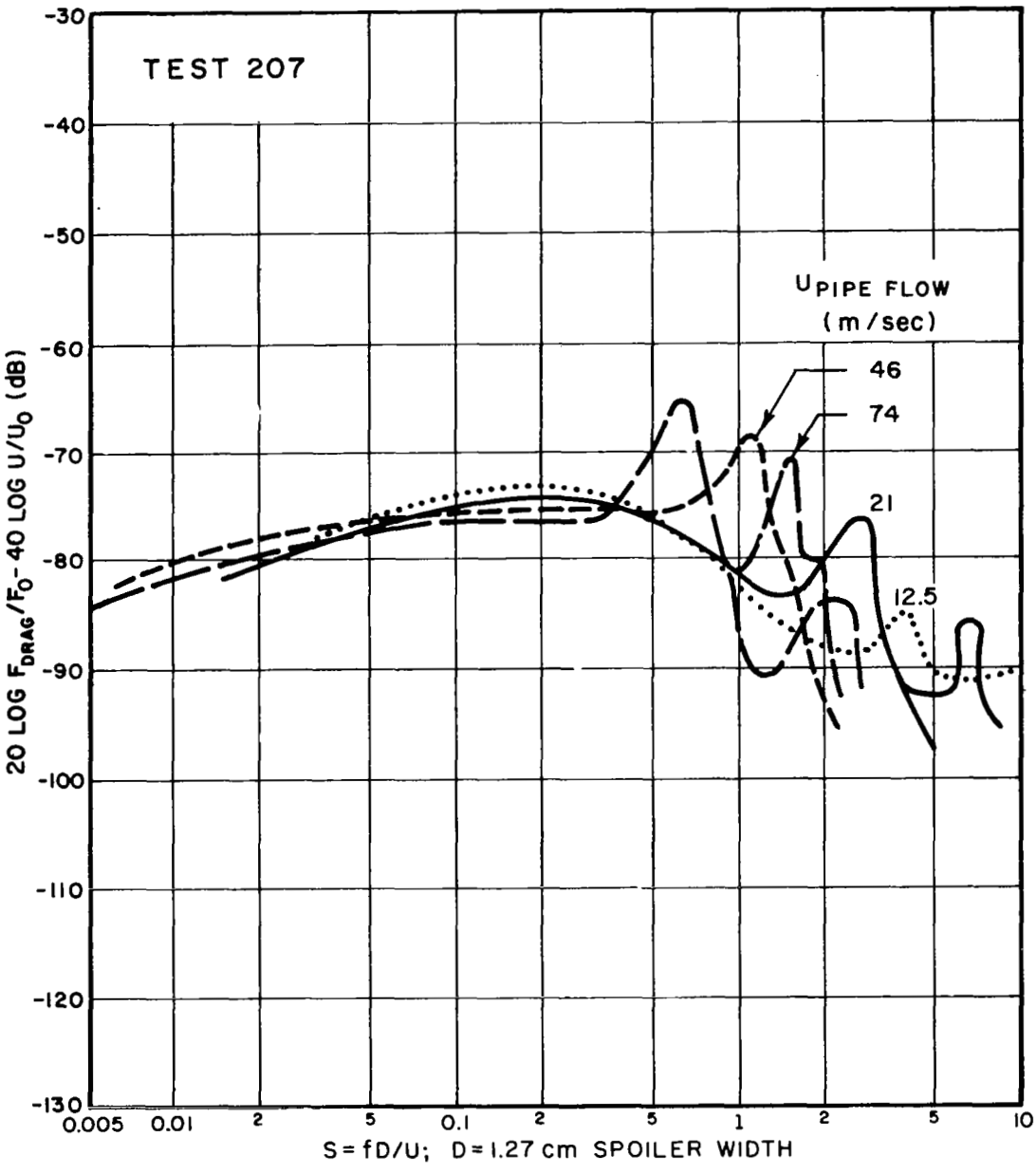

FIG. V-4 NORMALIZED FLUCTUATING DRAG FORCE LEVEL SPECTRUM (TEST 207: STRIP SPOILER 6 in UPSTREAM OF PIPE EXIT)

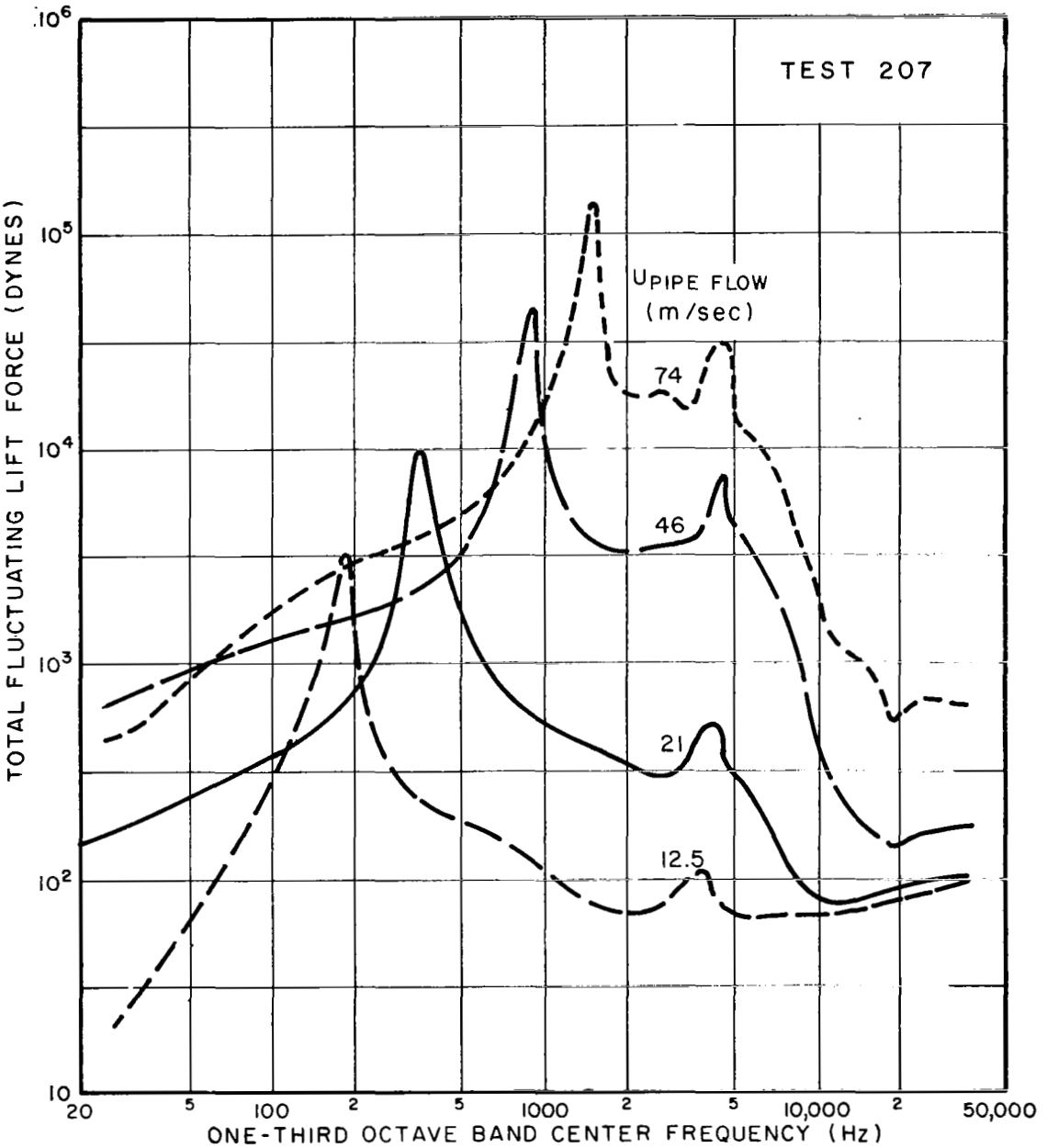

FIG. V-5 FLUCTUATING LIFT FORCE SPECTRA (TEST 207: STRIP SPOILER 6 in UPSTREAM OF PIPE EXIT)

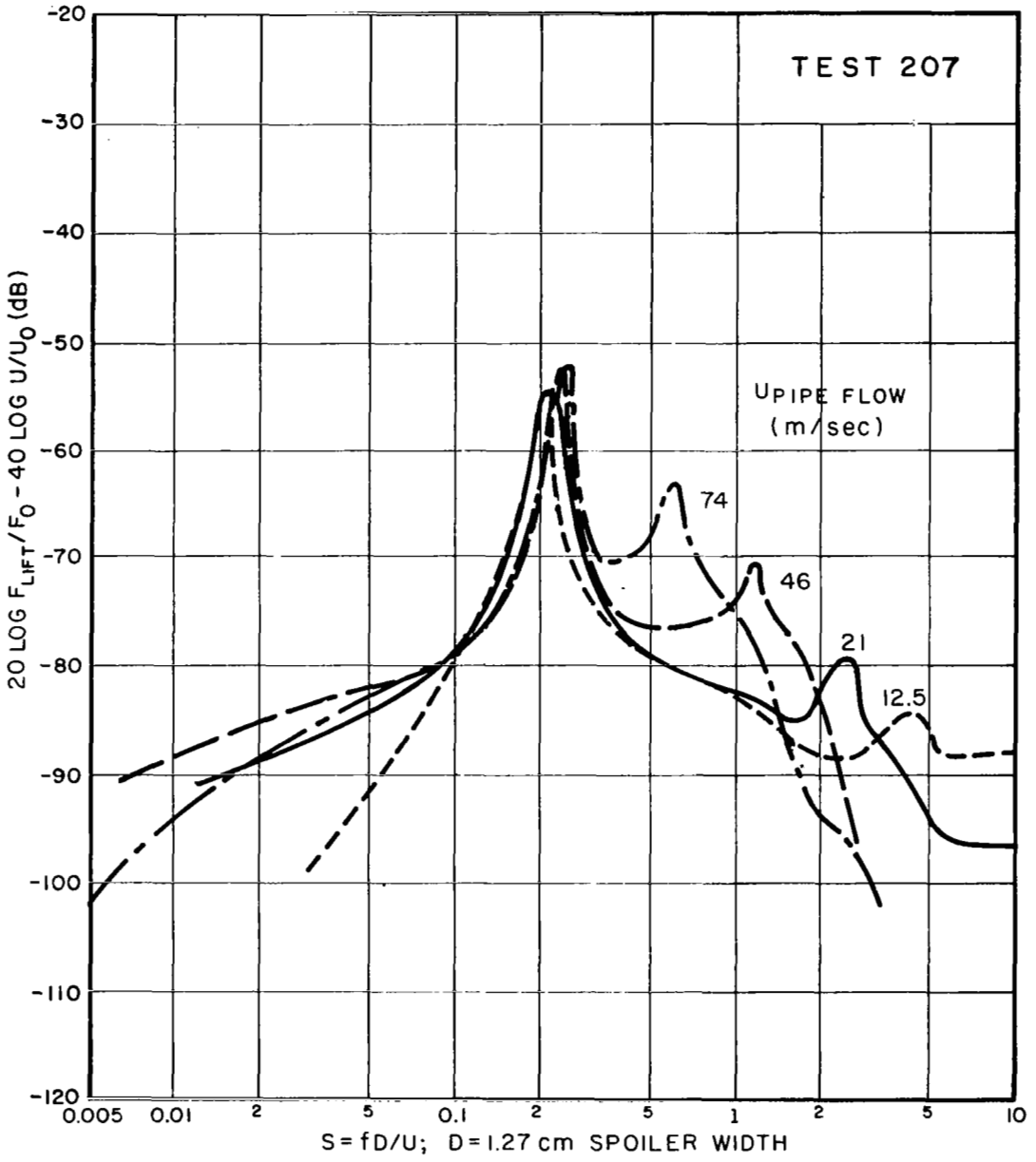

FIG. V-6 NORMALIZED LIFT FORCE LEVEL SPECTRUM (TEST 207: STRIP SPOILER 6 in UPSTREAM OF PIPE EXIT)

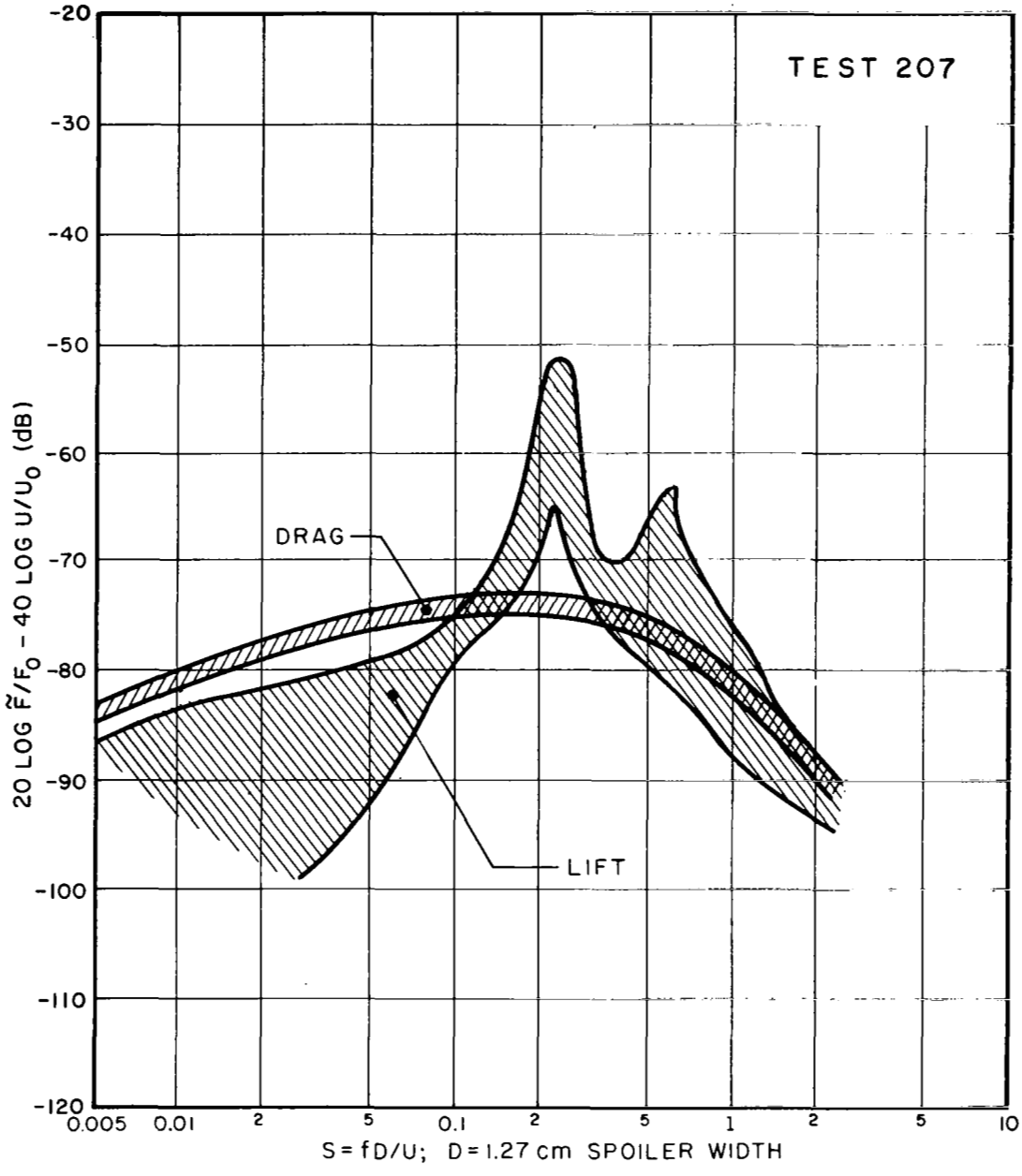

FIG. V-7 COMPARISON OF NORMALIZED LIFT AND DRAG FORCE LEVEL SPECTRUM (TEST 207: STRIP SPOILER 6 in UPSTREAM OF PIPE EXIT)

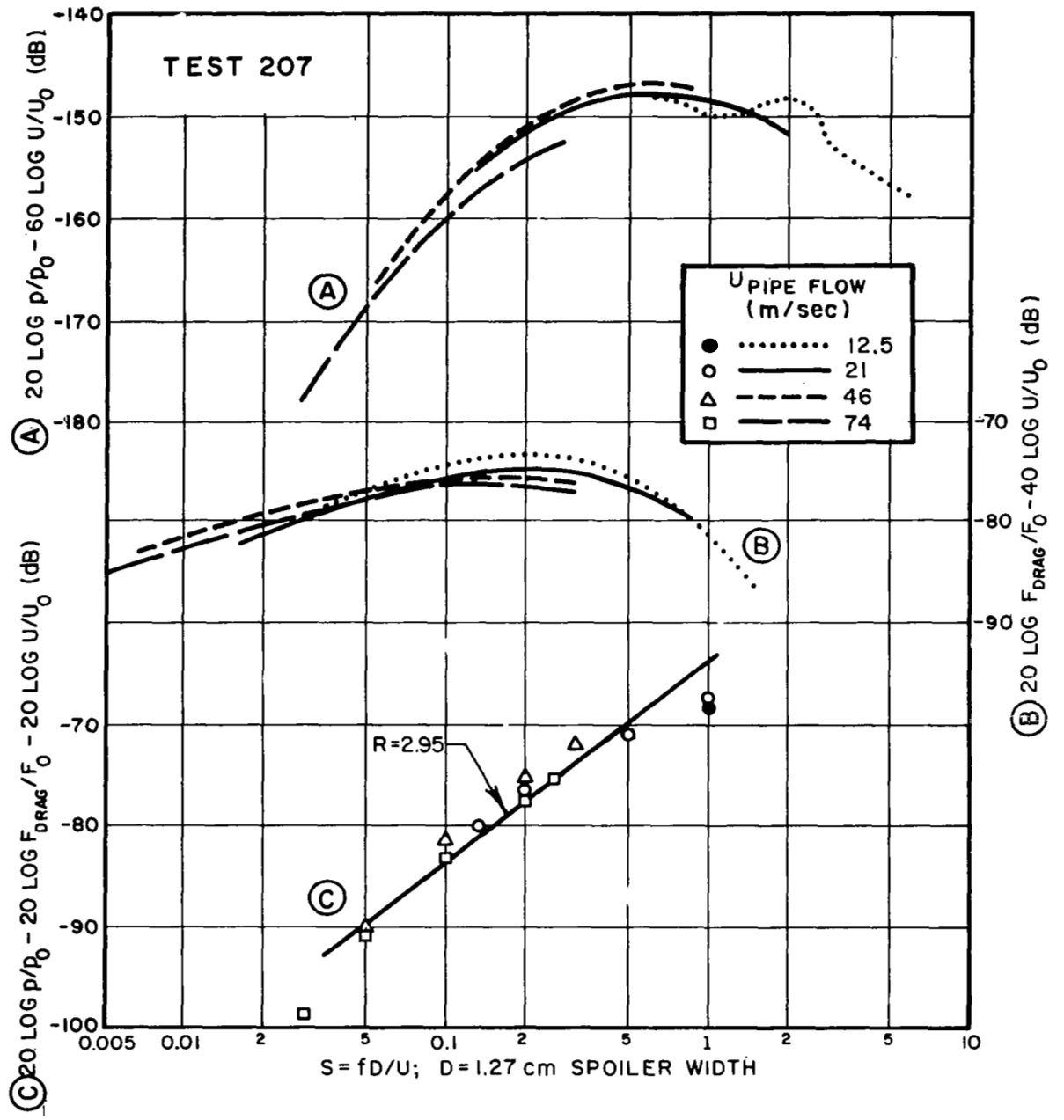

FIG. V-8 SUMMARY OF TEST RESULTS FOR STRIP SPOILER 6 in UPSTREAM OF PIPE EXIT (TEST 207):

Ⓐ Normalized sound pressure level spectrum
Ⓑ Normalized drag force level spectrum
Ⓒ Difference spectrum

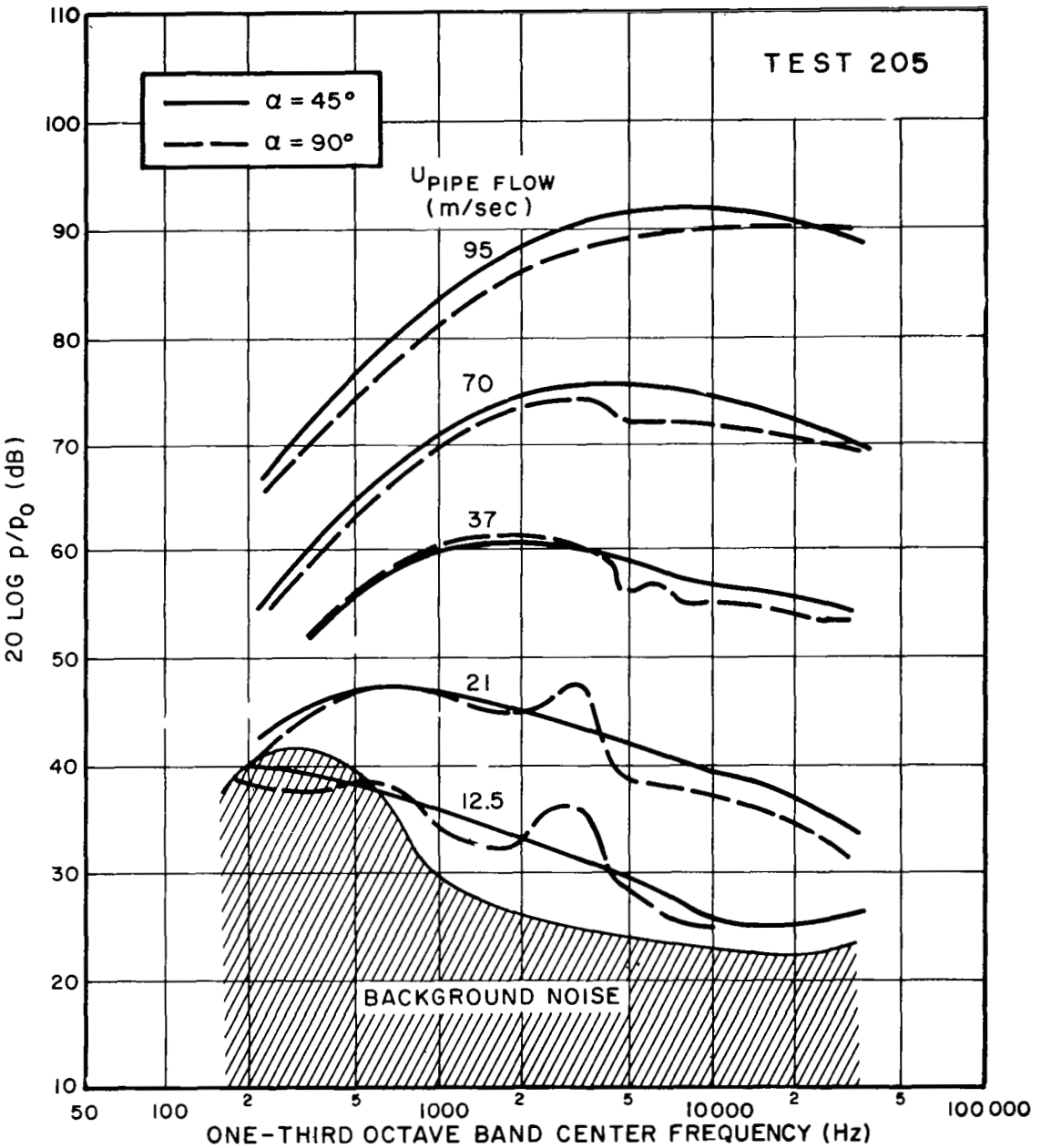

FIG. V-9 SOUND PRESSURE LEVEL SPECTRA (TEST 205: STRIP SPOILER AT PIPE EXIT)

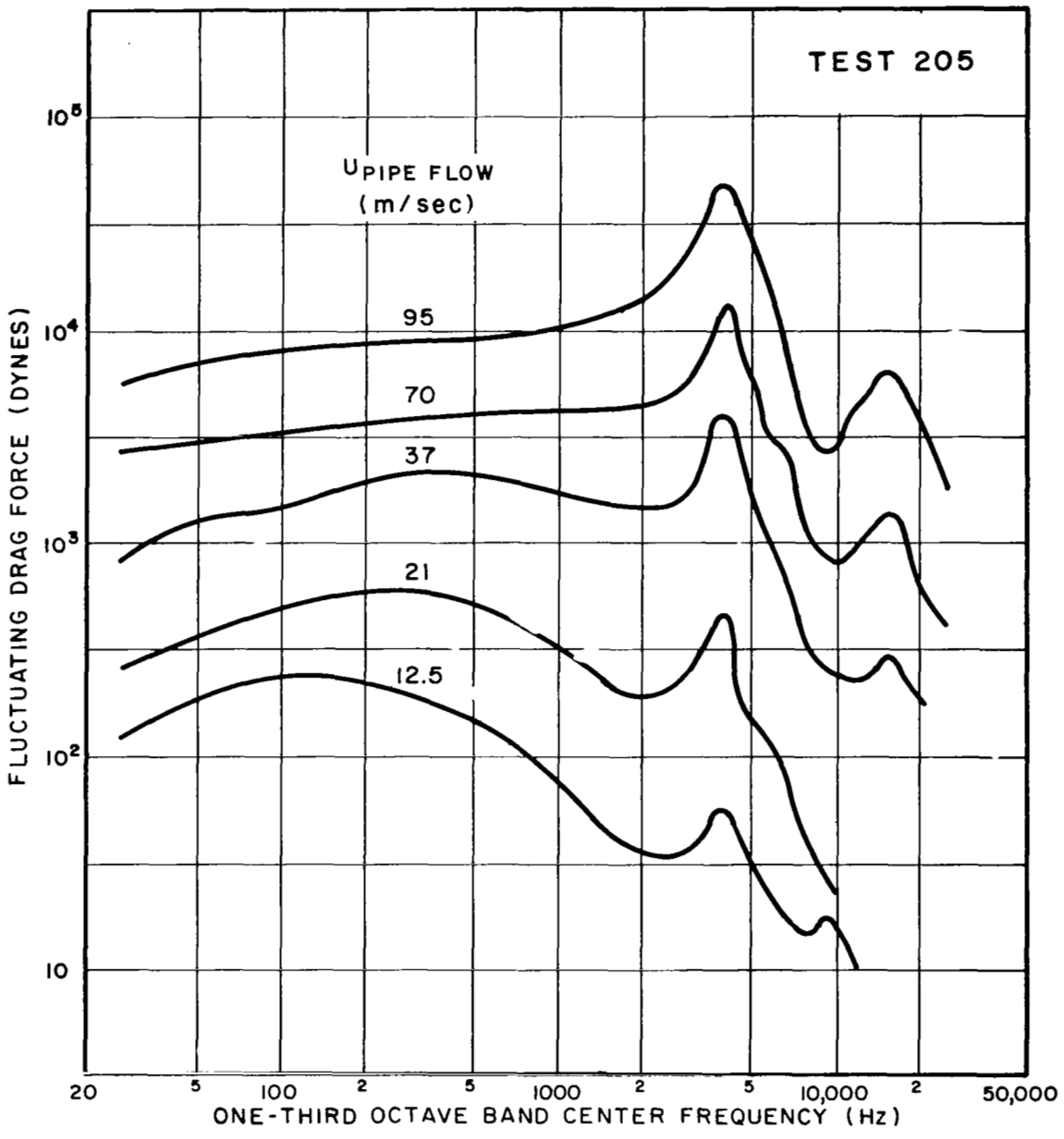

FIG. V-10 FLUCTUATING DRAG FORCE SPECTRA (TEST 205: STRIP SPOILER AT PIPE EXIT)

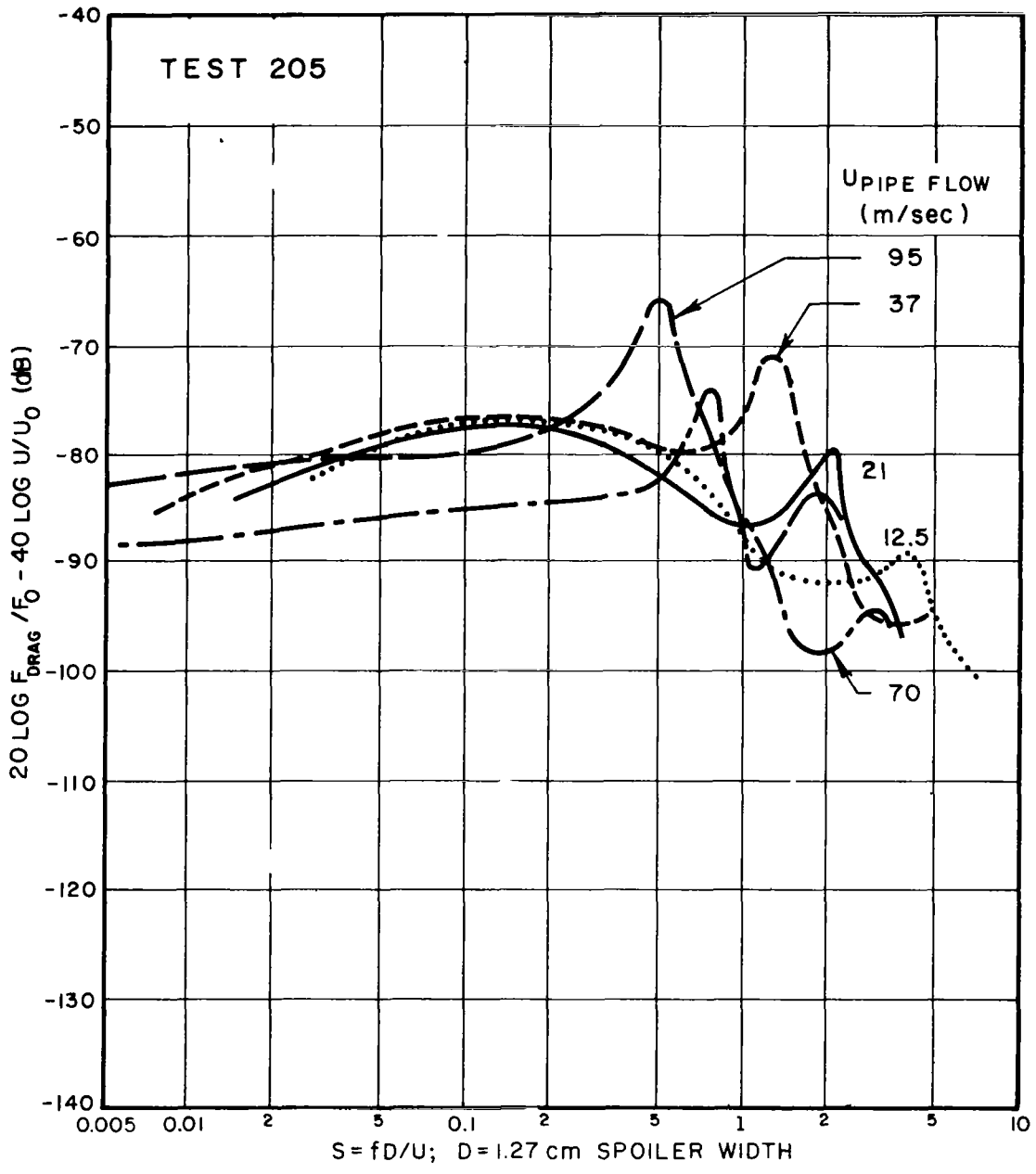

FIG. V-11 NORMALIZED DRAG FORCE LEVEL SPECTRUM (TEST 205: STRIP SPOILER AT PIPE EXIT)

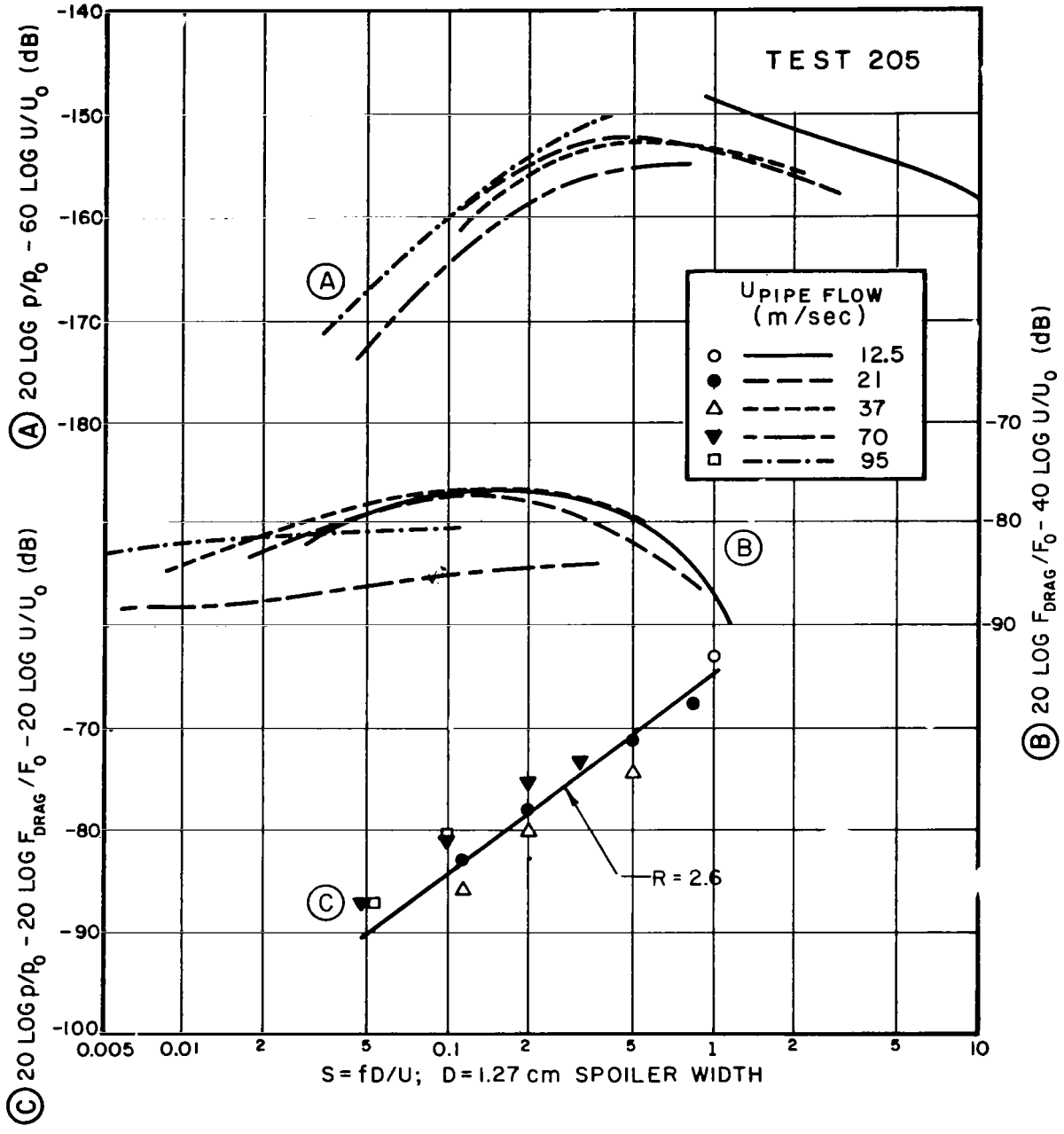

FIG. V-12 SUMMARY OF TEST RESULTS FOR STRIP SPOILER AT EXIT PLANE (TEST 205):

Ⓐ Normalized sound pressure level spectrum

Ⓑ Normalized drag force level spectrum

Ⓒ Difference spectrum

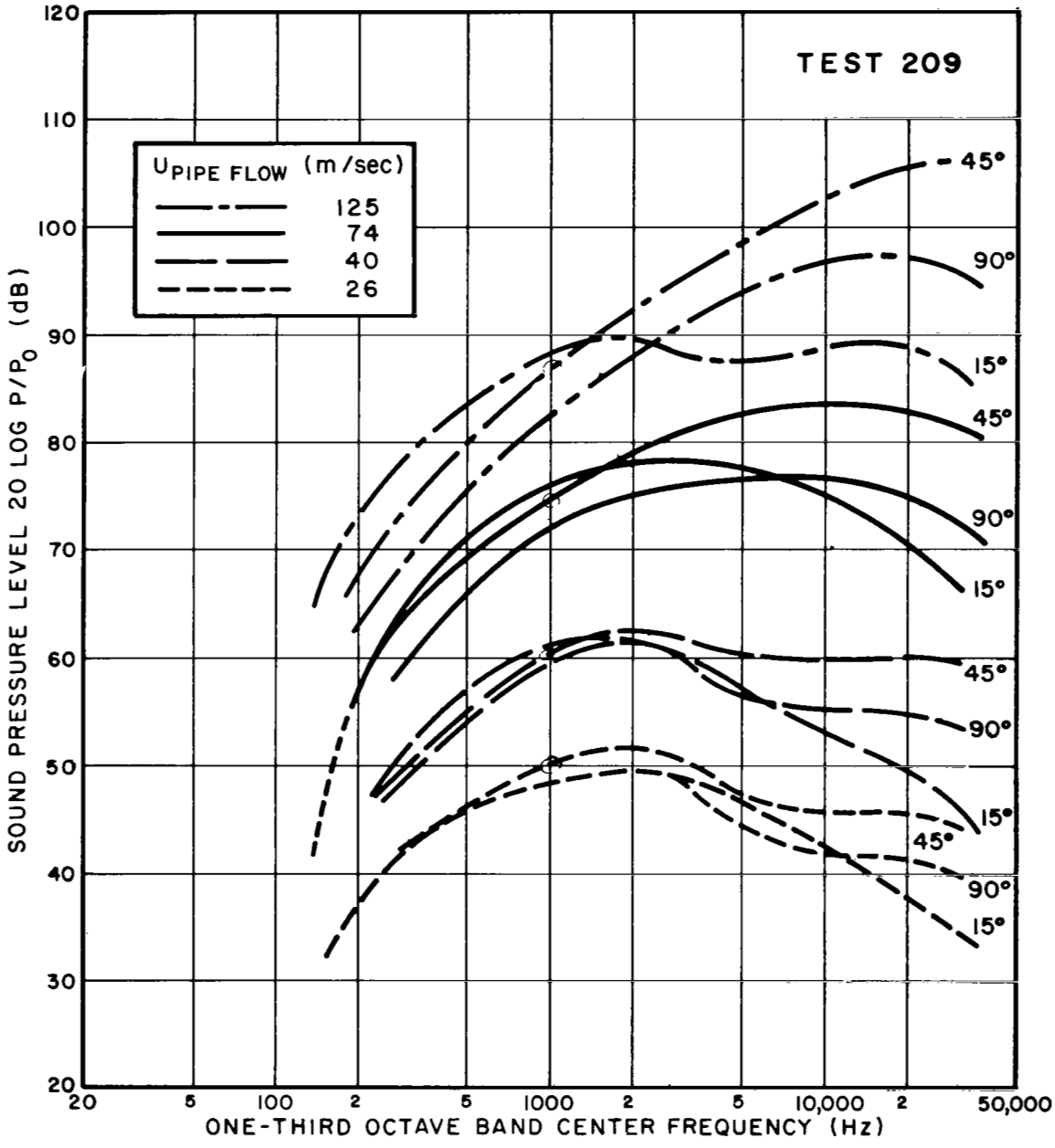

FIG. V-13 SOUND PRESSURE LEVEL SPECTRA (TEST 209: STRIP SPOILER 18 in UPSTREAM OF PIPE EXIT)

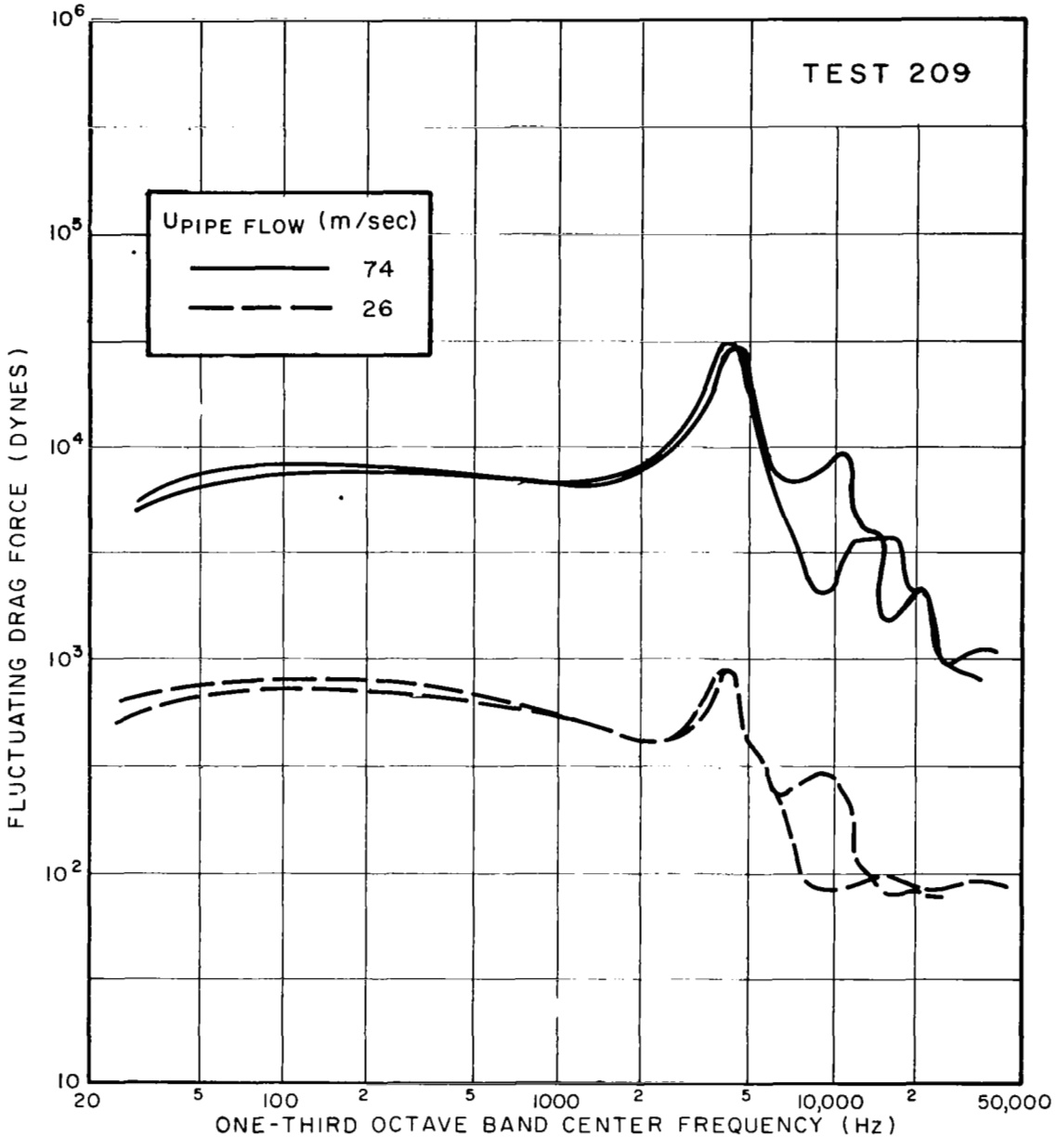

FIG. V-14 FLUCTUATING DRAG FORCE SPECTRA (TEST 209: STRIP SPOILER 18 in UPSTREAM OF PIPE EXIT)

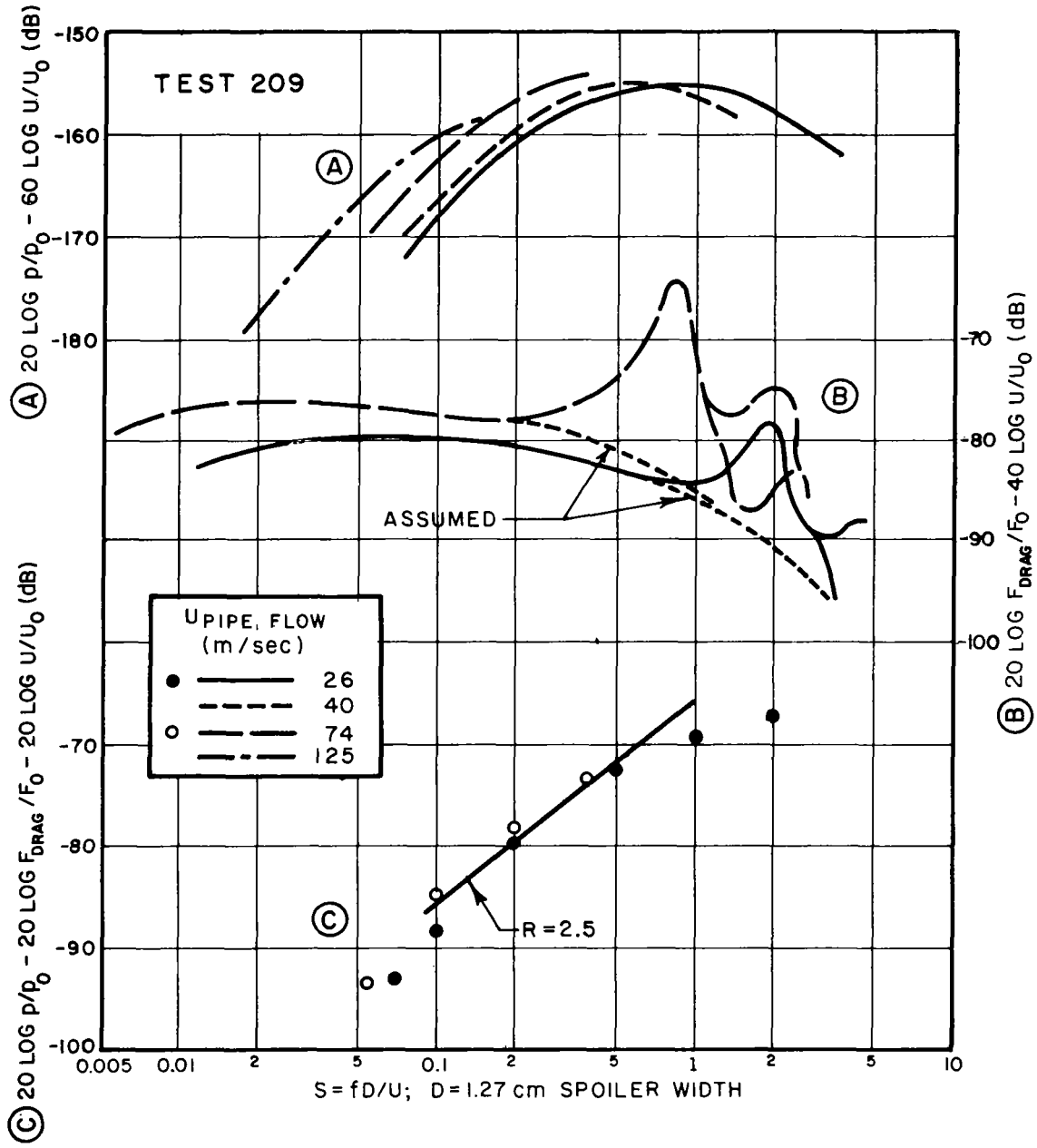

FIG. V-15 SUMMARY OF TEST RESULTS FOR STRIP SPOILER 18 in UPSTREAM OF PIPE EXIT (TEST 209):

Ⓐ Normalized sound pressure level spectrum

Ⓑ Normalized drag force level spectrum

Ⓒ Difference spectrum

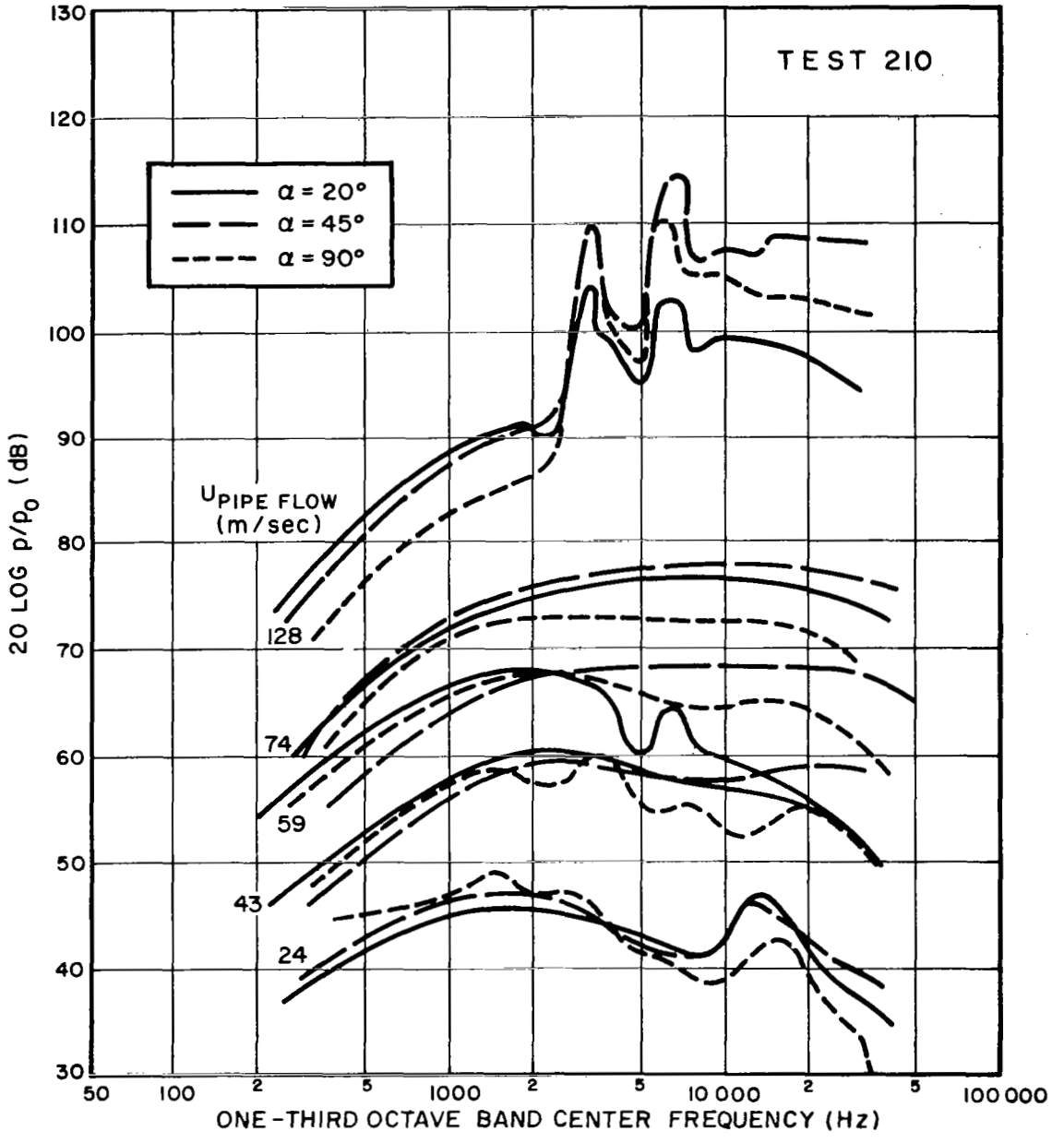

FIG. V-16 SOUND PRESSURE LEVEL SPECTRA (TEST 210: CYLINDRICAL SPOILER 18 in UPSTREAM OF EXIT PIPE)

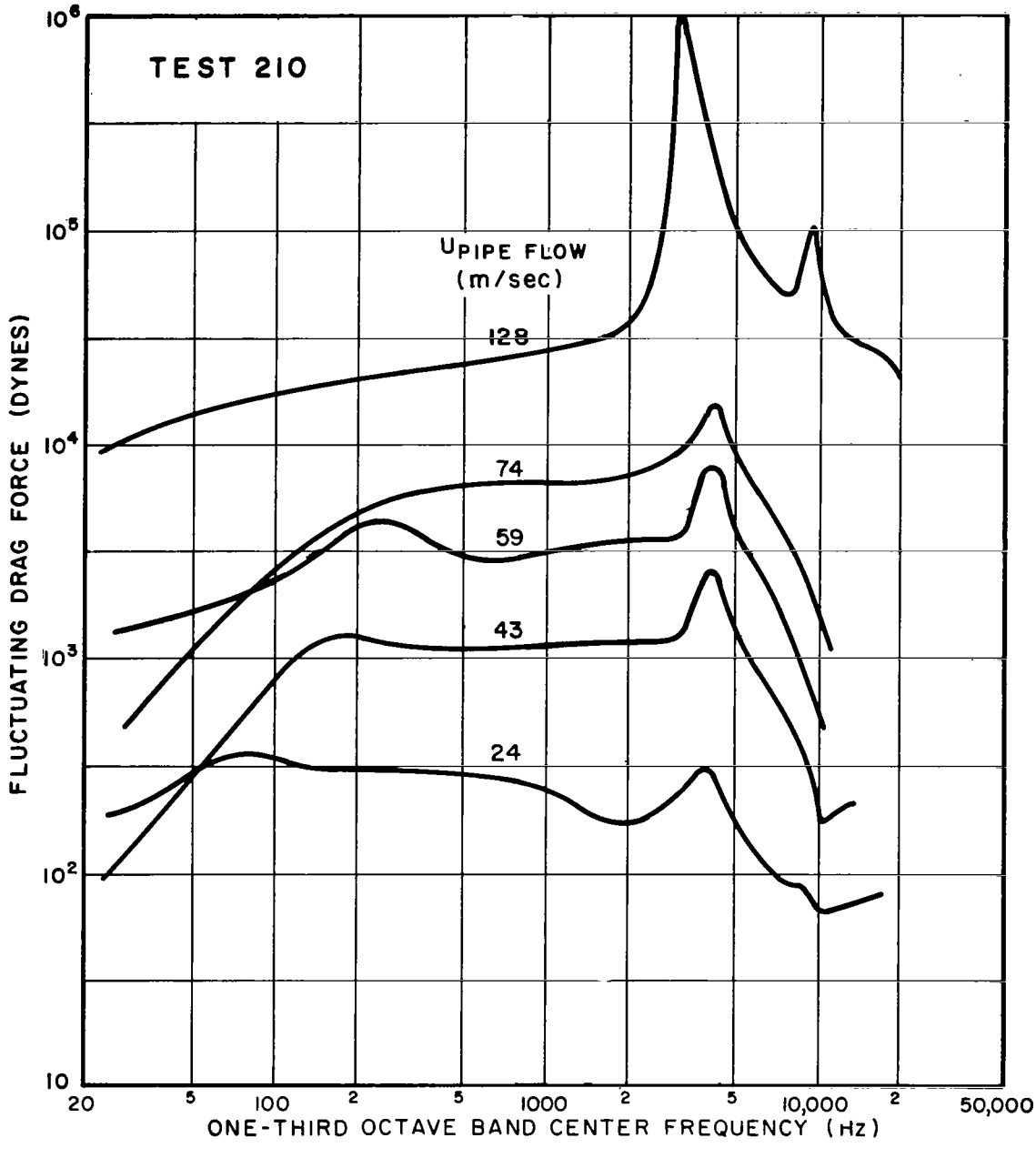

FIG. V-17 FLUCTUATING DRAG FORCE SPECTRA (TEST 210: CYLINDRICAL SPOILER 18 in UPSTREAM OF PIPE EXIT)

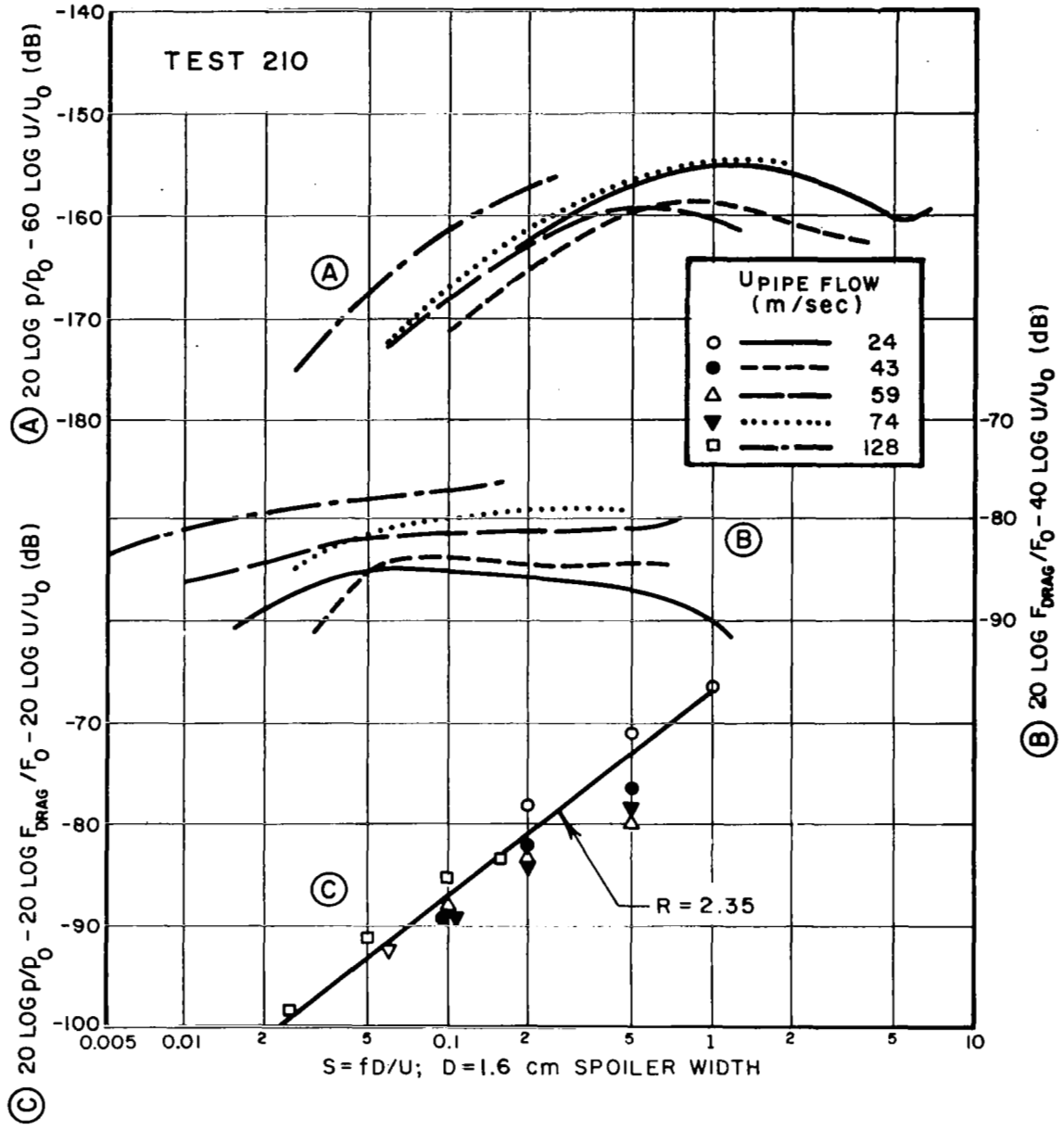

FIG. V-18 SUMMARY OF TEST RESULTS FOR CYLINDRICAL SPOILER 18 in UPSTREAM OF PIPE EXIT (TEST 210):

Ⓐ Normalized sound pressure level spectrum

Ⓑ Normalized drag force level spectrum

Ⓒ Difference spectrum

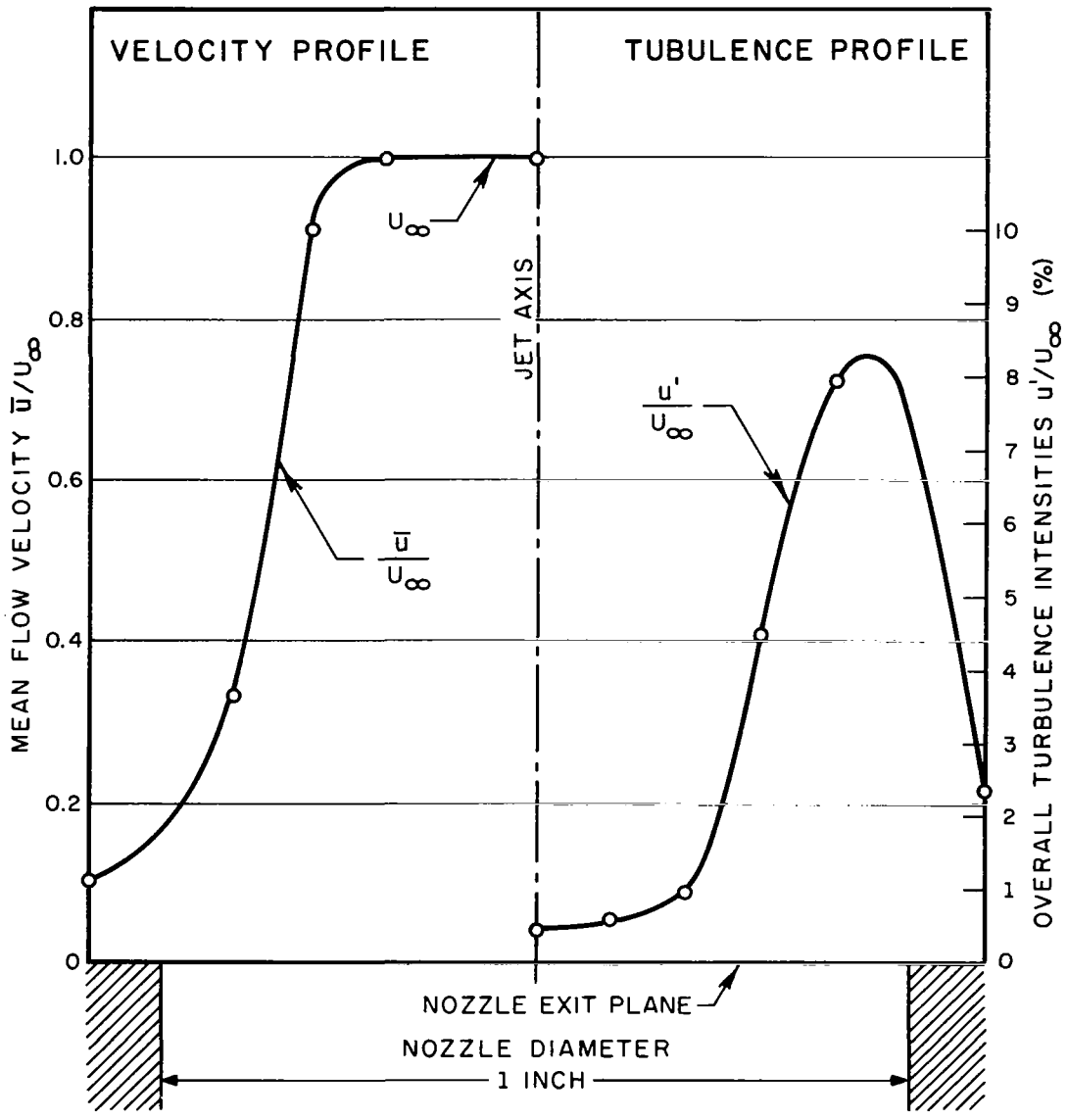

FIG. V-19 VELOCITY PROFILE AND TURBULENCE PROFILE ONE NOZZLE DIAMETER DOWNSTREAM OF NOZZLE EXIT PLANE

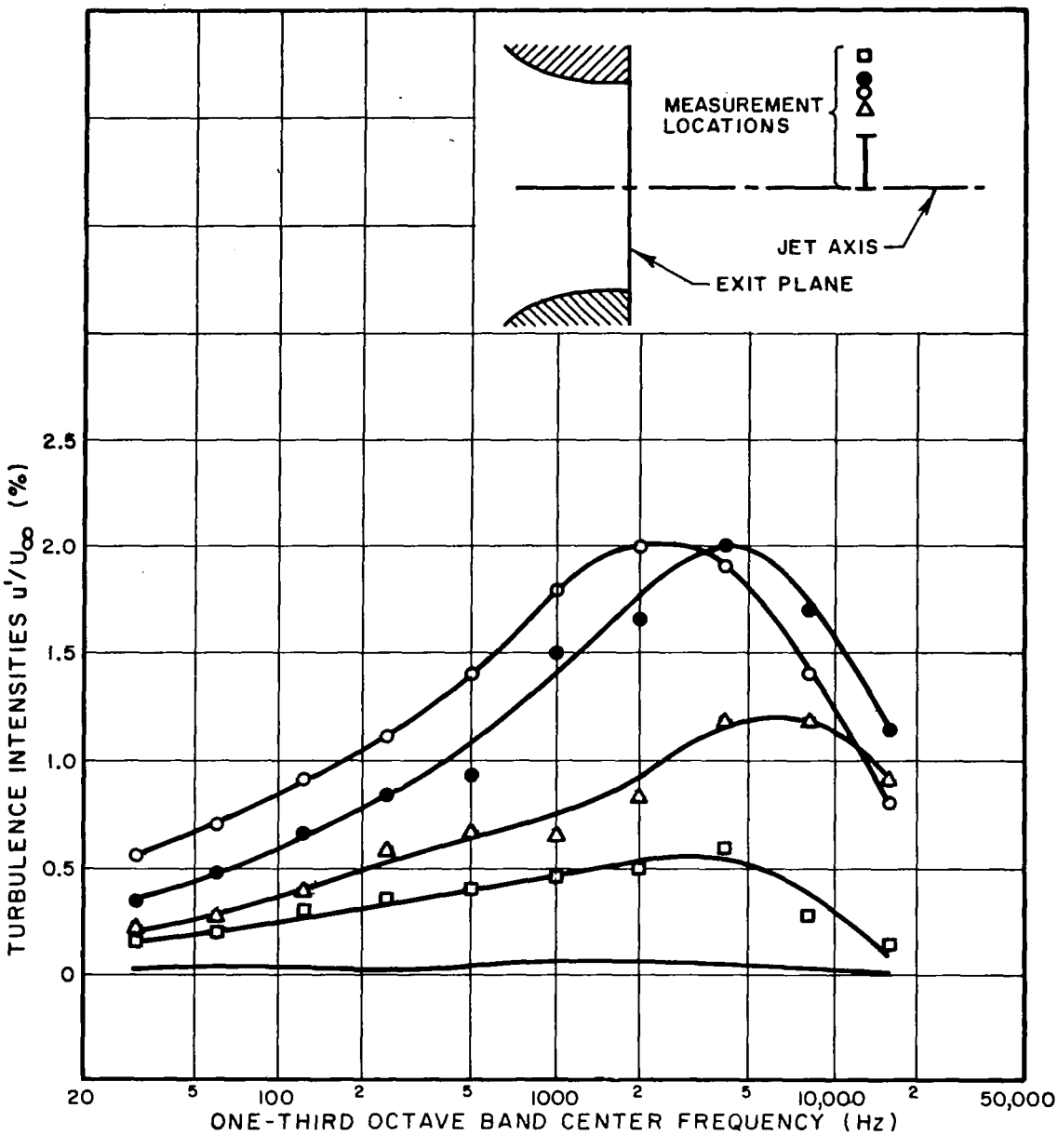

FIG. V-20 TURBULENCE SPECTRA MEASURED ONE NOZZLE DIAMETER DOWNSTREAM OF NOZZLE EXIT PLANE U_{jet} = 130 m/sec

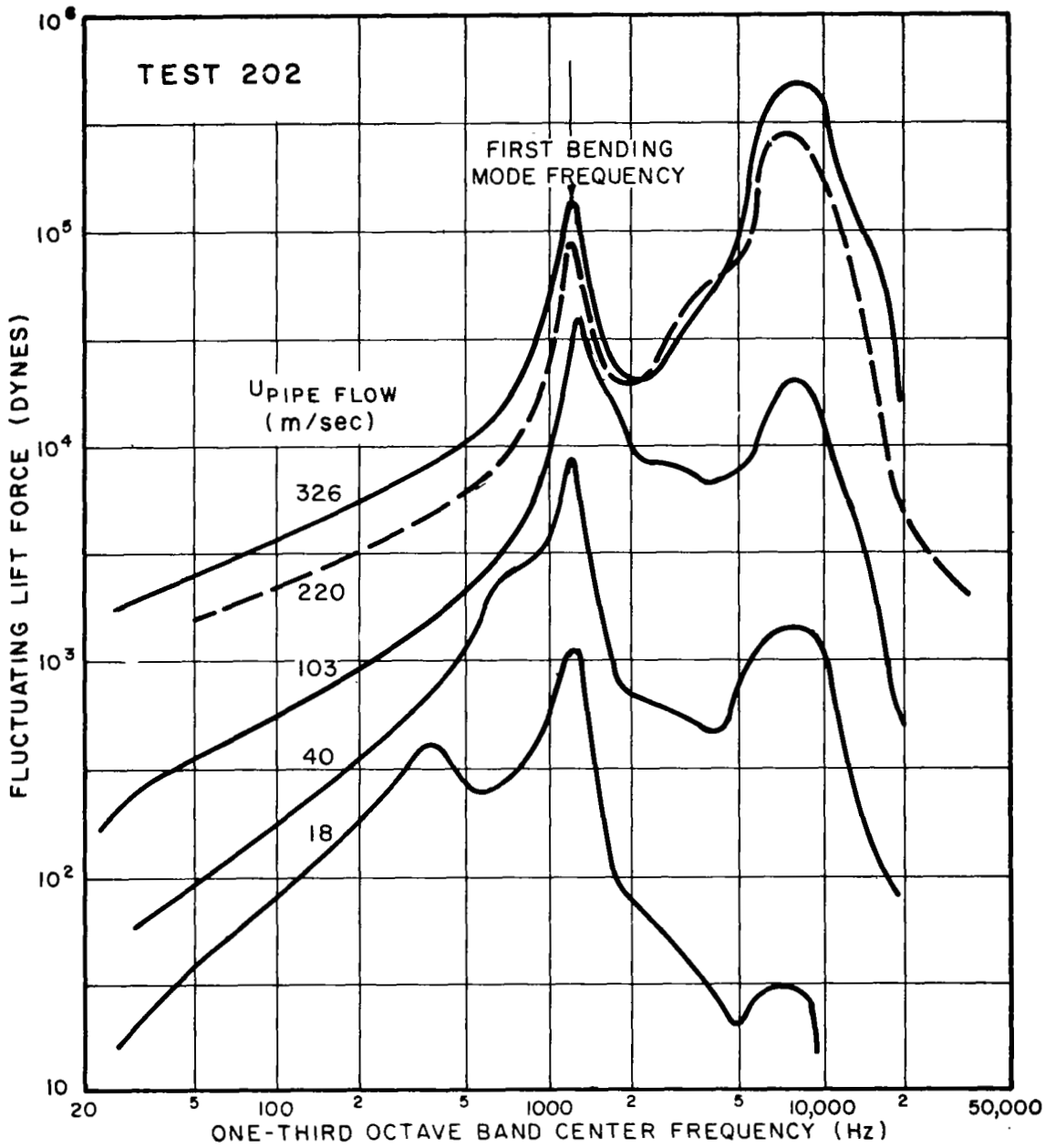

FIG. V-21 FLUCTUATING LIFT FORCE SPECTRA (TEST 202: AIRFOIL IN FREE JET)

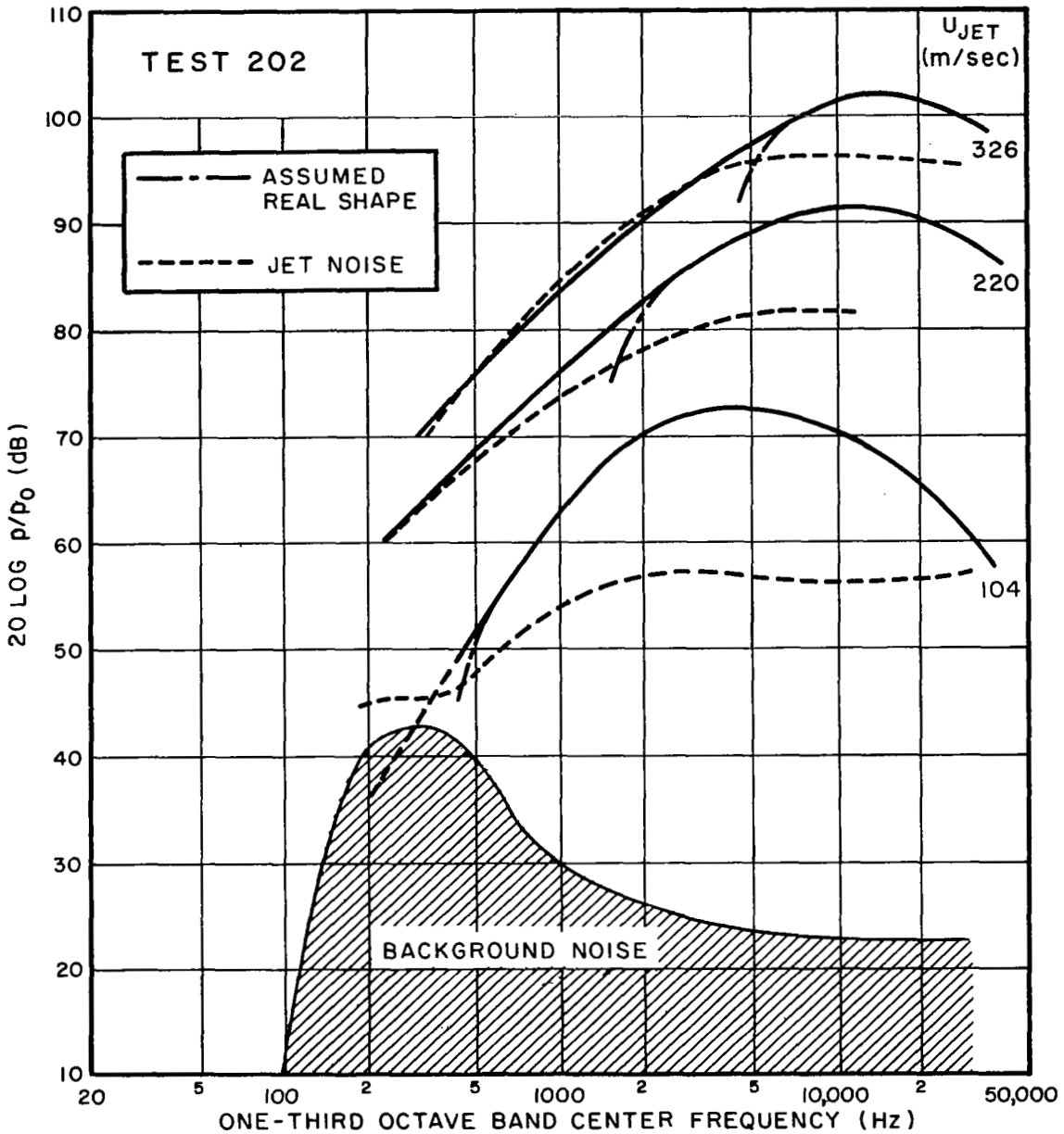

FIG. V-22 SOUND PRESSURE LEVEL SPECTRA (TEST 202: AIRFOIL IN FREE JET)

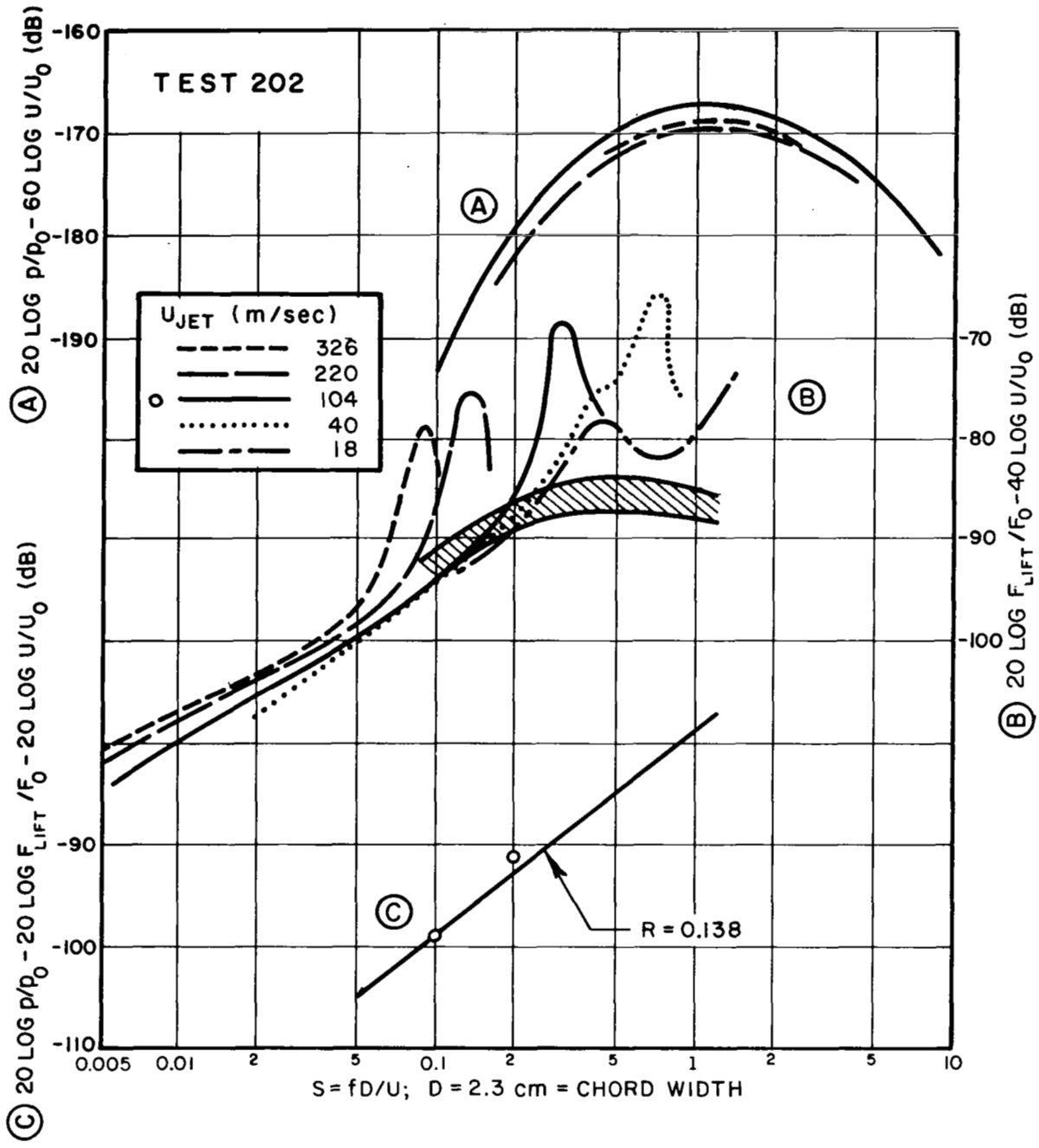

FIG. V-23 SUMMARY OF TEST RESULTS FOR AIRFOIL IN FREE JET (TEST 202):

Ⓐ Normalized sound pressure level spectrum

Ⓑ Normalized lift force level spectrum

Ⓒ Difference spectrum

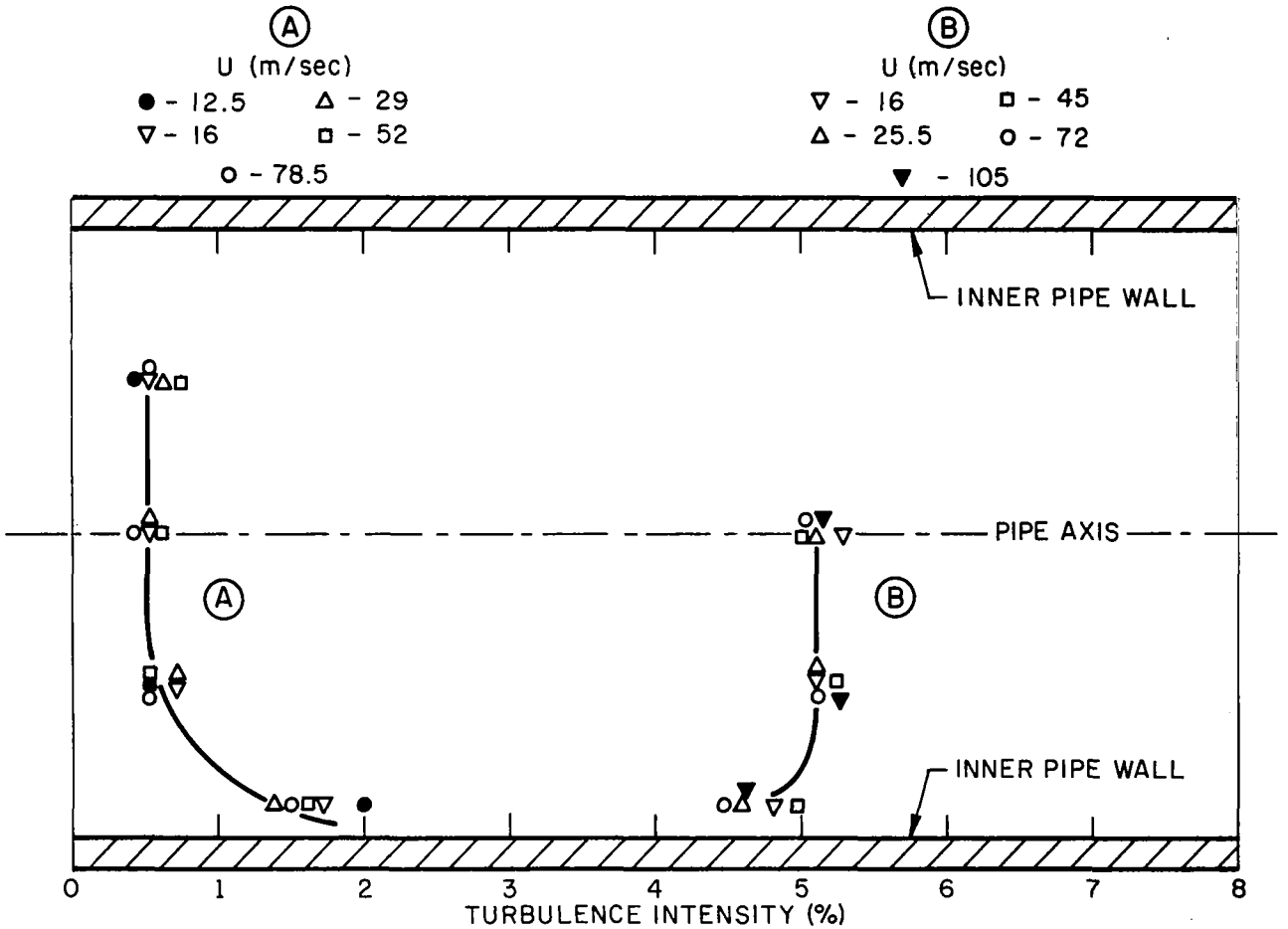

FIG. V-24 TURBULENCE PROFILES ACROSS PIPE (TEST 181):
(A) 2 in downstream of silk screens
(B) Fully developed pipe flow

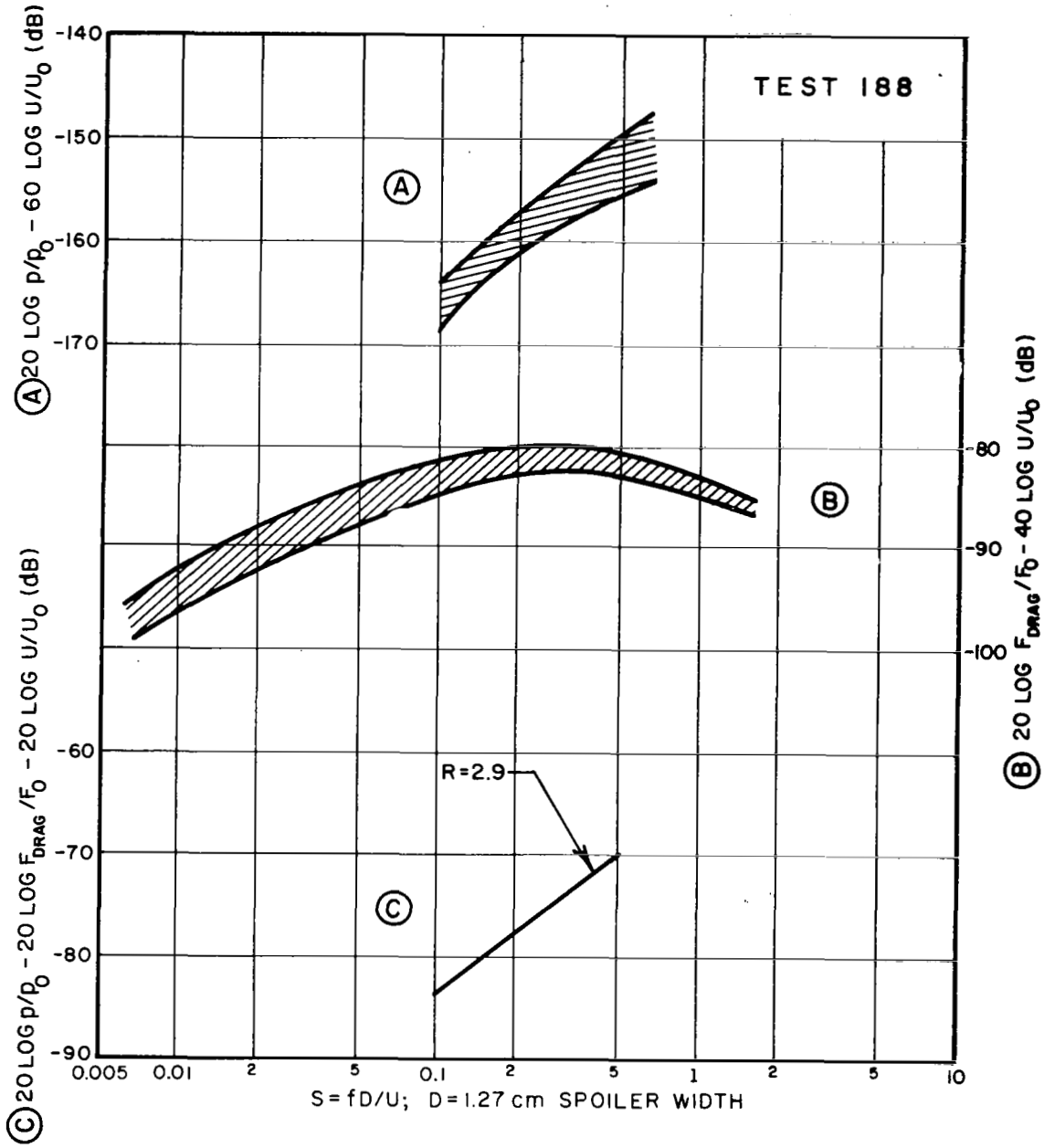

FIG. V-25 SUMMARY OF TEST RESULTS FOR STRIP SPOILER 9 in UPSTREAM OF PIPE EXIT (TEST 188, REDUCED TURBULENCE LEVEL):

Ⓐ Normalized sound pressure level spectrum

Ⓑ Normalized drag force level spectrum

Ⓒ Difference spectrum

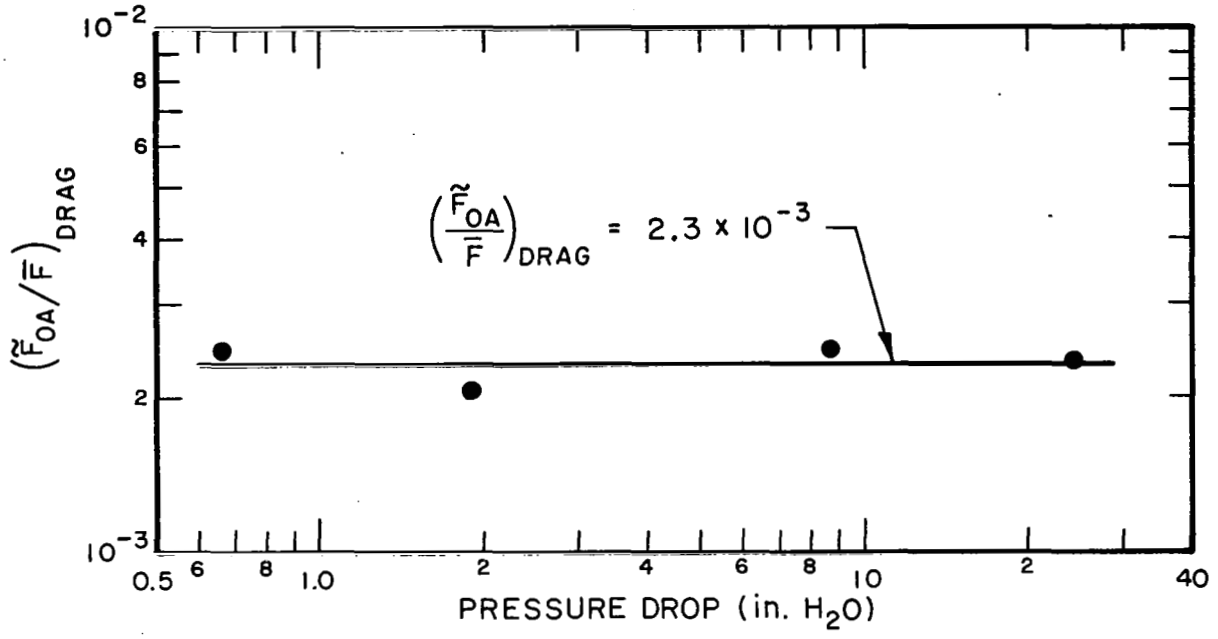

FIG. V-26 RELATIONSHIP BETWEEN OVERALL FLUCTUATING DRAG FORCE AND STEADY-STATE DRAG FORCE

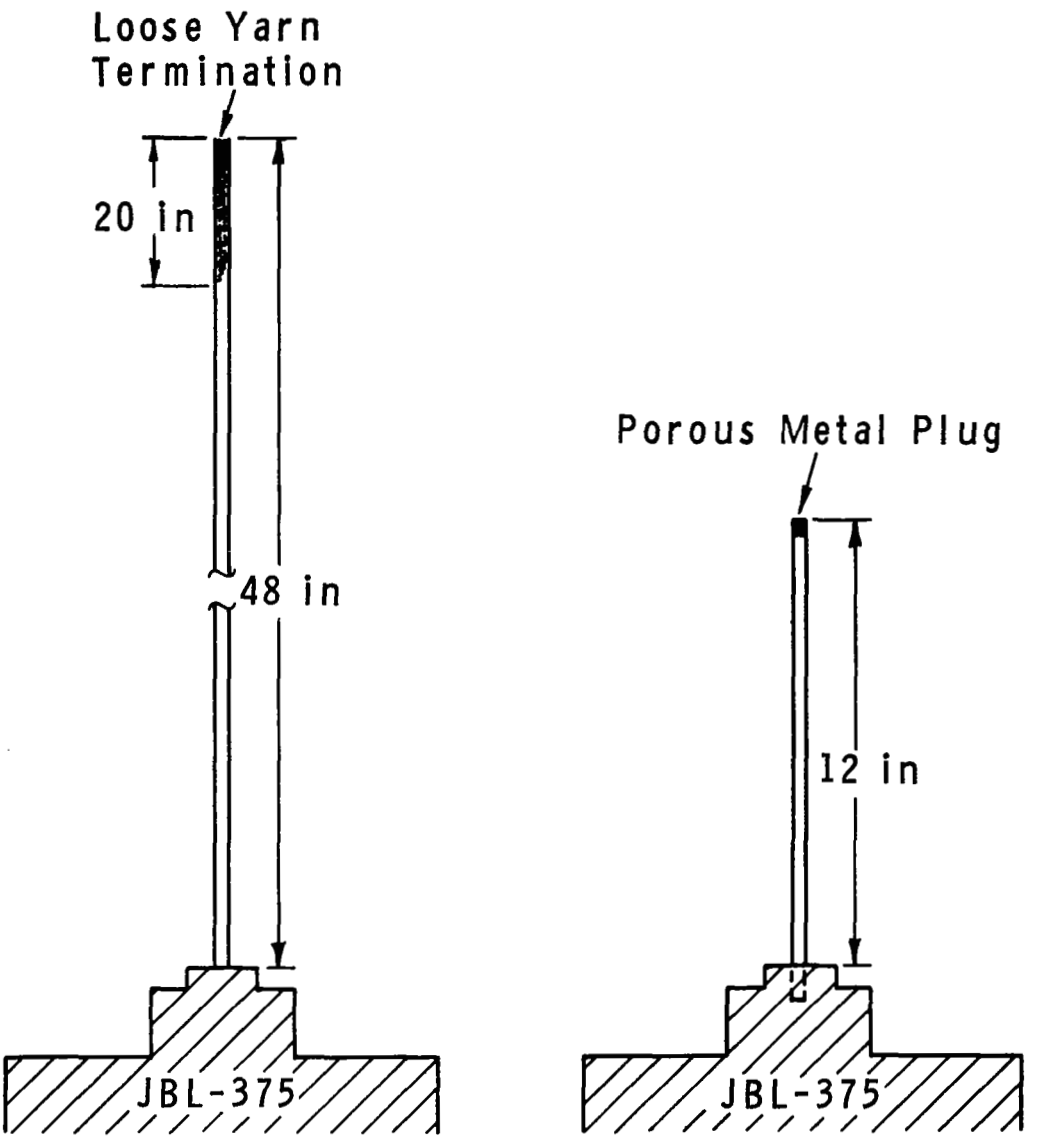

FIG. A-1 SOURCE DESIGN

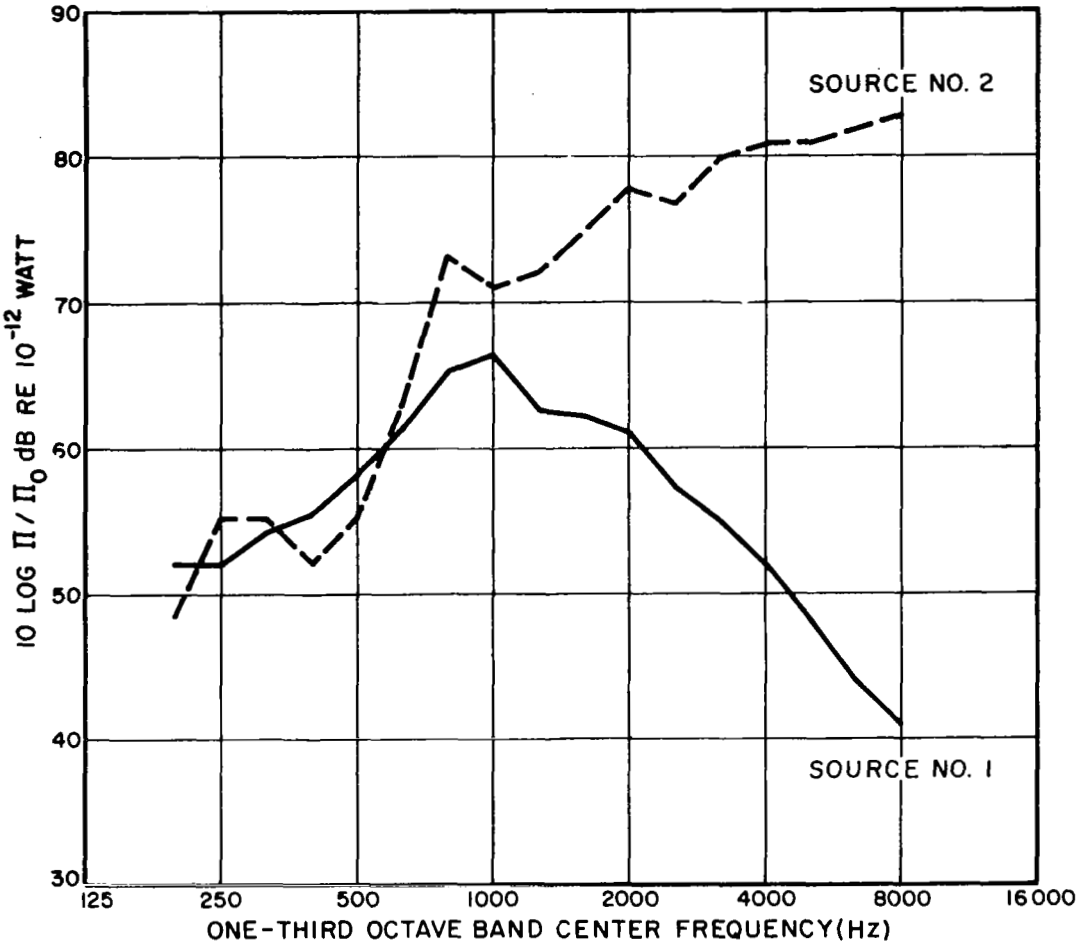

FIG. A-2 FREE-FIELD RADIATION FROM ACOUSTIC MONOPOLE SOURCE

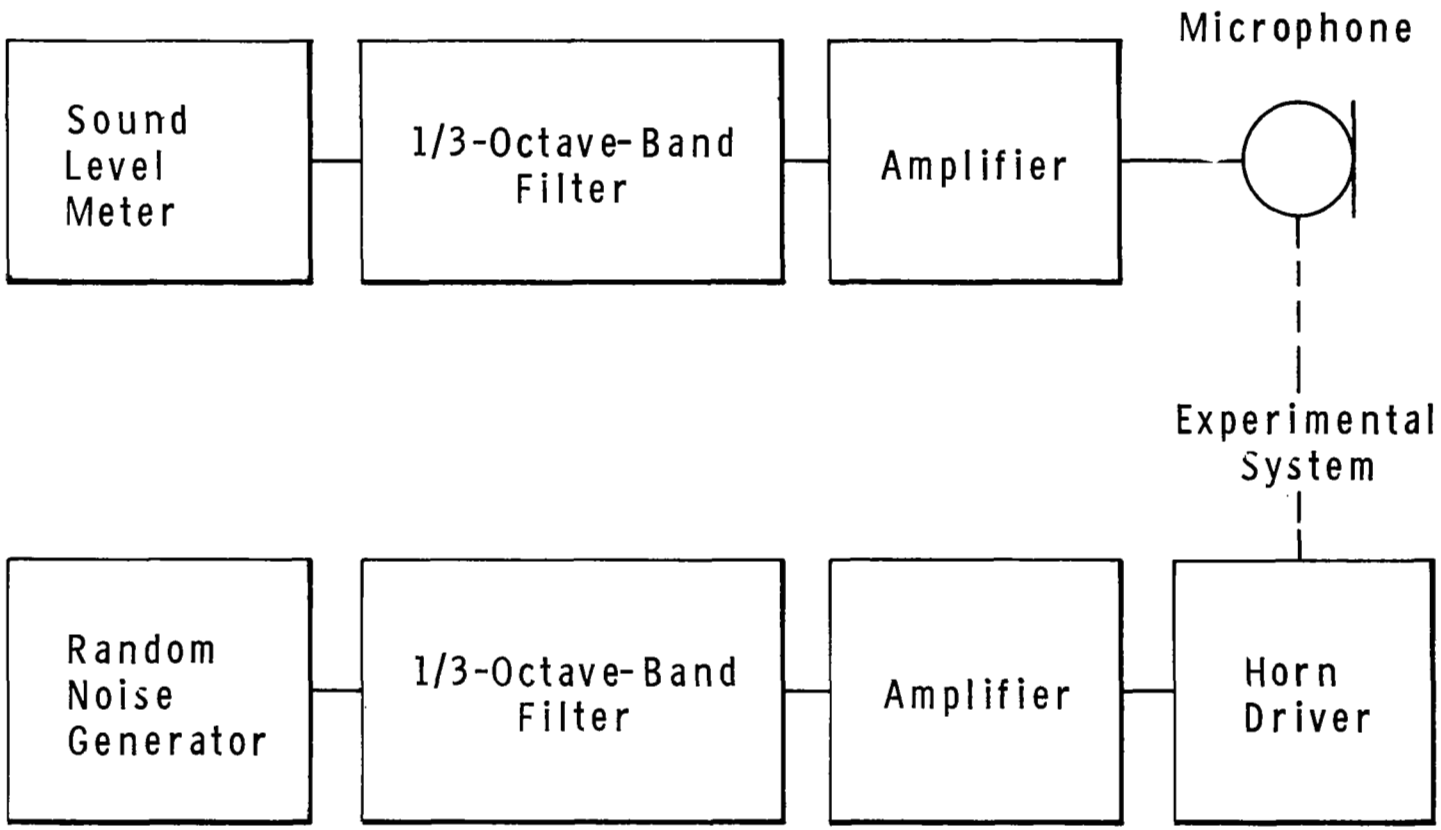

FIG. A-3 SCHEMATIC OF MEASUREMENT SYSTEM

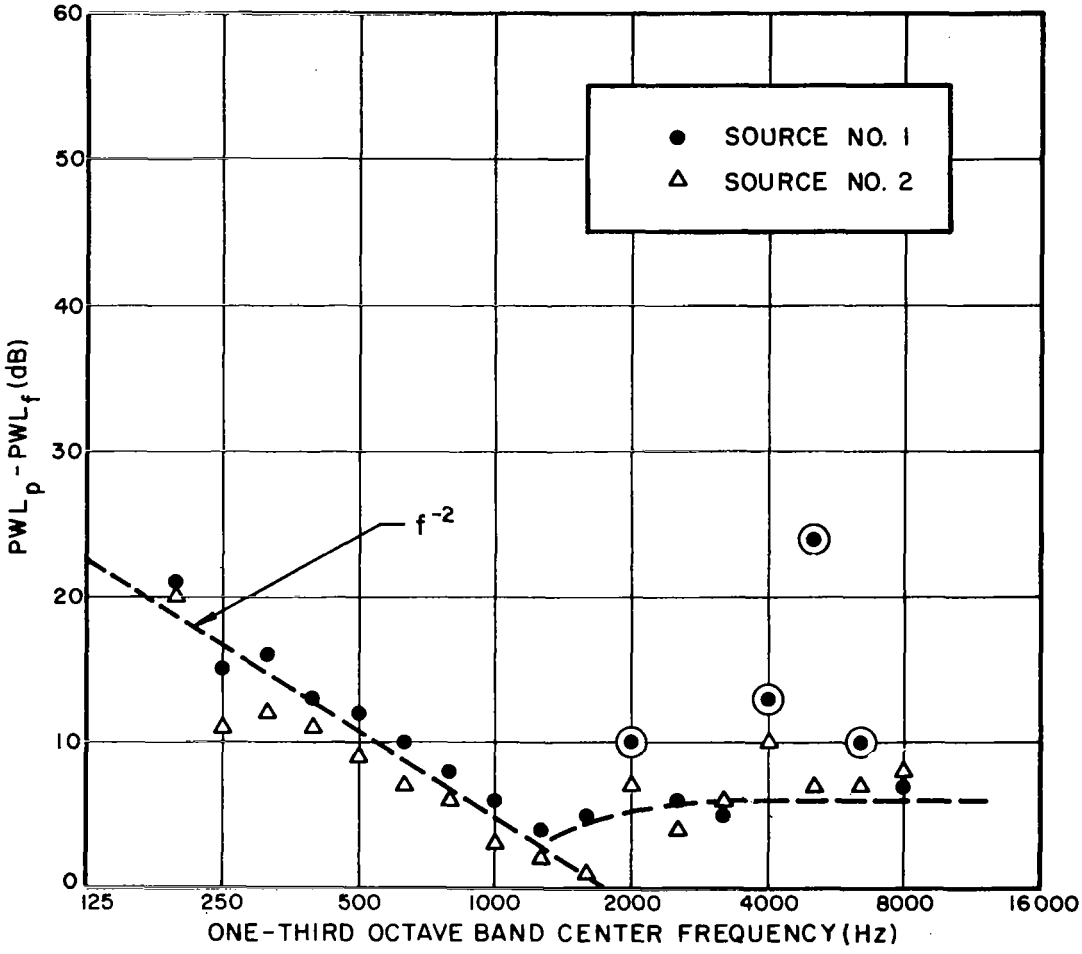

FIG. A-4 INFLUENCE OF INFINITE PIPE ON SOURCE

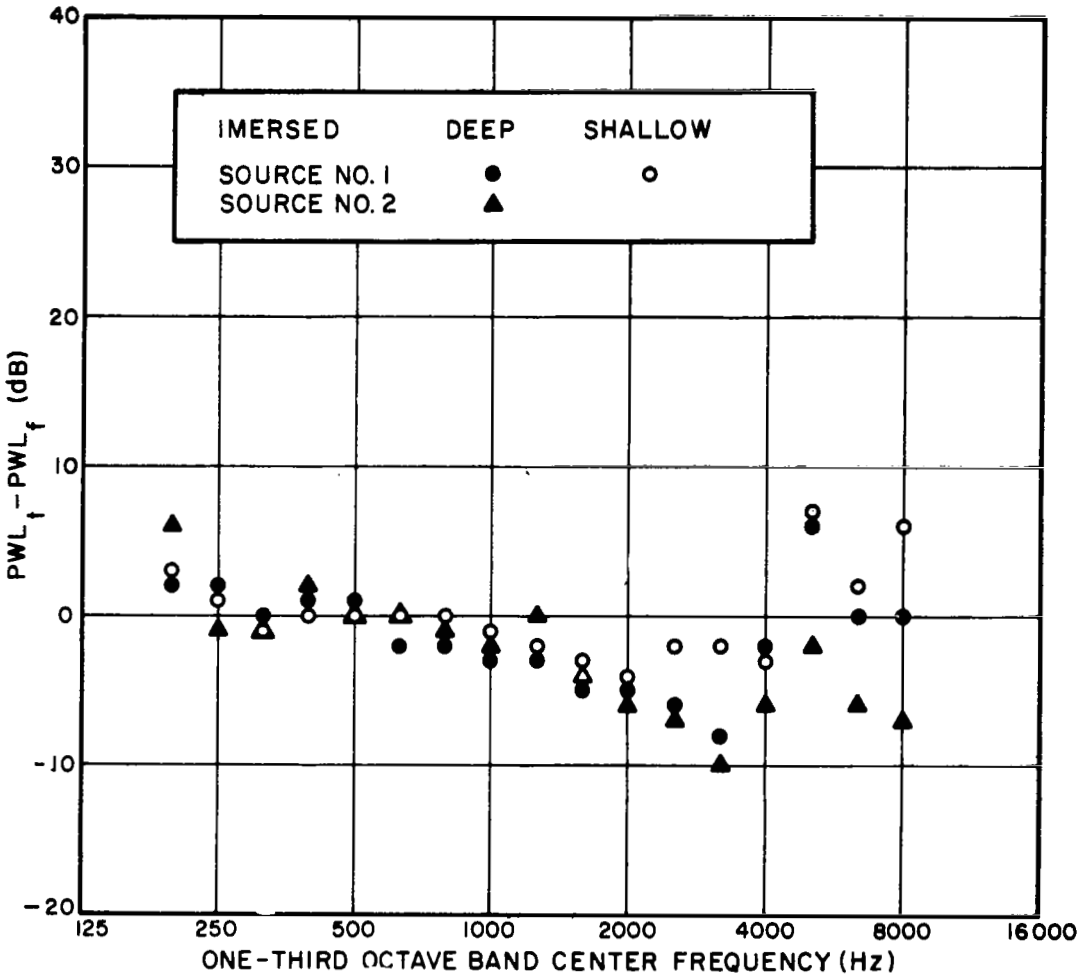

FIG. A-5 INFLUENCE OF TRUNCATED PIPE ON SOURCE

NASA-Langley, 1969 —— 23 CR-1340